Chapter IV

Results

4.1. *In-silico* Screening

4.1.1. Virtual screening of chemical repositories

Large collections of compounds are frequently tested experimentally to find potential hits, but the time and expense required can be significantly reduced by *in-silico* screening and docking of compound repositories. The probable binding conformations are seen using molecular docking, which also shows hydrogen bonds, π-π interactions, and close ties to important residues. Using molecular docking, 30,417 compounds from three different libraries of chemical compounds were computationally assessed for their ability to block three different target enzymes of the *Mycobacterium* cell wall biosynthesis pathway.

4.1.2. *Mycobacterial* Mycolic Acid membrane protein *MmpL* 11D2 (4YOL)

The 2.4 Å *MmpL* 11D2 structures have two anti-parallel helices (helixes α2 and α3), establishing a *"βαββαβ"* fold that encloses an aquaphobic core of residues resting on top of four standard anti-parallel sheets. A bulge created by two proline residues (Proline 463 and Proline 464) interrupts the three residues β2. Five hydrogen bonds with β2 and β3 stabilize the loop linking them.[186] Additionally, stacking between Phe 431 and His 441 provides stability to a prolonged twist region between β1 and α2.

Another factor stabilizing the overall globular structure is an ion couple that lies among Arg 430 and Asp 509, as well as many H-bonds.[186]

A crucial component of contemporary drug design is the virtual screening and discovery of potential inhibitors through the virtual screening of a large chemical library for biological activities. Through virtual screening, it may be possible to identify a chemical that has a lower free binding energy when binding to macromolecules like protein and DNA. The anticipated *MmpL* 11D2 enzymes were molecularly docked with a set of molecules. Fifty-one compounds were found utilizing *in-silico* screening, and thirteen (Figure 4.1) of the top hits were selected for further study.

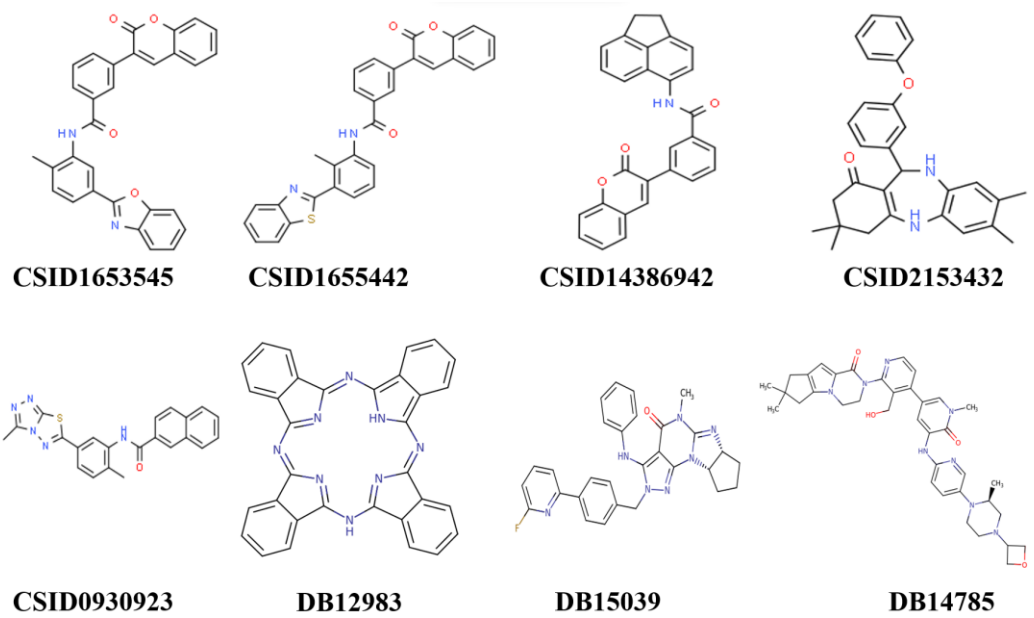

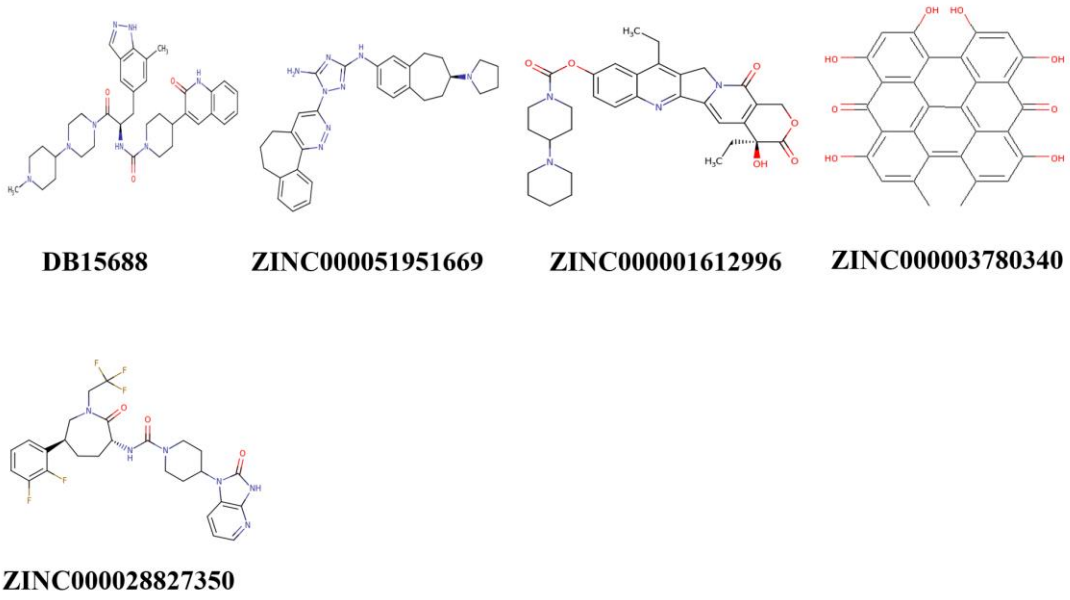

Figure 4.1. 2D structure of top thirteen hits identified against MTB's protein *MmpL* 11D2.

The thirteen top-ranked compounds were chosen with strong binding affinity grounded on the "XP G-score", which quantifies the "binding energy" (Table 4.1). The binding affinity lies between -9.9 to -8.0 kcal/mol (Figure 4.2). The top thirteen compounds in terms of binding energy are From ChemSpider, CSID1653545 (-9.9 Kcal/mol) with *KI* 4.04 nM, CSID1655442 (-9.0 Kcal/mol) with *KI* 35.48 nM, CSID1438694 (-8.4 Kcal/mol) with *KI* 5.03 nM, CSID2153432 (-8.0 Kcal/mol) with *KI* 83.30 nM, CSID0930923 (-8.0 Kcal/mol) with *KI* 28.82 nM; From Drug Bank, DB12983 (-8.8 Kcal/mol) with *KI* 165.48 nM, DB15039 (-8.2 Kcal/mol) with *KI* 129.60 nM, DB14785 (-8.1 Kcal/mol) with *KI* 21.64 nM, DB15688 (-8.0 Kcal/mol) with *KI* 22.34 nM; ZINC000051951669 (-8.6 Kcal/mol) with *KI* 50.12 nM, ZINC000001612996 (-8.4 Kcal/mol) with *KI* 120.67 nM, ZINC000003780340 (8.3 Kcal/mol) with *KI* 49.28 nM, ZINC000028827350 (-8.1 Kcal/mol) with *KI* 107.39 nM.

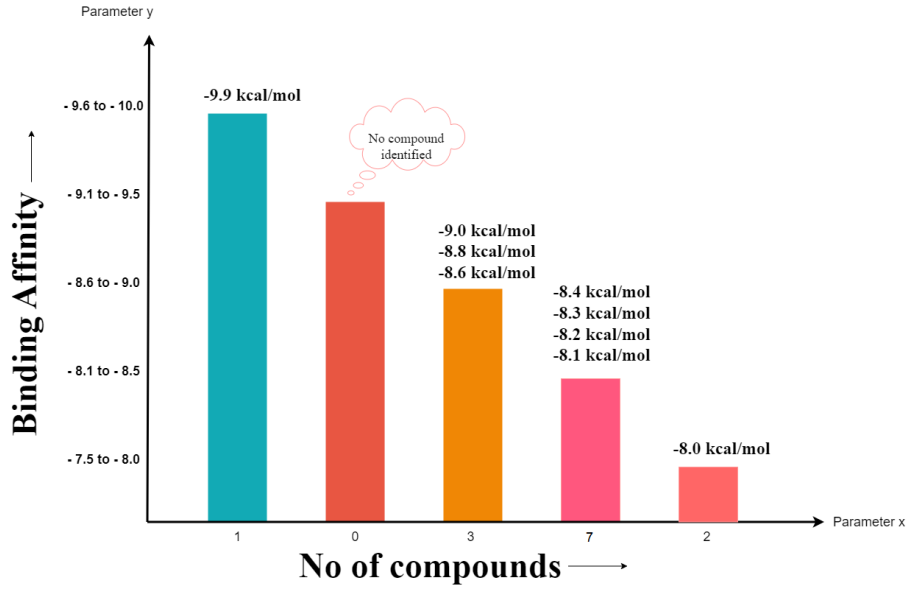

Figure 4.2. The free binding affinity of selected compounds against *MmpL* 11D2.

4.1.3. Identified compounds-*MmpL* 11D2 interactions

Using the simulated screening process, thirteen compounds were selected from three different repositories. These compounds were examined in tests involving the *MmpL* 11D2 proteins. These compounds all match the cavity of the goal construction the best. The graphics below display these substances' positions and interaction patterns with the *MmpL* 11D2 proteins (Figure 4.3). The compound from the ChemSpider with CSID1653545 (Fig 4.3.1) shows eight hydrophobic interactions with Gln 426, Leu 428, Leu 474, Arg 496, Pro 500, Ala 503, Val 508, Asp 509 and five interactions by a hydrogen bond with residues Arg 496 (two contacts), Asp 509 (two contacts), and Val 510. The second compound with CSID1655442 (Fig 4.3.2) shows hydrophobic interaction with four residues including Arg 496, Pro 500, Val 508, and Val 510, and four interactions with hydrogen bonds with resides Arg 496, Val 508, Asp 509, and Val 510.

Table 4.1. Drug likeness characteristics of top thirteen hits against target *MmpL* 11D2.

S.NO	Compound ID	Binding Affinity	Inhibition constant (KI)	Molecular Weight	LOGP	H-Bond Acceptors	H-Bond Donors	Drug-likeness Score
1	CSID1653545	-9.9	4.04 nM	472.49	7.04	6	1	-0.52
2	CSID1655442	-9	35.48 nM	488.55	7.29	5	1	-0.33
3	CSID1438694	-8.4	5.03 nM	417.45	6.41	4	1	-0.26
4	CSID2153432	-8.1	83.30 nM	438.56	6.32	4	2	0.14
5	CSID0930923	-8	28.82 nM	399.46	5.16	6	1	-0.1
6	DB12983	-8.8	165.48 nM	514.55	4.79	6	2	-1.06
7	DB15039	-8.2	129.60 nM	507.53	5.04	6	1	1.23
8	DB14785	-8.1	21.64 nM	664.81	2.82	9	2	0.98
9	DB15688	-8	22.34 nM	638.81	2.85	6	3	1.33
10	ZINC000051951669	-8.6	50.12 nM	506.65	4.88	7	3	0.06
11	ZINC000001612996	-8.4	120.67 nM	586.68	4.09	8	2	1.54
12	ZINC000003780340	-8.3	49.28 nM	504.45	5.08	8	4	-1.01
13	ZINC000028827350	-8.1	107.39 nM	566.53	3.68	5	2	1.49

The third compound with CSID1438694 (Fig 4.3.3) shows hydrophobic interaction with Arg 496, Pro 500, Gln 507, Val 508 (two contacts), and Val 510, and three hydrogen bond interactions with residues Val 508 (two contacts) and Val 510. The fourth compound with CSID2153432 (Fig 4.3.4) shows a total of nine interactions, eight hydrophobic interactions with residue Pro 500 (two contacts), Ala 503, Val 508 (two contacts), Asp 509, and Val 510, and one interaction by a hydrogen bond with residues Val 508. The fifth compound with CSID0930923 (Fig 4.3.5) shows five hydrophobic interactions with residues Gln 426, Leu 428, Leu 474, Arg 496, Asp 509, and five interactions by a hydrogen bond with residues Arg 496 (two contacts), Asp 509 (two contacts), and Val 510. The sixth compound is from Drug Bank with DBID: DB12983 (Fig 4.3.6) showing five hydrophobic interactions with residues Ile 445, Pro 463, Pro 464, Arg 465, and Phe 466. The next and seventh compound is DB15039

(Fig 4.3.7) showing seven hydrophobic interactions with residues Arg 496 (two contacts), Pro 500 (two contacts), Ala 503, Val 508, and Val 510, and four hydrogen bond interactions with residues Arg 496 (two contacts), Val 508, Val 510. The eighth compound, DB14785 (Fig 4.3.8) shows interaction with Arg 496, Pro 500, Gln 507, and Val 508 by hydrophobic mode and three interactions by a hydrogen bond with Thr 493, and Val 508 (two contacts). The ninth compound, DB15688 (Fig 4.3.9) shows the interaction with six hydrophobic residues including Glu 440 (two contacts), Ala 447, Arg 501, and Val 502 (two contacts), and four interactions via hydrogen bonds including Gln 443, Thr 444 (two contacts), and Arg 501.

The tenth compound from Zinc Database with Zinc ID: ZINC000051951669 (Fig 4.3.10) shows interaction with nine hydrophobic residues including Phe 431 (two contacts), Asp 432, Thr 444, Ala 447 (two contacts), Val 502, Ala 505, Ala 506 and four interactions by a hydrogen bond with residues Asp 432, Gln 443, Val 502 (two contacts). The eleventh compound, ZINC000001612996 (Fig 4.3.11) shows two hydrophobic interactions with residues His 450, and Gln 454 and two hydrogen bonds with residues Arg 449, and Asn 457.

The next and twelve compounds are ZINC000003780340 (Fig 4.3.12) which shows hydrophobic interaction with Gln 454 (two contacts), Pro 456, and Trp 494, and six interactions by hydrogen bonds including Arg 451 (two contacts), Gln 454, Asn 457 (two contacts), and Trp 494. The thirteen compounds, ZINC000028827350 (Fig 4.3.13) show only one hydrophobic interaction with Ala 506 and six interactions via hydrogen bonds with residues Asp 432, Ala 433, His 441, Thr 444, Ala 503, and Ala 505.

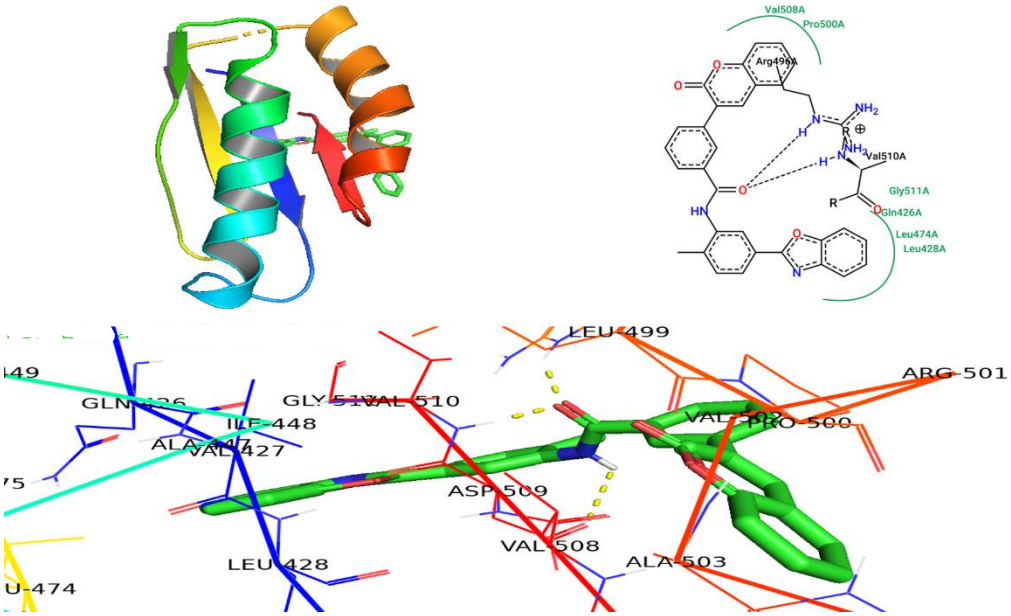

4.3.1 *MmpL* 11D2-CSID1653545

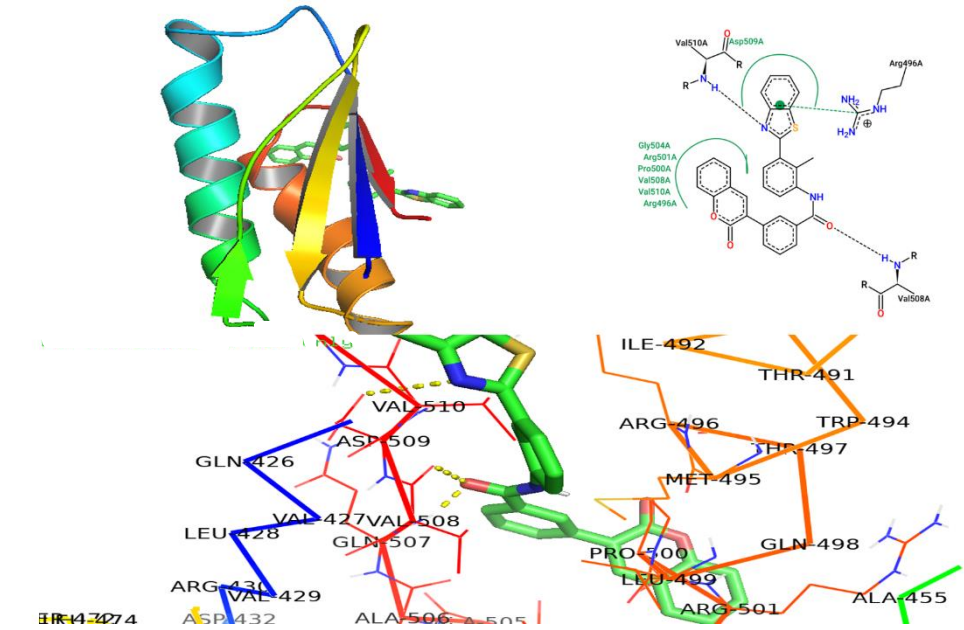

4.3.2 *MmpL* 11D2-CSID1655442

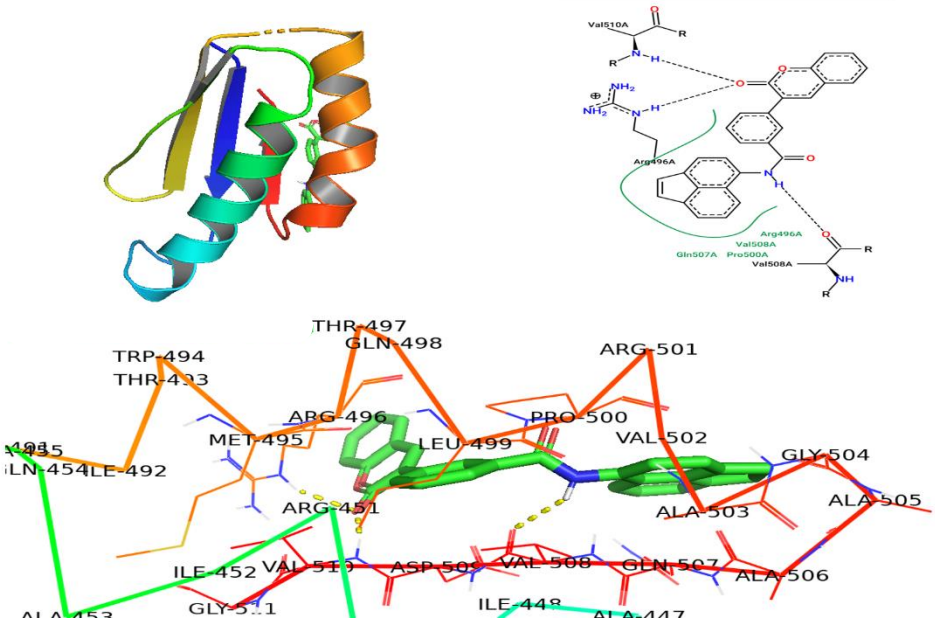

4.3.3 *MmpL* 11D2-CSID1438694

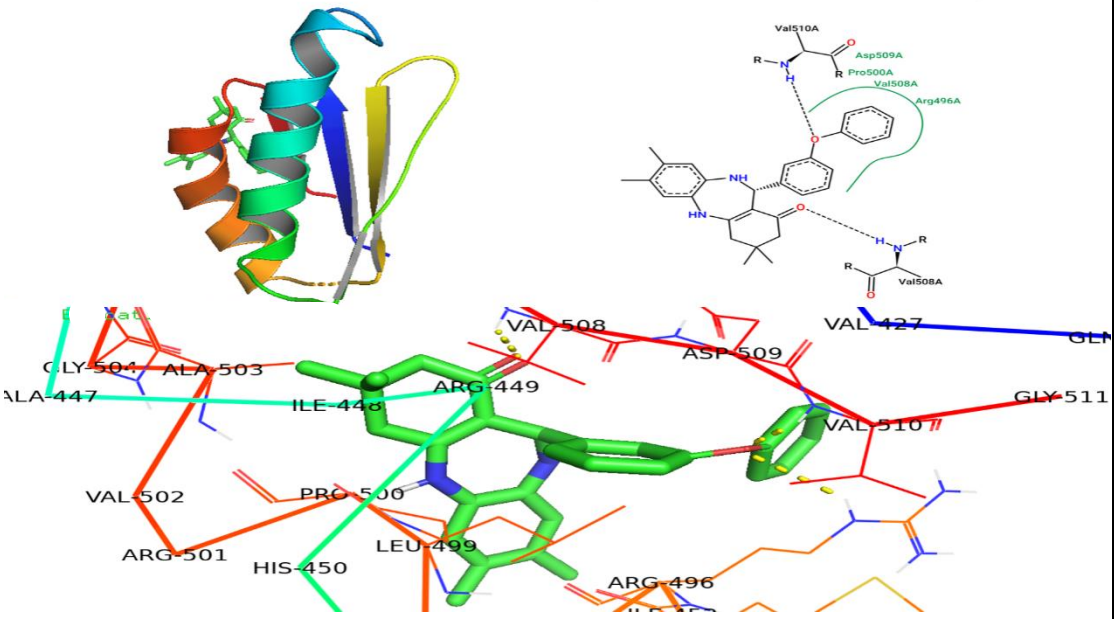

4.3.4 *MmpL* 11D2-CSID2153432

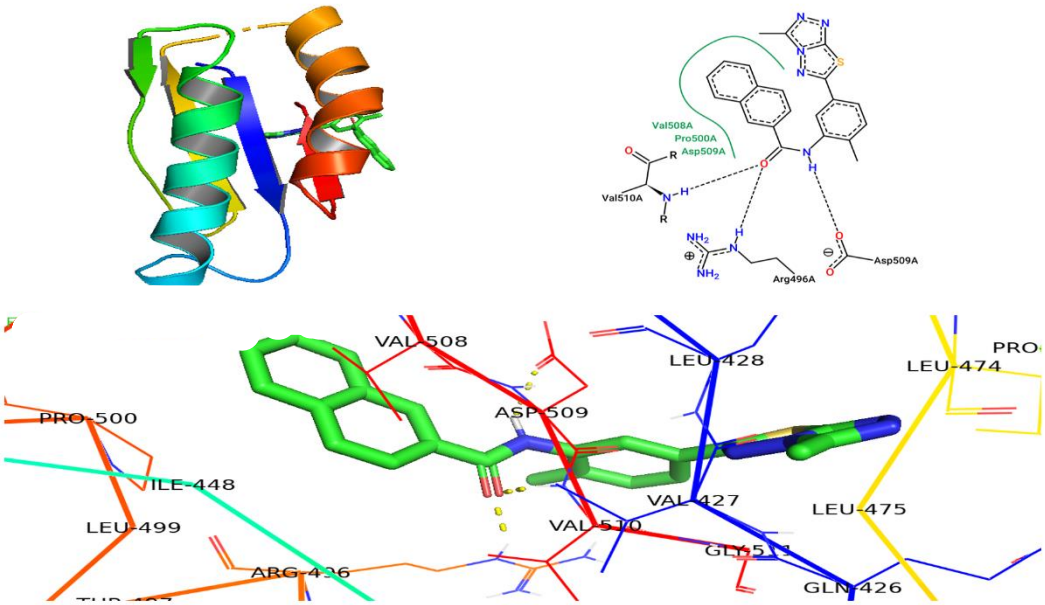

4.3.5 *MmpL* 11D2-CSID930923

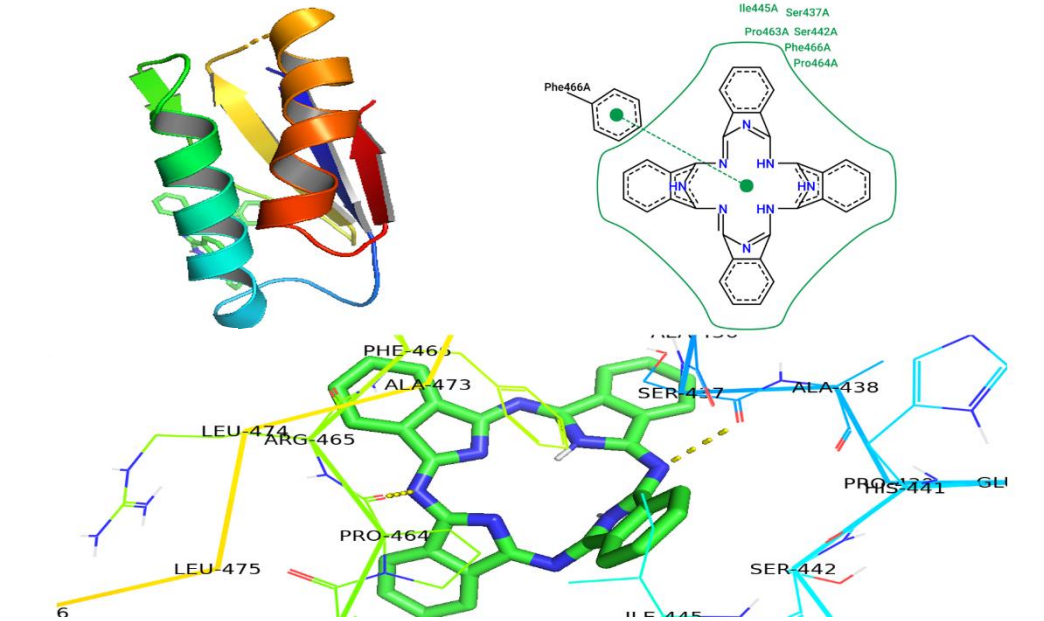

4.3.6 *MmpL* 11D2-DB12983

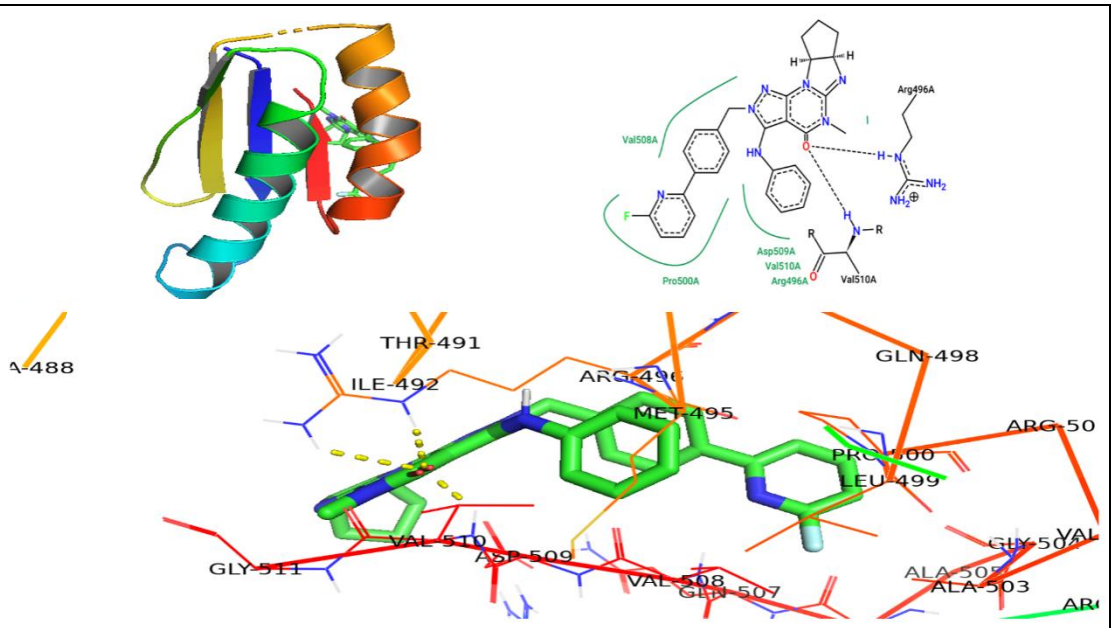

4.3.7 *MmpL* 11D2-DB15039

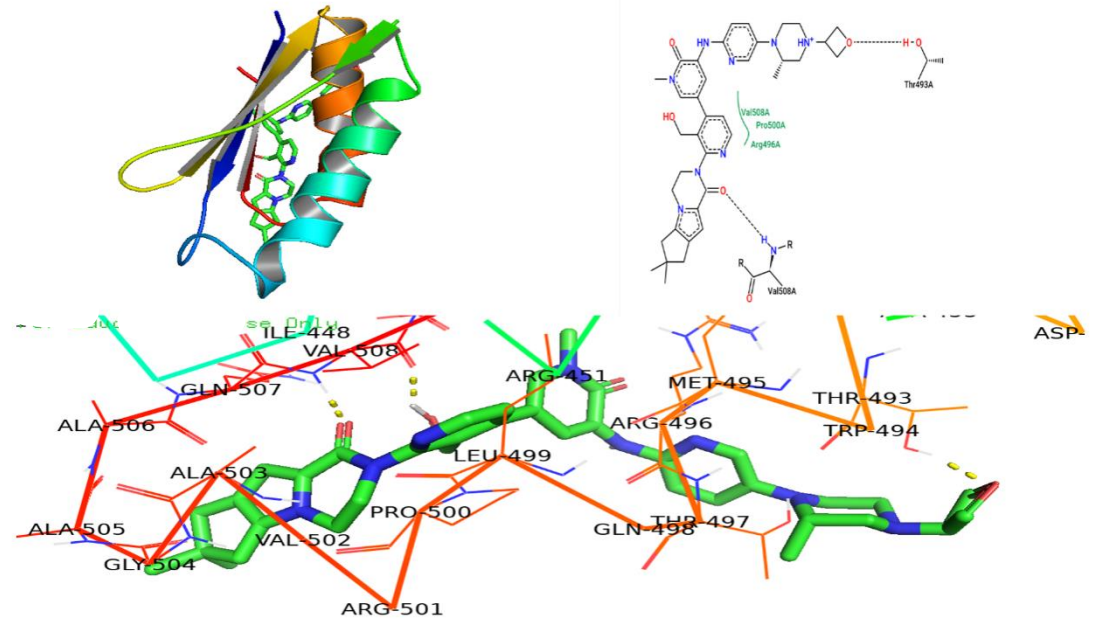

4.3.8 *MmpL* 11D2-DB14785

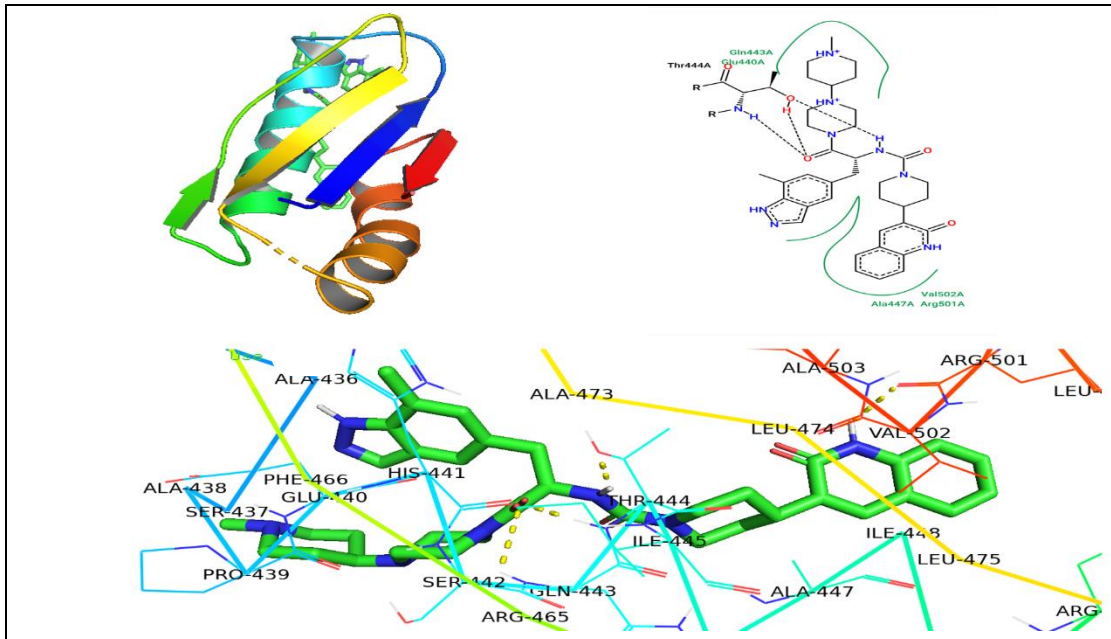

4.3.9 *MmpL* 11D2-DBI5688

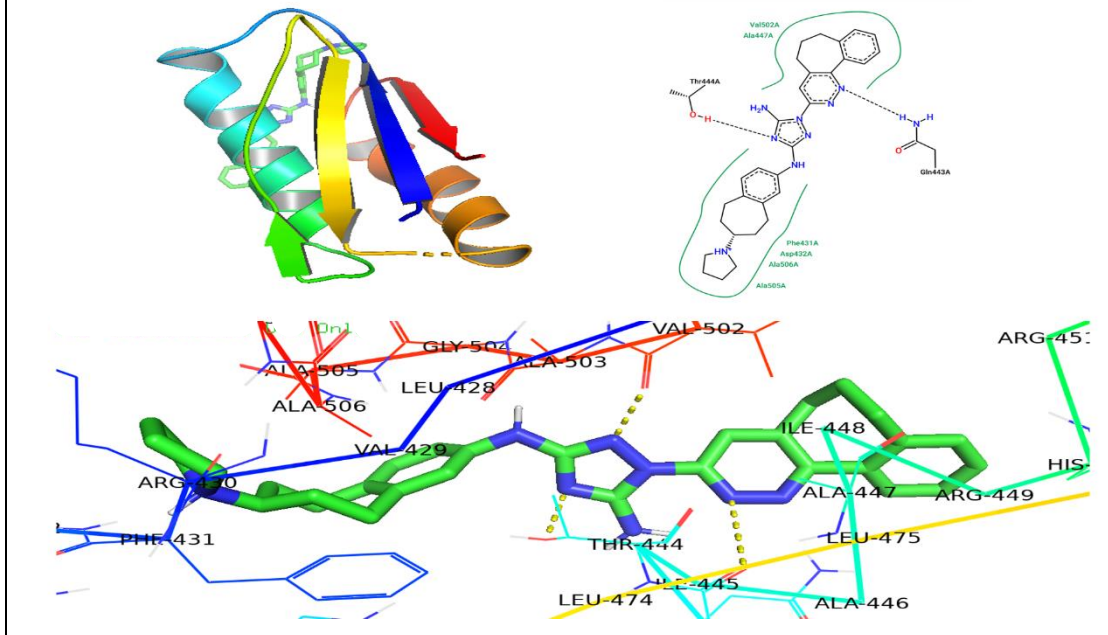

4.3.10 *MmpL* 11D2-ZINC000051951669

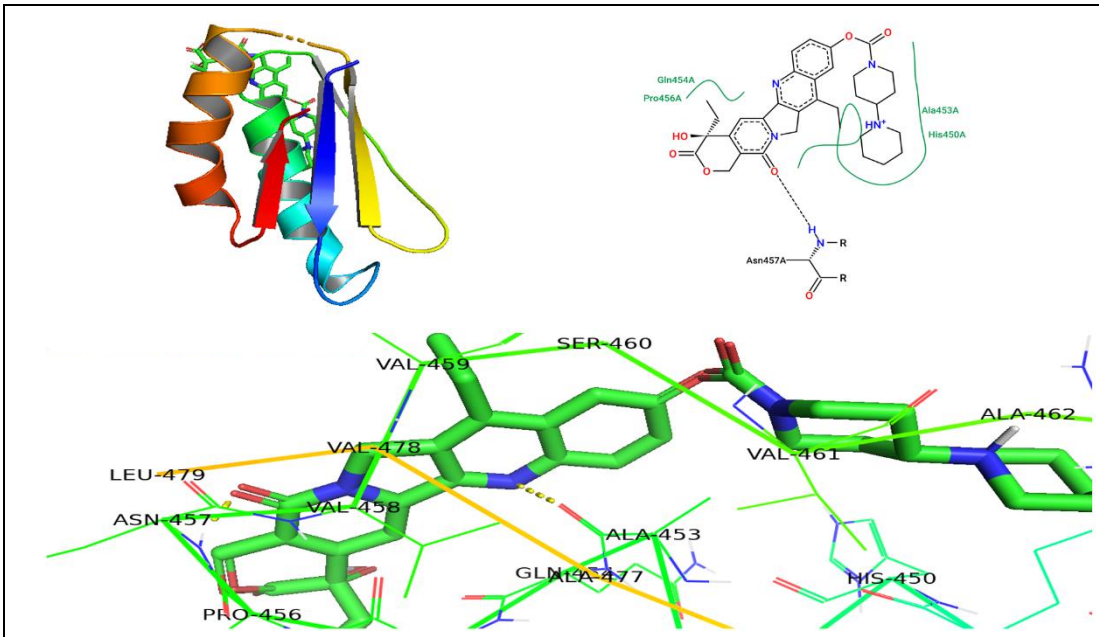

4.3.11 *MmpL* 11D2-ZINC000001612996

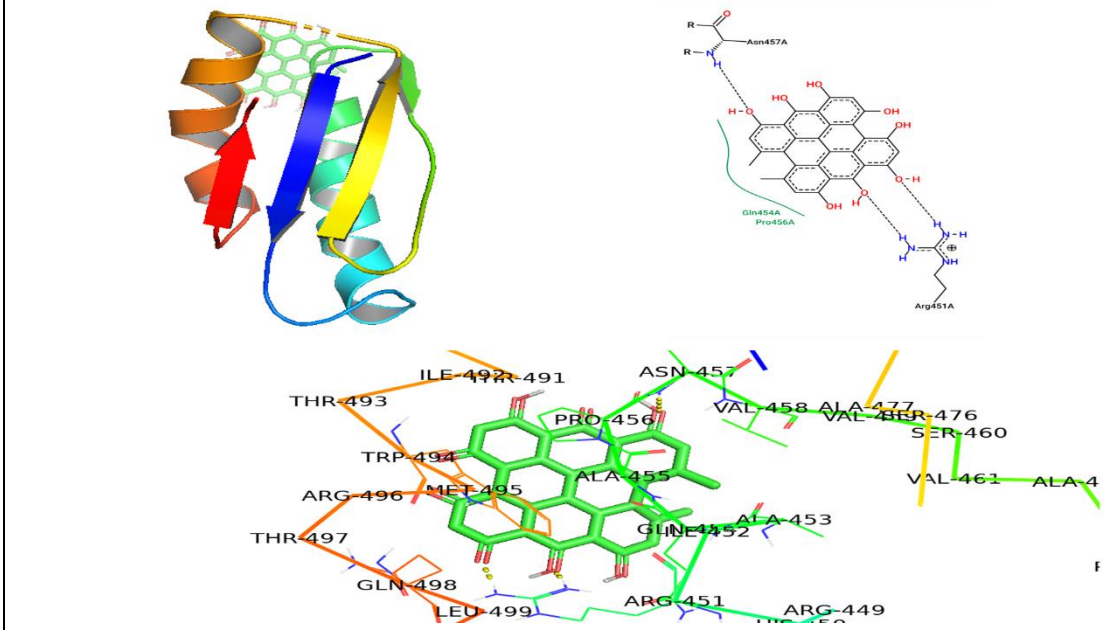

4.3.12 *MmpL* 11D2-ZINC000003780340

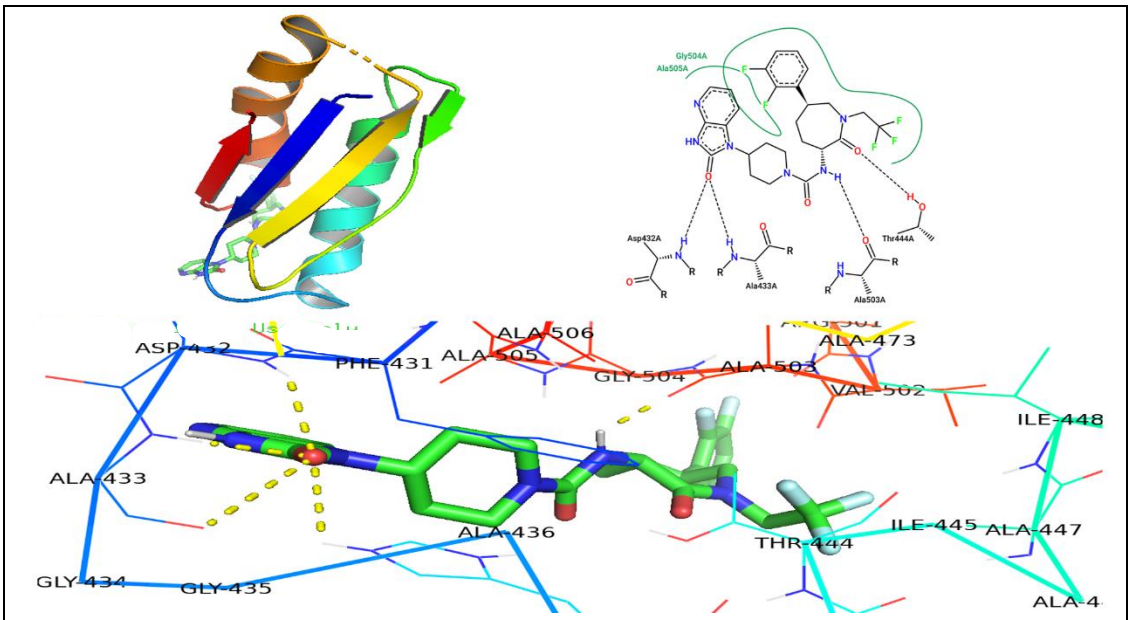

4.3.13 *MmpL* 11D2-ZINC000028827350

Figure 4.3. Top thirteen best hits against *MmpL* 11D2 of MTB's cell wall. *MmpL* 11D2-containing molecules are shown docked (left screen) and in touch with antagonistic residues (right screen). In 3D postures, docked molecules are shown next to interfacing receptor residues. Yellow dotted lines show hydrogen bond interactions.

4.1.4. *Mycobacterial* Arabinogalactan membrane protein *GlfT2* (4fIX)

GlfT2 (Rv3808c) is a galactofuranosyltransferases enzyme responsible for the polymerization of the galactan component of the Mycolylarabinogalactan complex, which is the primary constituent of the *Mycobacterial* cell wall. The majority of the galactan potion of the Mycolylarabinogalactan complex is synthesized by *GlfT2*.

X-ray crystallography was employed to elucidate the crystal structure of *GlfT2*, revealing a resolution of 2.45 Å, displaying an uncommon multidomain structure with a core GT-A domain flanked by two primarily "α-helical c-terminal" domains and an

"N-terminal β-barrel" domain. The protomers were kidney-shaped and came together to form a C4-symmetric homotetramer with an exposed hydrophobic and positively charged residue on the surface that is probably important in membrane interaction.[187]

Mycobacterial galactan synthesis, *GlfT1*, and *GlfT2* are two bifunctional GTs. They use a rising "polyprenol-bound oligosaccharide" as the acceptor and "UDP-d-galactofuranose" (*UDP-Galf*) as the donor.[187] *GlfT2*, a polymerizing glycosyltransferase, is responsible for producing the final 30 monosaccharides in the galactan component of the Mycolylarabinogalactan complex. *GlfT2* forms both β-(1→5) and β-(1→6) linkages between galactofuranosyl (*Galf*) residues, contributing to the elongation of the galactan chain. On the other hand, *GlfT1* only adds the first two *Galf* moieties to initiate the galactan synthesis process.[187]

More research has been done on *GlfT2* than on *GlfT1*. Saturation transfer difference-NMR studies and mass spectrometry findings are of special interest. It demonstrates that *GlfT2* only uses one active site to create the β-(1→5) and β-(1→6) linkages.[188] A group of 30,417 molecules was docked molecularly with the expected *GlfT2* enzyme. By using *in-silico* screening, a total of fifty-one compounds were discovered, and thirty (Figure 4.4) of the top hits were chosen for additional research.

From the pool of compounds, thirty of the highest-ranked compounds were selected based on their strong binding affinities as determined by the "XP G-score", a gauge of binding energy (Table 4.2). The range of the binding affinity is from -13.2 to -9.2 Kcal/ mol (Figure 4.5).

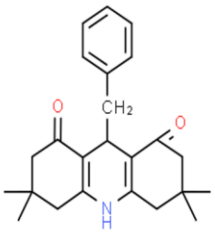

CSID541554

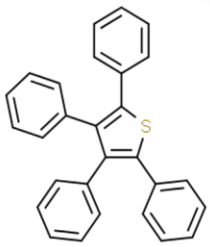

CSID67239

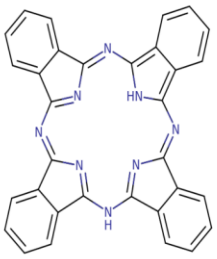

DB12983

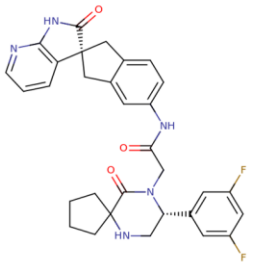

DB12424

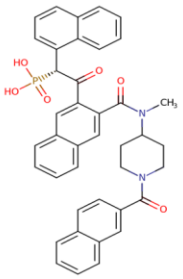

DB04016

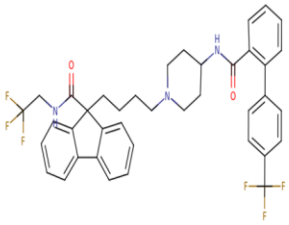

DB08827

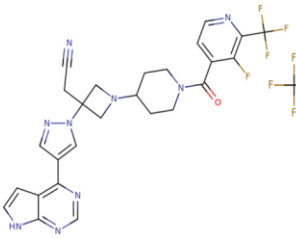

DB12154

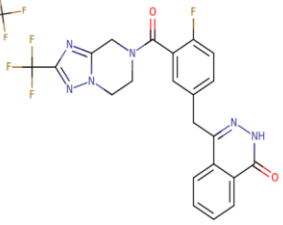

DB15637

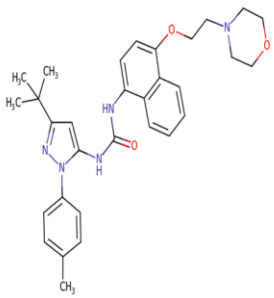

DB03044

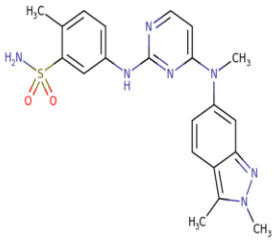

DB06589

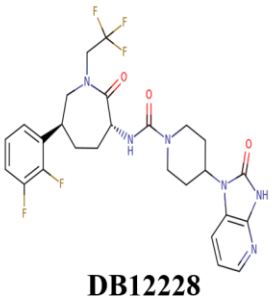

DB12228

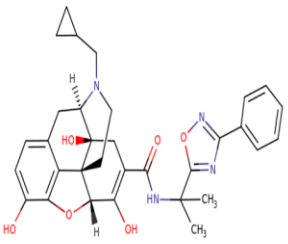

DB11691

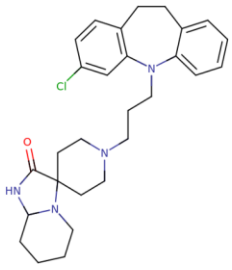

DB13676

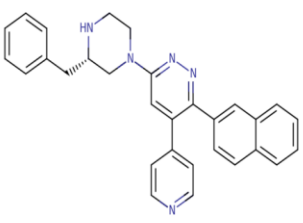

DB01988

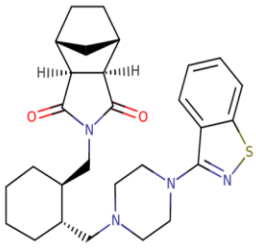

DB08815

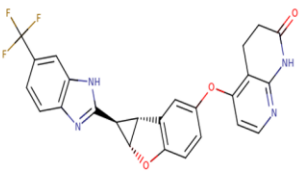

DB14773

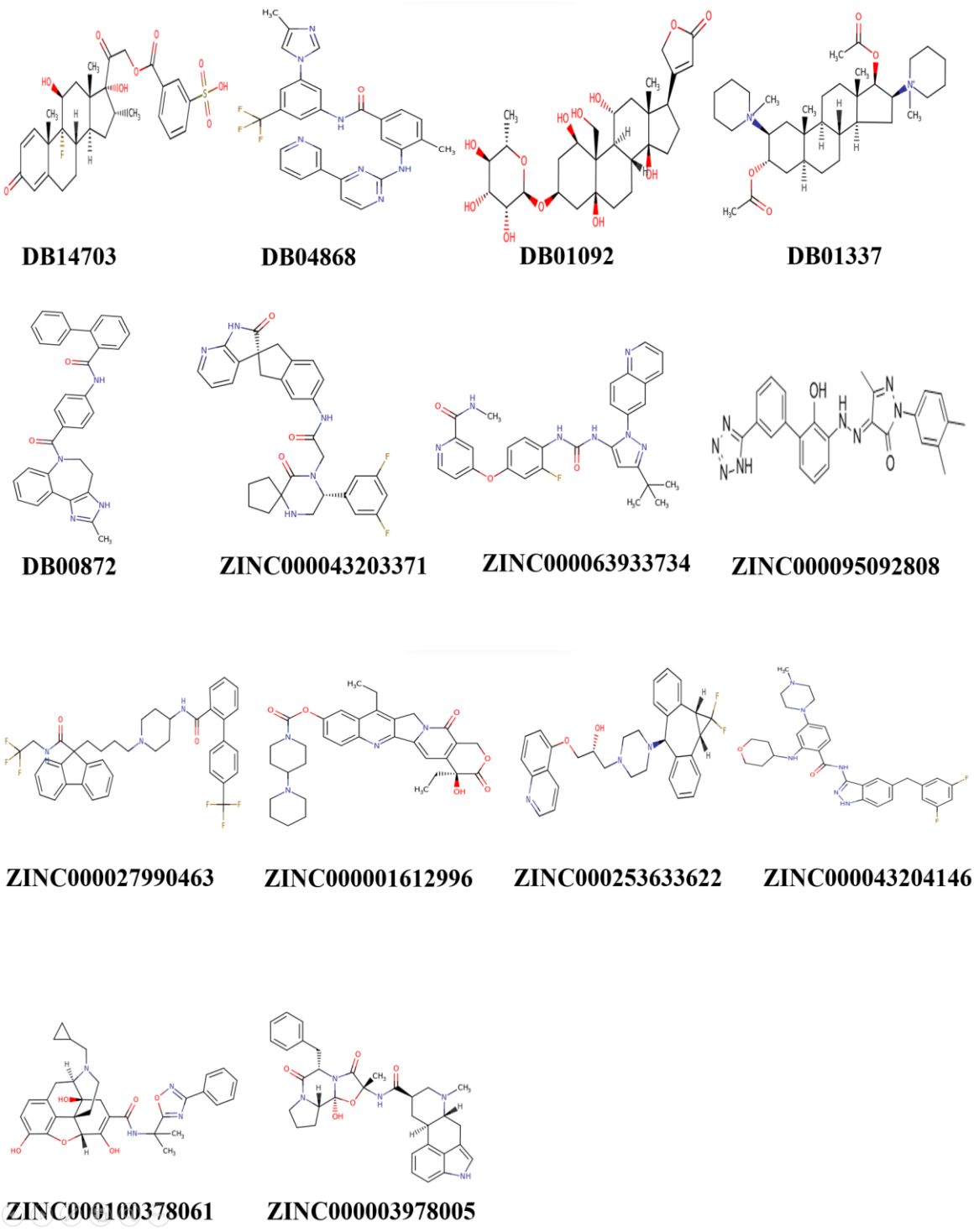

Figure 4.4. 2D structure of top thirty hits identified against MTB's protein *GlfT2*.

When it comes to binding energy, the top thirty compounds are: from ChemSpider, CSID541554 (-10.7 Kcal/mol) with *KI* 475.24 pM, CSID67239 (-9.2 Kcal/mol) with *KI* 138.09 µM.

From Drug Bank, DB12983 (-13.5 Kcal/mol) with *KI* 1.05 nM, DB12324 (-12.8 Kcal/mol) with *KI* 2.57 nM, DB04016 (-12.0 Kcal/mol) with *KI* 4.64 nM, DB08827 (-11.9 Kcal/mol) with *KI* 28.20 nM, DB12154 (-11.9 Kcal/mol) with *KI* 1.20 nM, DB15637 (-11.7 Kcal/mol) with *KI* 562.24 pM, DB03044 (-11.6 Kcal/mol) with *KI* 544.98 pM, DB06589 (-11.5 Kcal/mol) with *KI* 789.85 pM, DB12228 (-11.5 Kcal/mol) with *KI* 4.04 nM, DB11691 (-11.5 Kcal/mol) with *KI* 4.35 nM, DB13676 (-11.5 Kcal/mol) with *KI* 3.99 nM, DB01988 (-11.5 Kcal/mol) with *KI* 26.18 nM, DB08815 (-11.5 Kcal/mol) with *KI* 33.98 nM, DB14773 (-11.4 Kcal/mol) with *KI* 518.63 pM, DB14703 (-11.4 Kcal/mol) with *KI* 4.37 nM, DB04868 (-11.4 Kcal/mol) with *KI* 10.04 nM, DB1092 (-11.4 Kcal/mol) with *KI* 3.71 pM, DB01337 (-11.4 Kcal/mol) with *KI* 10.57 nM, DB00872 (-11.4 Kcal/mol) with *KI* 5.96 nM.

From the ZINC database, ZINC000043203371 (-12.2 Kcal/mol) with *KI* 1.70 nM, ZINC000063933734 (-12.2 Kcal/mol) with *KI* 296.76 pM, ZINC000095092808 (-12.2 Kcal/mol) with *KI* 4.02 nM, ZINC000027990463 (-12.0 Kcal/mol) with *KI* 6.11 nM, ZINC000001612996 (-11.9 Kcal/mol) with *KI* 24.55 pM, ZINC000253633622 (-11.9 Kcal/mol) with *KI* 16.26 nM, ZINC000043204146 (-11.7 Kcal/mol) with *KI* 12.17 nM, ZINC000100378061 (-11.6 Kcal/mol) with *KI* 368.53 pM, ZINC000003978005 (-11.6 Kcal/mol) with *KI* 4.26 nM.

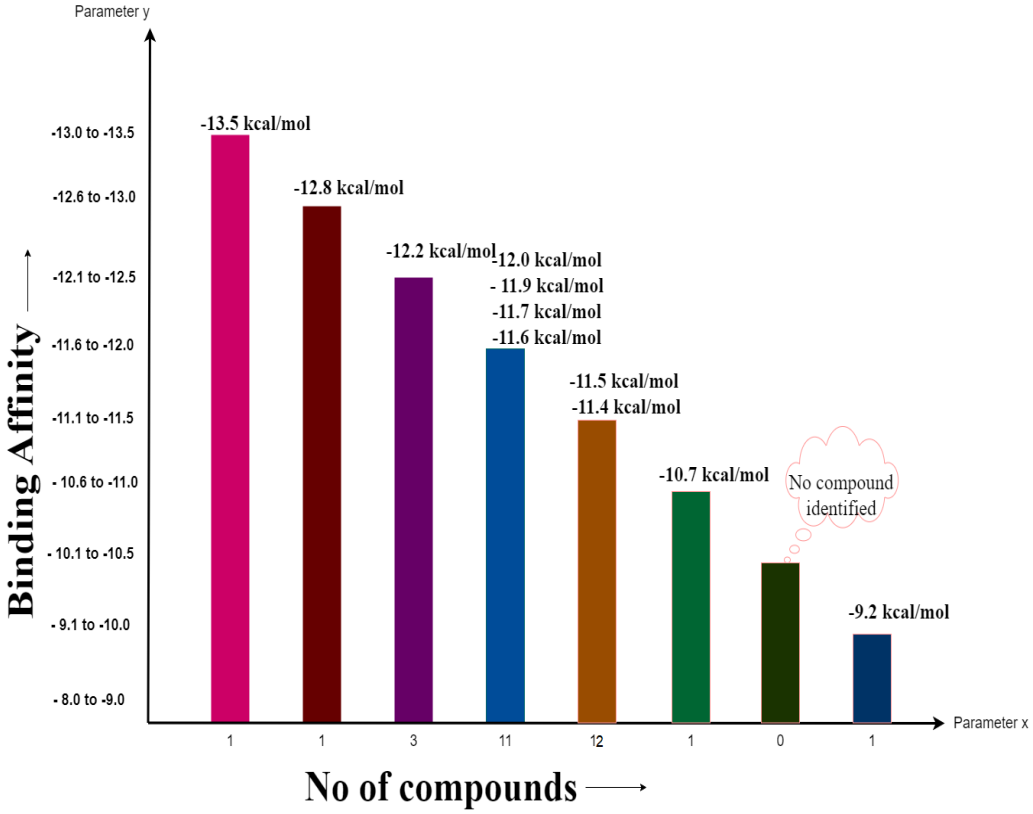

Figure 4.5. The free binding affinity of selected compounds against *GlfT2*.

4.1.5. Identified compounds-*GlfT2* interactions

Thirty compounds from three different libraries using the simulated screening procedure were selected. Tests utilizing the *GlfT2* protein looked at these compounds. These compounds all best fit the goal constructions' cavity. These compounds' position and interactions with the *GlfT2* protein are shown in the figures below (Figure 4.6). The compound with CSID541554 (Fig 4.6.1) shows nine hydrophobic interactions and one interaction via hydrogen bond. The hydrophobic interaction includes Trp 309, Tyr 344, Trp 347, Lys 369, Trp 370, Asp 372, Ala 373, Trp399 (two contacts), and Trp 370 hydrogen bond interaction. The second compound with CSID67239 (Fig 4.6.2) shows a total of thirteen hydrophobic with zero hydrogen bond

interactions. These hydrophobic interactions are Tyr 236, Trp 309 (three contacts), Tyr 344, Trp 348 (two contacts), Ile 368, Lys 369, Trp 370 (two contacts), Ala 373, and Trp 399. The third compound is from Drug Bank with DBID, DB12983 (Fig 4.6.3) which shows seven hydrophobic interactions including two interactions with a hydrogen bond. The hydrophobic interactions are Tyr 317 (two contacts), Asp 318, Trp 399 (two contacts), Asp 403, and Ala 405. The hydrogen bond interactions are Trp 399 and Asp 401. The fourth compound, DB12424 (Fig 4.6.4) shows a total of ten interactions with five hydrophobic and hydrogen bonds respectively. The hydrophobic interactions are Trp 399, Asp 403, Asp 404, Ala 405, and Ile 406 while hydrogen bond interactions are Lys 369, Ala 405, Gln 409 (two contacts), and Glu 451. The next compound is DB04016 (Fig 4.6.5) which shows six hydrogen bond interactions including Ala 405, Glu 451, Thr 550, Ala 553, Arg 577 (two contacts), and five hydrophobic interactions including Ile 406, Lys 445 (two contacts), Thr 550, and Arg 554. The sixth compound is DB08827 (Fig 4.6.6) shows five hydrophobic interactions with Try 236, Trp 347, Trp 348, Ile 368, and Met 397 and four interactions via hydrogen bonding including Asp 256, Lys 369, Trp 370, and His 396. The seventh compound DB12154 (Fig 4.6.7) shows hydrophobic interaction which includes Trp 309, Trp 399, Asp 403, Ala 405, and Try 344, Asp 401 by hydrogen bonding. The eighth compound is DB15637 (Fig 4.6.8) showing two hydrophobic interactions with Trp 348, and Lys 369 and six hydrogen bond interactions with His 296, Tyr 344, Trp 347, Trp 348, and Asp 372. The ninth compound is DB03044 (Fig 4.6.9) showing hydrophobic interactions with Asp 318, Trp 399, Asp 401, and Asp 403 while Asp 401, and Asp 403 (two contacts) via hydrogen bond interaction.

Table 4.2. Drug-likeness characteristic of top thirty hits against target *GlfT2*.

S.NO	Compound ID	Binding Affinity	Inhibition constant (KI)	Molecular Weight	LOGP	H-Bond Acceptors	H-Bond Donors	Drug-likeness Score
1	CSID541554	-10.7	475.24 pM	363.49	3.79	3	1	-0.21
2	CSID67239	-9.2	138.09 uM	388.52	8.66	1	0	-1.69
3	DB12983	-13.5	1.05 nM	514.55	4.79	6	2	-1.06
4	DB12424	-12.8	2.57 nM	557.6	2.85	5	3	1.11
5	DB04016	-12	4.64 nM	670.68	4.49	6	2	1.09
6	DB08827	-11.9	28.20 nM	693.72	7.19	3	2	0.76
7	DB12154	-11.9	1.20 nM	553.52	2.35	7	1	0.08
8	DB15637	-11.7	562.24 pM	472.4	2.79	5	1	1.32
9	DB03044	-11.6	544.98 pM	527.65	5.32	5	2	0.86
10	DB06589	-11.5	789.85 pM	437.51	3.59	7	2	-0.69
11	DB12228	-11.5	4.04 nM	566.52	2.44	4	2	1.15
12	DB11691	-11.5	4.35 nM	570.64	3.14	8	4	1.34
13	DB13676	-11.5	3.99 nM	479.07	4.68	4	1	1.64
14	DB01988	-11.5	26.18 nM	457.56	4.75	5	1	0.61
15	DB08815	-11.5	33.98 nM	492.67	5.25	5	0	0.82
16	DB14773	-11.4	518.63 pM	478.43	4.24	4	2	0.4
17	DB14703	-11.4	4.37 nM	576.63	1.87	8	3	0.66
18	DB04868	-11.4	10.04 nM	529.51	4.51	6	2	0.19
19	DB01092	-11.4	3.71 pM	584.65	-2.8	11	8	1.15
20	DB01337	-11.4	10.57 nM	572.86	1.04	2	0	0.76
21	DB00872	-11.4	5.96 nM	498.57	5.23	3	2	0.66
22	ZINC000043203371	-12.2	1.70 nM	557.6	3.77	5	3	1.11
23	ZINC000063933734	-12.2	296.76 pM	553.59	6.04	7	3	-0.43
24	ZINC000095092808	-12.2	4.02 nM	466.5	4.04	8	0	-0.74
25	ZINC000027990463	-12	6.11 nM	693.73	8.38	2	3	0.76
26	ZINC000001612996	-11.9	24.55 pM	586.68	4.09	8	2	1.54
27	ZINC000253633622	-11.9	16.26 nM	527.61	5.21	5	1	0.8
28	ZINC000043204146	-11.7	12.17 nM	560.64	5.02	5	4	1.19
29	ZINC000100378061	-11.6	368.53 pM	570.64	3.48	8	4	1.34
30	ZINC000003978005	-11.6	4.26 nM	583.68	2.08	5	4	0.97

The next compound is DB06589 (Fig 4.6.10) which shows a total of ten interactions. The hydrophobic interactions include Phe 169, Tyr 236, and Trp 348 (two contacts). The hydrogen bond interactions include Phe 169, Arg 171 (two contacts), Tyr 236, Asp 256, and Trp 370. The eleventh compound is DB12228 (Fig 4.6.11) which shows six hydrophobic interactions including Pro 167, Phe 169, Tyr 236, Trp 348, and Lys 369 while His 296, Glu 300, Tyr 344, and Lys 369 are interacting via hydrogen bonds. The next compound is DB11691 (Fig 4.6.12) showing a total of ten interactions with six hydrophobic and four interactions by a hydrogen bond. Hydrophobic interactions are Trp 309, Met 397, Trp 399 (three contacts), and Ala 405 while His 296, Lys 369, Ala 405, and His 413 are interacting via hydrogen bonds.

The thirteen compounds are DB13676 (Fig 4.6.13) shows six hydrophobic interactions including Trp 348, Trp 399 (three contacts), Asp 403, and Ala 405, and two hydrogen bond interactions including Lys 369, and His 413. The next compound with DBID is DB01988 (Fig 4.6.14) which shows four hydrophobic interactions and three interactions by a hydrogen bond. The hydrophobic interactions are Trp 399 (two contacts), Asp 403, and Arg 554 while Asp 401, Ala 405, and Ala 553 are showing hydrogen bond interactions. The fifteen compounds DB08815 (Fig 4.6.15), show three hydrophobic interactions with Trp 309, Tyr 344, and Ala 405 while Lys 369, and His 413 by a hydrogen bond. The sixteenth compound is DB14773 (Fig 4.6.16) which shows a total of fifteen interactions including both hydrophobic and hydrogen bonds. The hydrophobic interactions include Tyr 344 (two contacts), Trp 370, Ala 373, Asp 403 (two contacts), and Ala 405 while hydrogen bond interaction includes Trp 309 (two contacts), Lys 369, Trp 370, Trp 399 (two contacts), Asp 404, Ala 405. The

seventeenth compound with DBID is DB14703 (Fig 4.6.17) which shows five hydrophobic interactions including Tyr 236, Trp 347, Trp 348 (two contacts), and Trp 399 while five hydrogen bond interactions including Tyr 344 (two contacts), Lys 369, Trp 370, and Asp 372.

The next compound from Drug Bank is DB04868 (Fig 4.6.18) shows three hydrophobic kinds of interactions with Phe 169, Trp 399, and Asp 403 while four hydrogen bond interactions with Arg 171 (two contacts), Asp 258, and Lys 369. The nineteenth compound DB01092 (Fig 4.6.19) shows a total of thirteen interactions out of which three are hydrophobic and ten are hydrogen bond interactions. The hydrophobic interactions are Tyr 236, Ile 368, and Trp 399 while hydrogen bond interactions are Phe 169, Tyr 236, Tyr 344 (two contacts), Lys 369, Trp 370, and Asp 371 (four contacts). The next and twentieth compound is DB01337 (Fig 4.6.20) shows seven hydrophobic interactions with Trp 309 (three contacts), Ala 311, Tyr 317, Trp 399, and Ala 405 while two hydrogen bond interactions are Trp 309 and Tyr 317. The last compound from Drug Bank DB00872 (Fig 4.6.21) shows a total of twelve interactions out of which nine are hydrophobic and the rest are hydrogen bond interactions. The hydrophobic interactions are Pro 167, Phe 169, Trp 309 (two contacts), Trp 348, Phe 367, Ile 368, Lys 369, and Trp 399. Gly 232, Lys 369, and Trp 370 are hydrogen bond interactions.

The twenty-second compound is from the ZINC database ZINC000043203371 (Fig 4.6.22) and shows four hydrophobic interactions and three hydrogen bond interactions. The hydrophobic interactions are Trp 399 (three contacts), and Asp 403 while hydrogen bond interactions are Trp 309, Ala 311, and Asp 403. The next

compound is ZINC000063933734 (Fig 4.6.23) shows a total of ten interactions out of which seven hydrophobic interactions are Phe 169 (three contacts), Ile 368, Trp 408 (two contacts), and Leu 480 while hydrogen bond interactions are Gln 200, Asn 229, and Trp 370. The twenty-fourth compound ZINC000095092808 (Fig 4.6.24) shows three hydrophobic interactions including Trp 309, Lys 369, and Trp 399 while Gly 232, Ser 233, Lys 369 (two contacts), Asp 371, and His 413 interact via hydrogen bond. The twenty-fifth compound ZINC000027990463 (Fig 4.6.25) shows a total of twelve interactions. The hydrophobic interactions are Trp 309 (two contacts), Tyr 317, Tyr 344, Trp 399 (three contacts), and Asp 403. The hydrogen bond interactions are Trp 309, Lys 369, and His 413. The twenty-sixth compound with ZINC ID ZINC000001612996 (Fig 4.6.26) shows hydrophobic interactions with Phe 169, Trp 309, Tyr 344, Trp 348, and Trp 399 while Gln 299 and His 396 interactions via hydrogen bond.

The next compound is ZINC000253633622 (Fig 4.6.27) shows a total of thirteen interactions. The first eight are hydrophobic interactions with Trp 399, Asp 403, Asp 404, Ala 405, Ile 406 (two contacts), Thr 550, and Val 566 while the next five are hydrogen bond interactions which include Asp 401, Asp 403 (three contacts), Ala 405. The twenty-eight compound ZINC000043204146 (Fig 4.6.28) shows hydrophobic interactions with Trp 309, Lys 369, and Trp 399 (two contacts). The hydrogen bond interactions are Lys 369, Trp 370, and His 413. The next and twenty-ninth compound ZINC000100378061 (Fig 4.6.29) shows six hydrophobic interactions with Tyr 236, Trp 347 (two contacts), Ile 368, Met 397, and Trp 399 while the hydrogen bond interactions are Arg 171 (two contacts), Tyr 236, and Asp 403. The last and thirtieth

compound ZINC000003978005 (Fig 4.6.30) shows a total of eleven interactions out of which six are hydrophobic and the rest are hydrogen bond interactions. The hydrophobic interactions are Trp 399, Asp 403, Asp 404, Ile 406, Thr 550, and Ala 569, and the hydrogen bond interactions are Asp 401, Asp 403 (two contacts), Asp 403, Ala 405, and Ala 553.

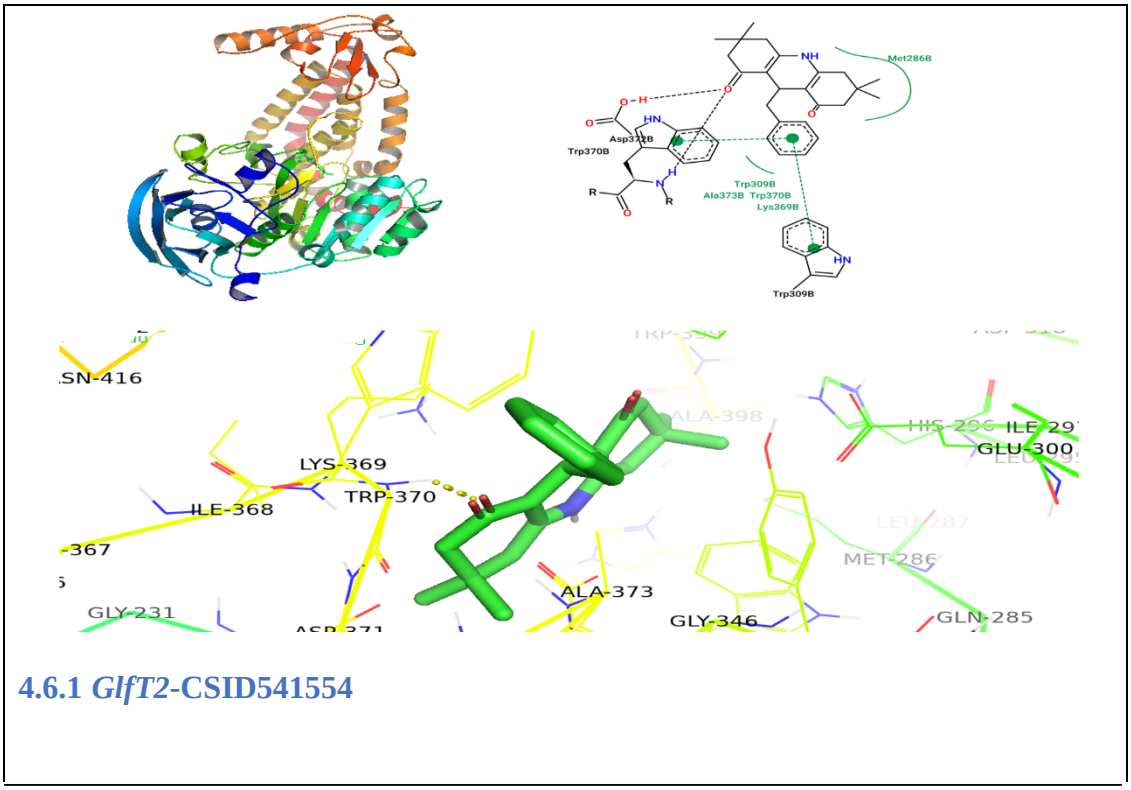

4.6.1 *GlfT2*-CSID541554

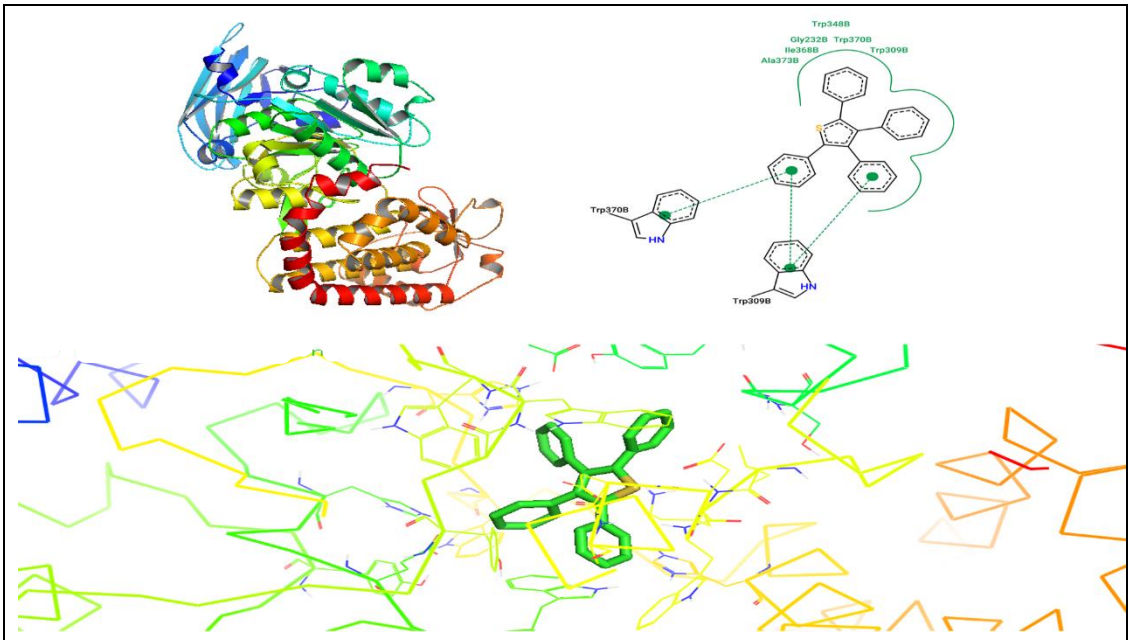

4.6.2 GlfT2-CSID67239

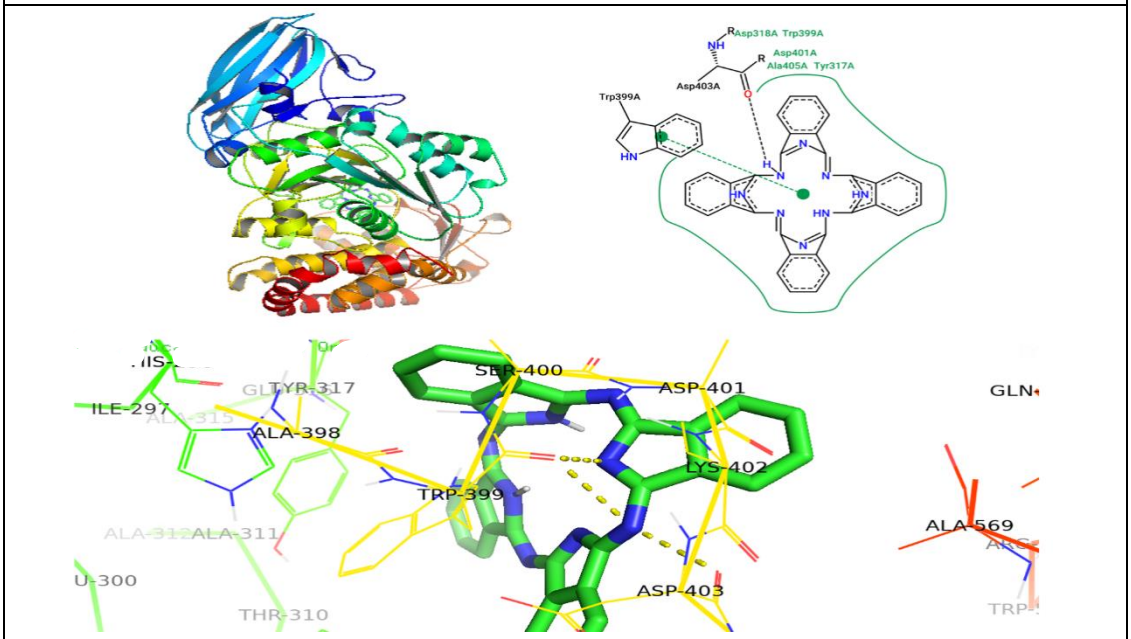

4.6.3 *GlfT2*-DB12983

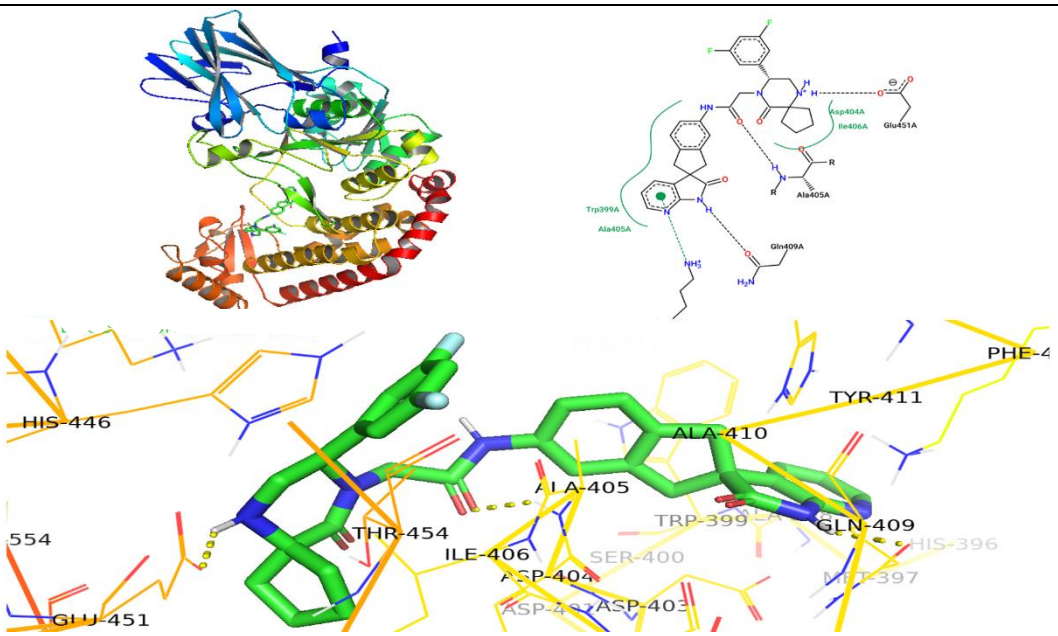

4.6.4 *GlfT2*-DB12424

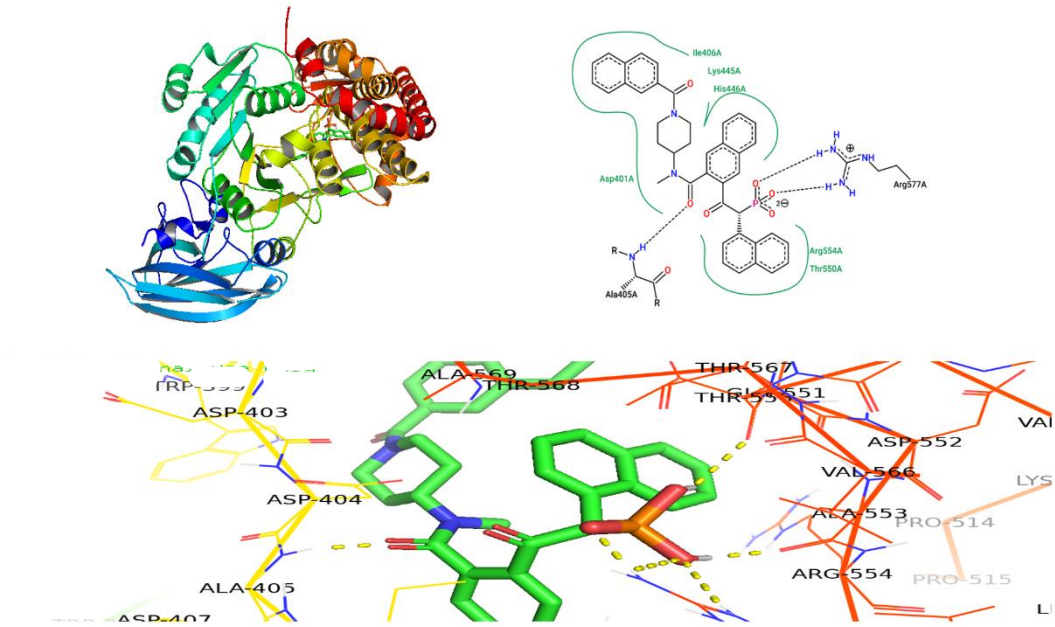

4.6.5 *GlfT2*-DB04016

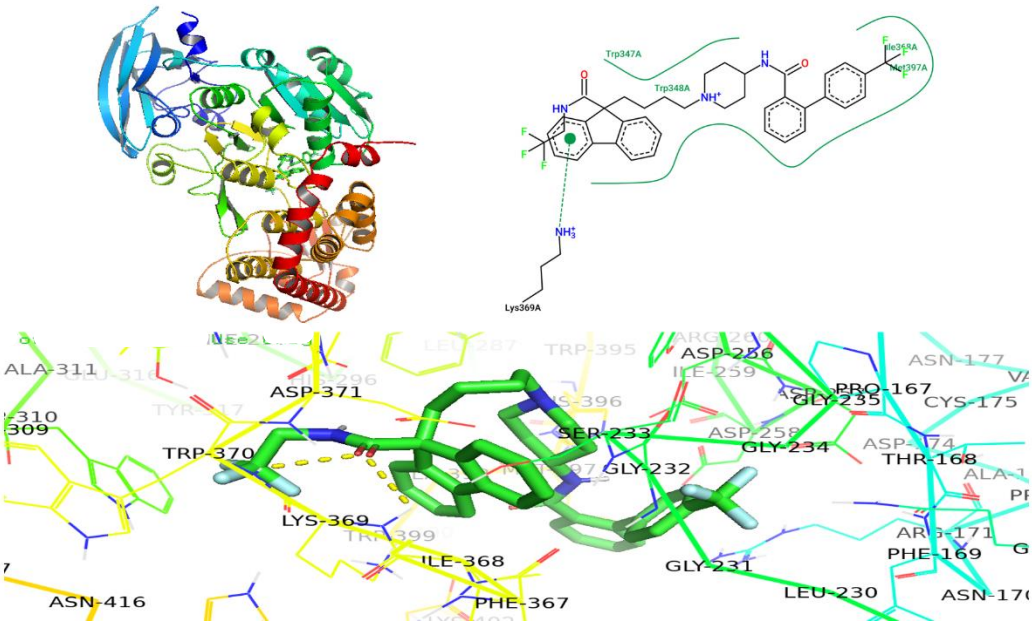

4.6.6 *GlfT2*-DB08827

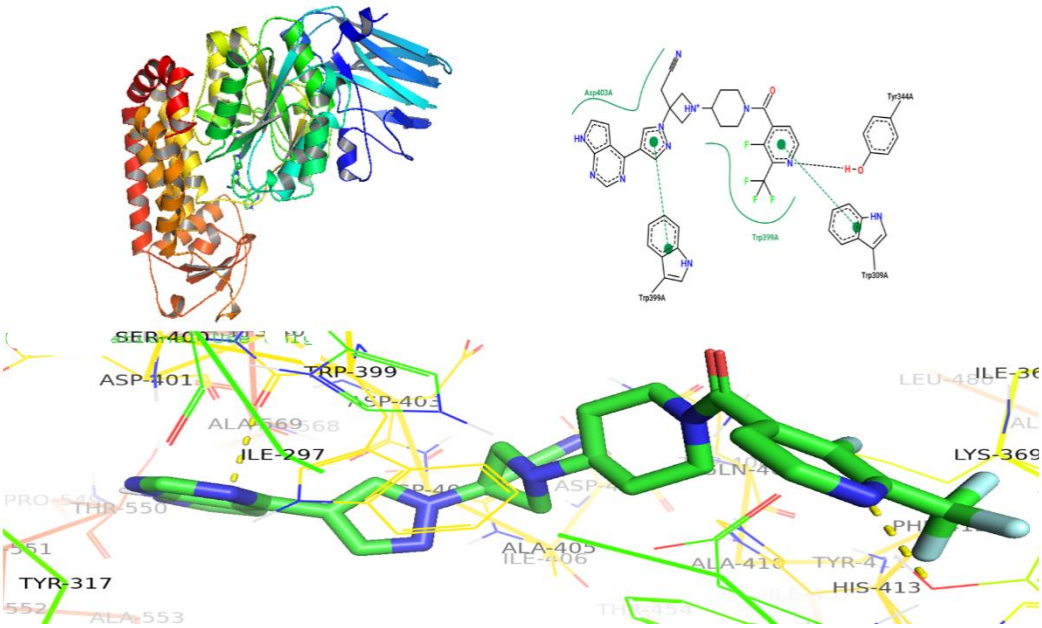

4.6.7 *GlfT2*-DB12154

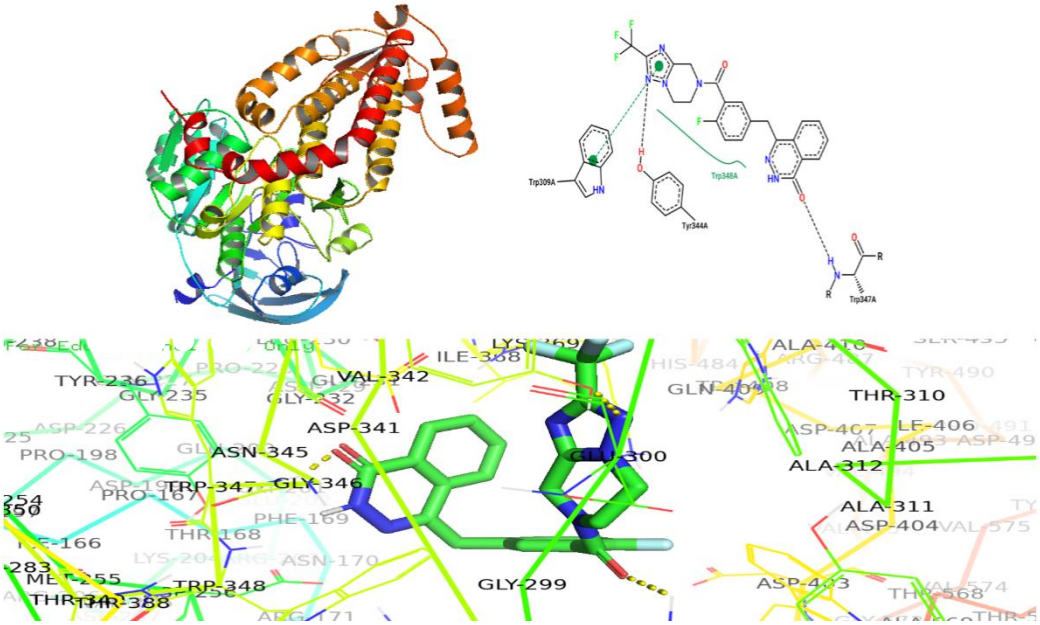

4.6.8 *GlfT2*-DB15637

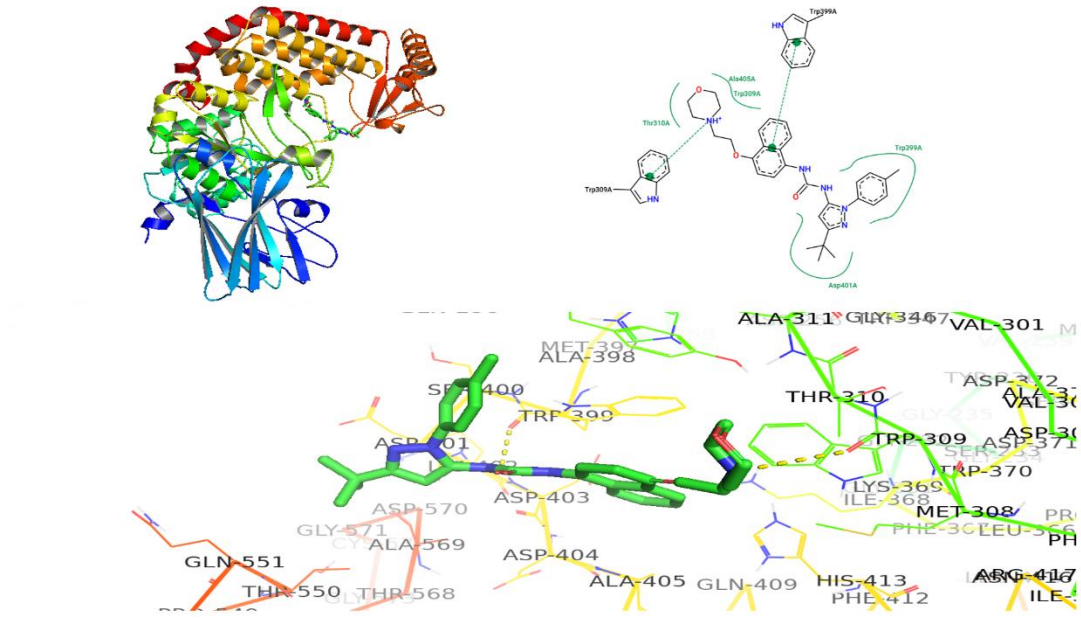

4.6.9 GlfT2-DB03044

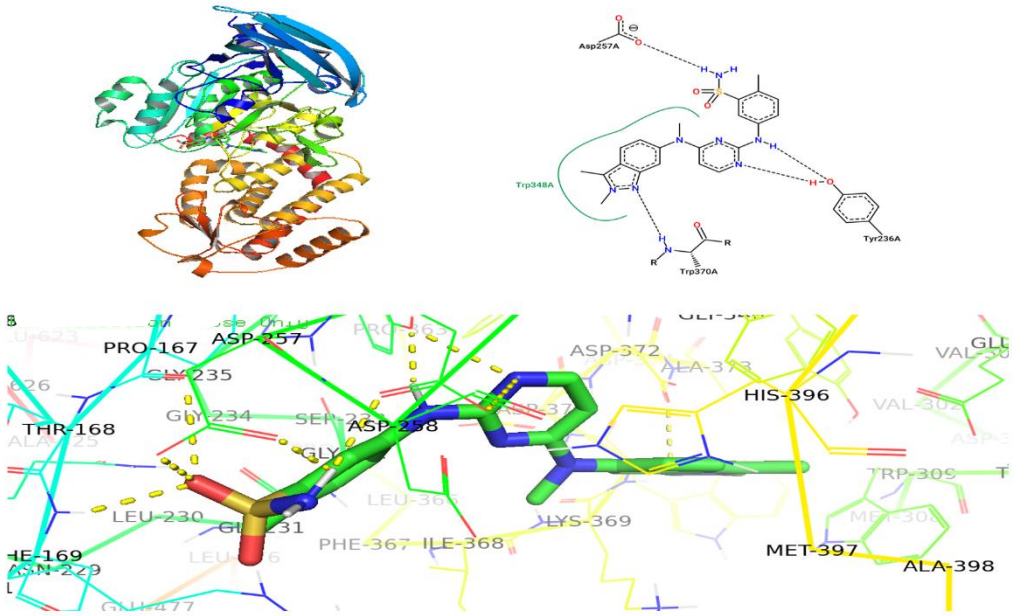

4.6.10 *GlfT2*-DB06589

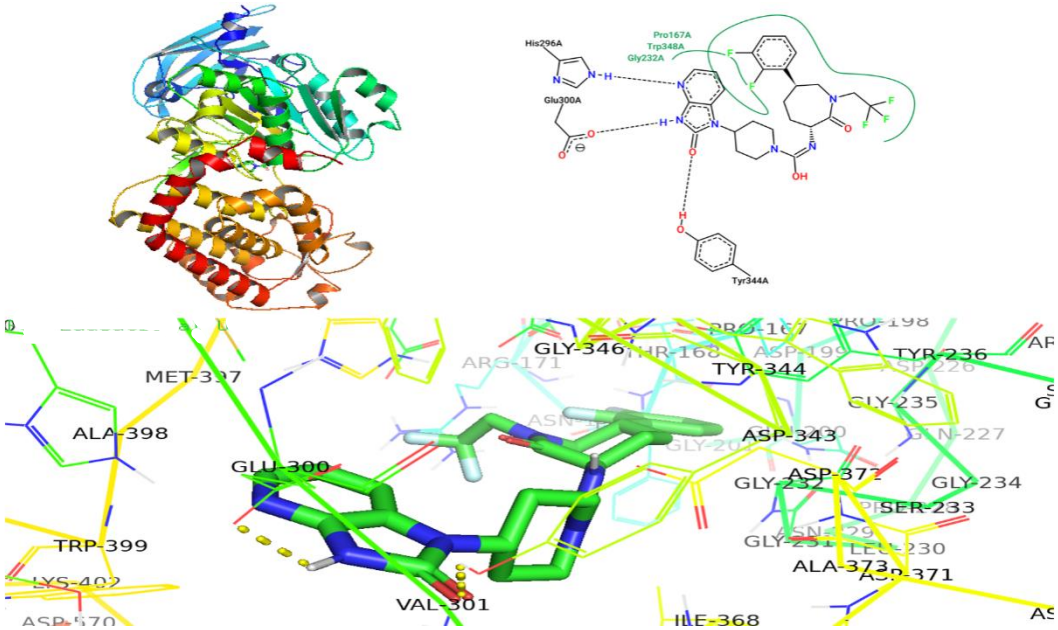

4.6.11 *GlfT2*-DB12228

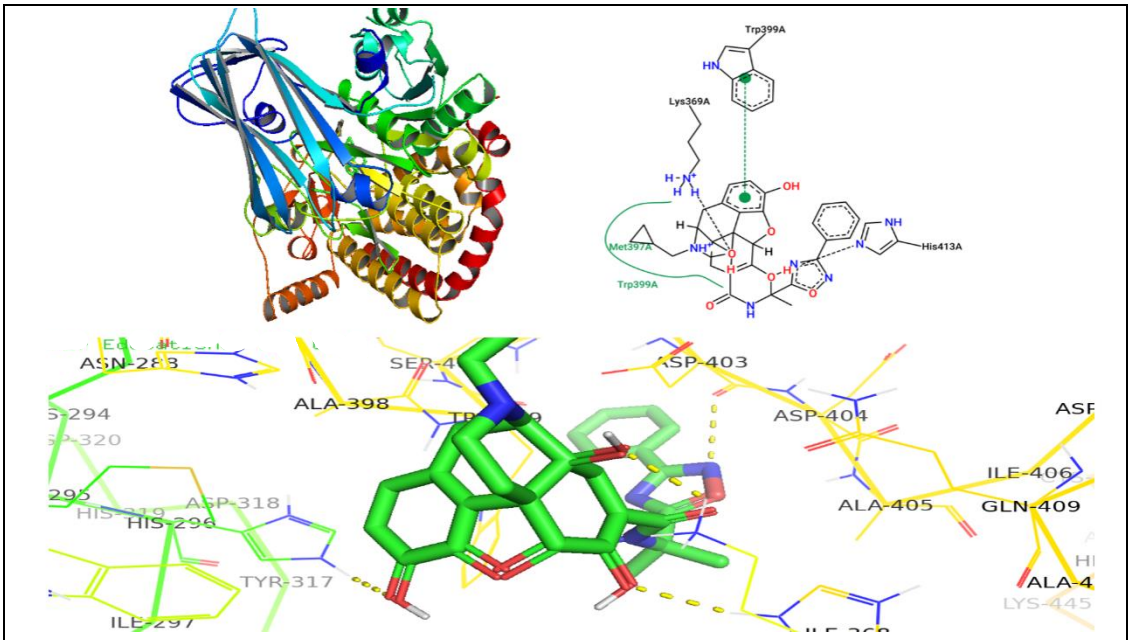

4.6.12 *GlfT2*-DB11691

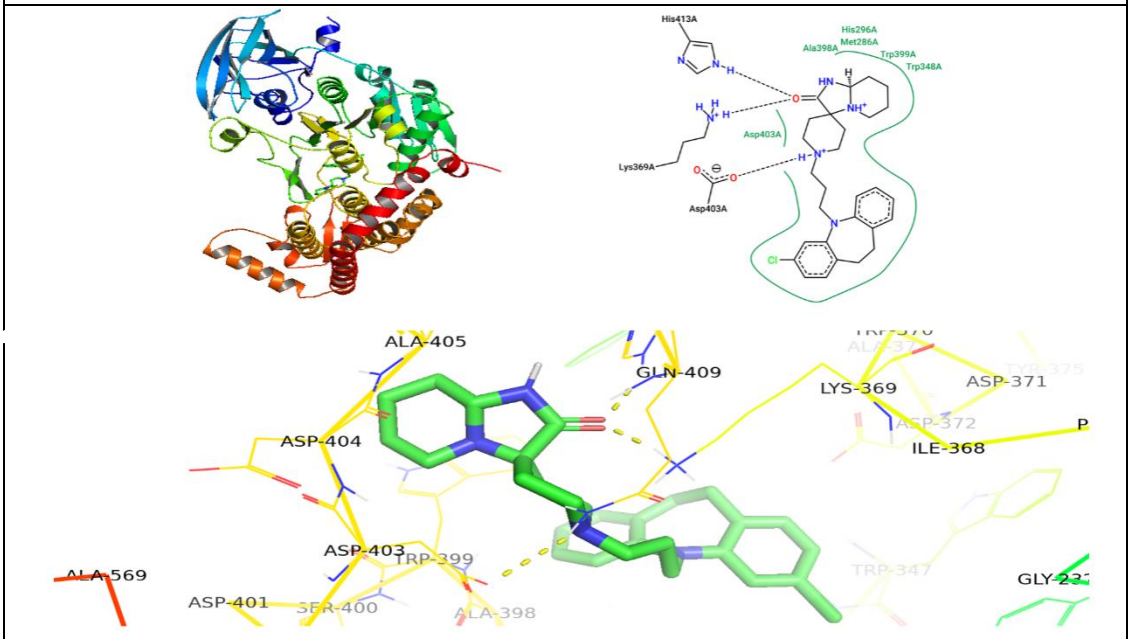

4.6.13 *GlfT2*-DB13676

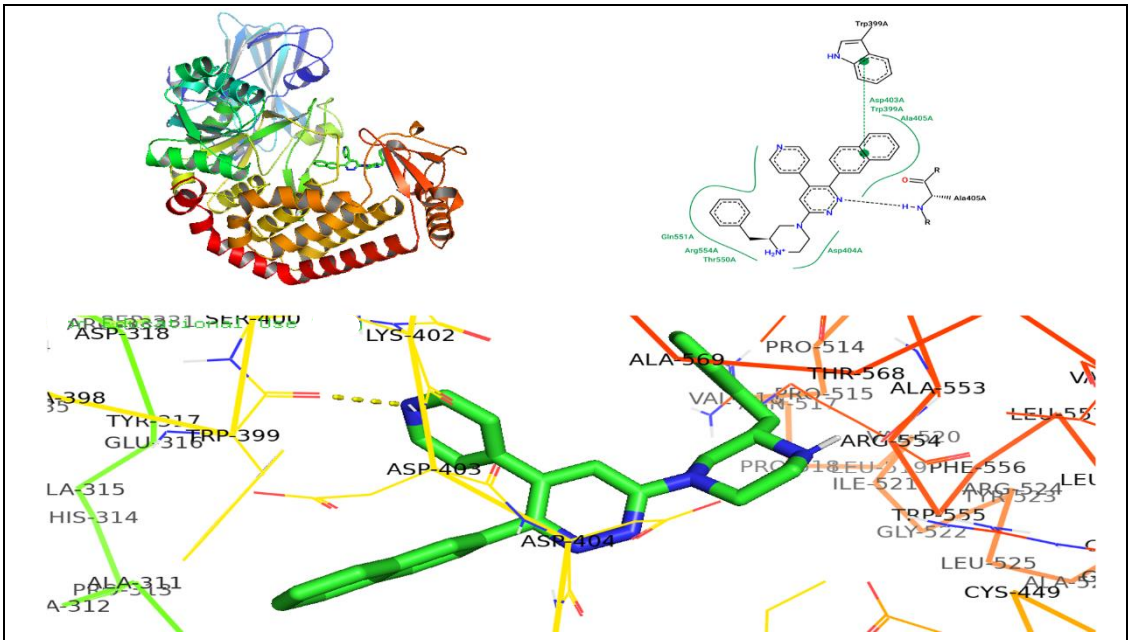

4.6.14 *GlfT2*-DB01988

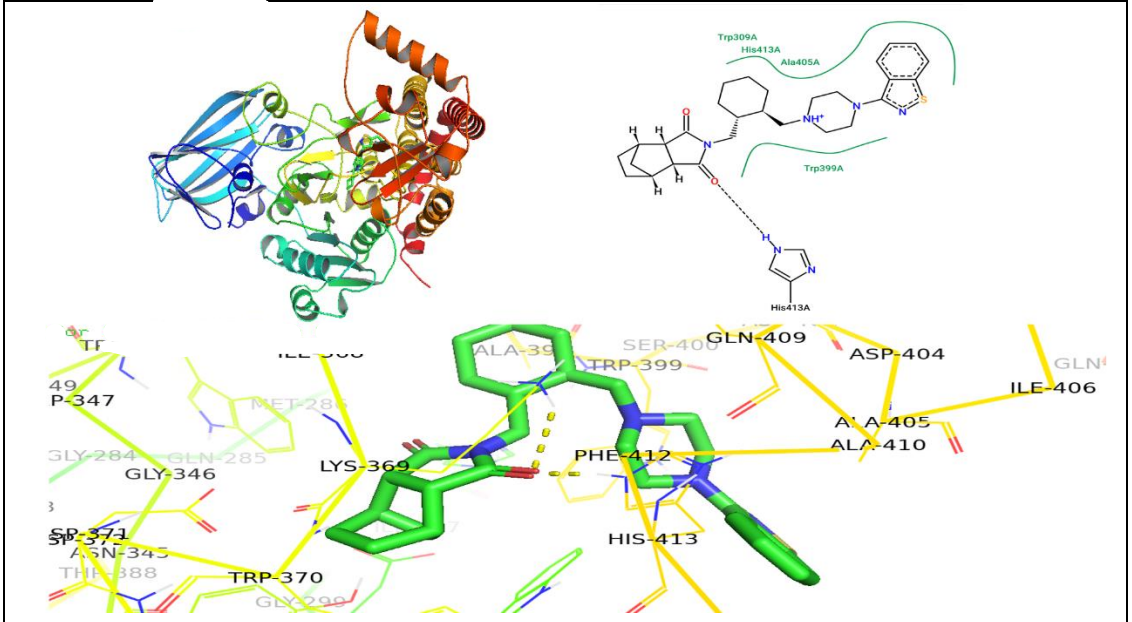

4.6.15 *GlfT2*-DB08815

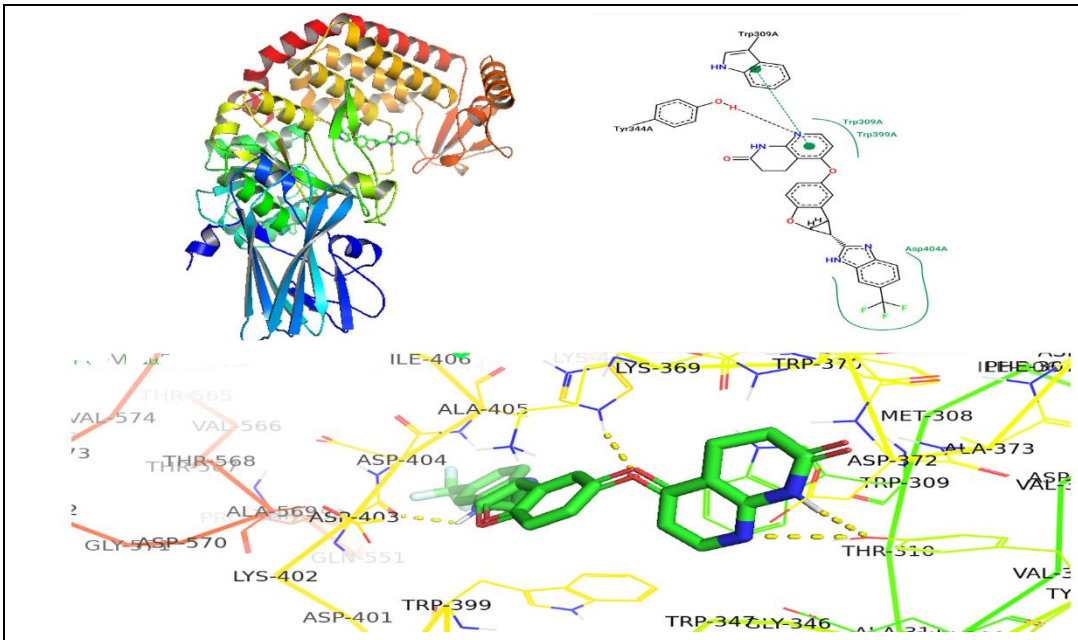

4.6.16 *GlfT2*-DB14773

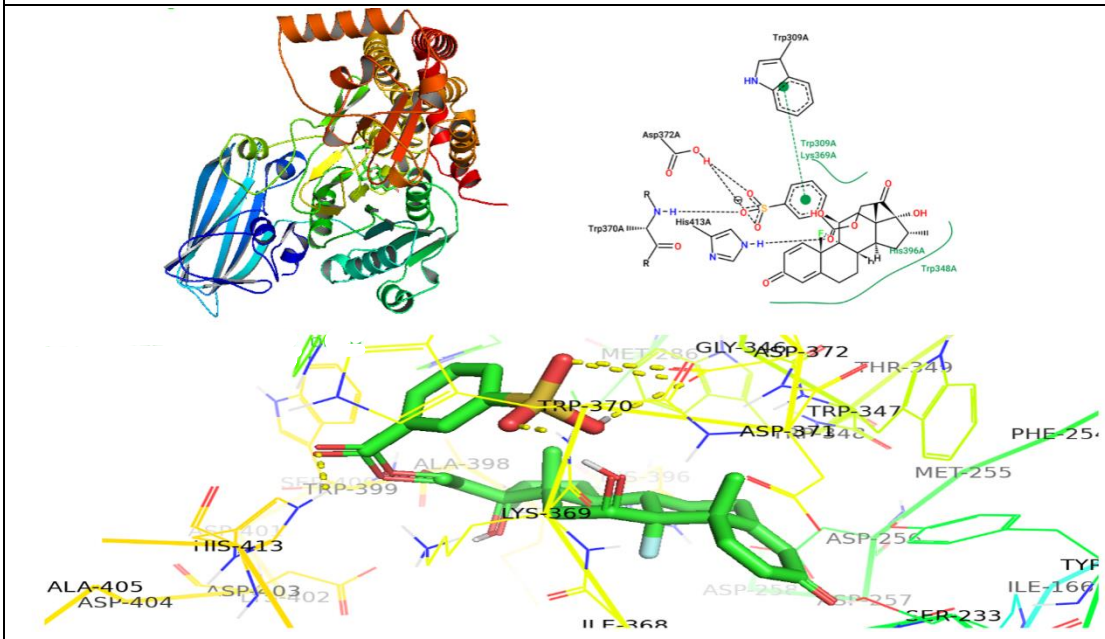

4.6.17 *GlfT2*-DB14703

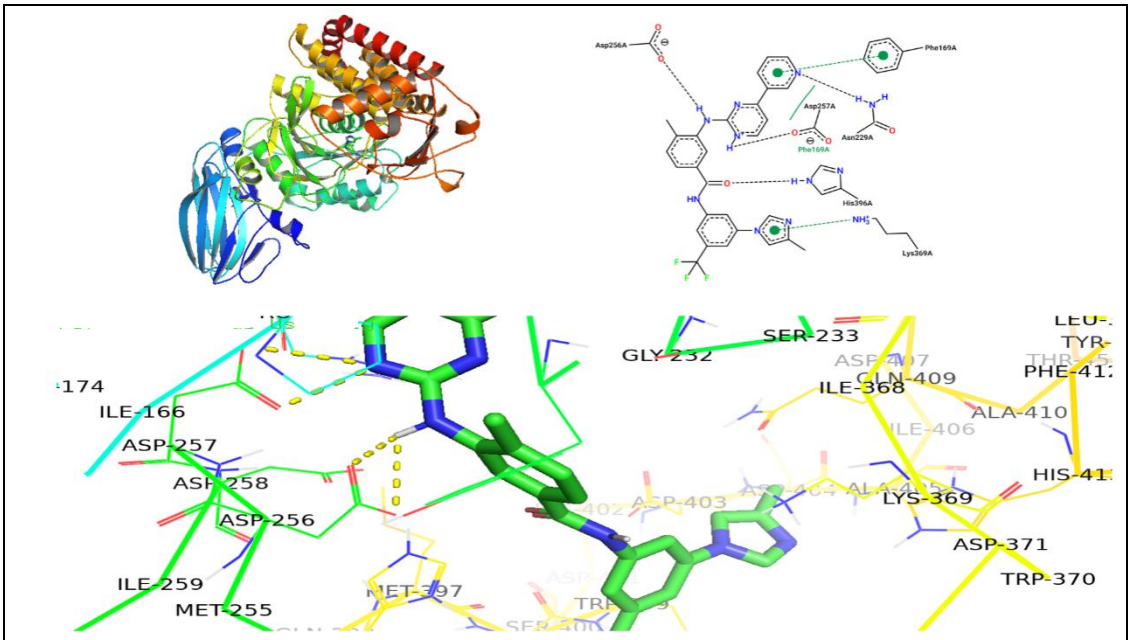

4.6.18 *GlfT2*-DB04868

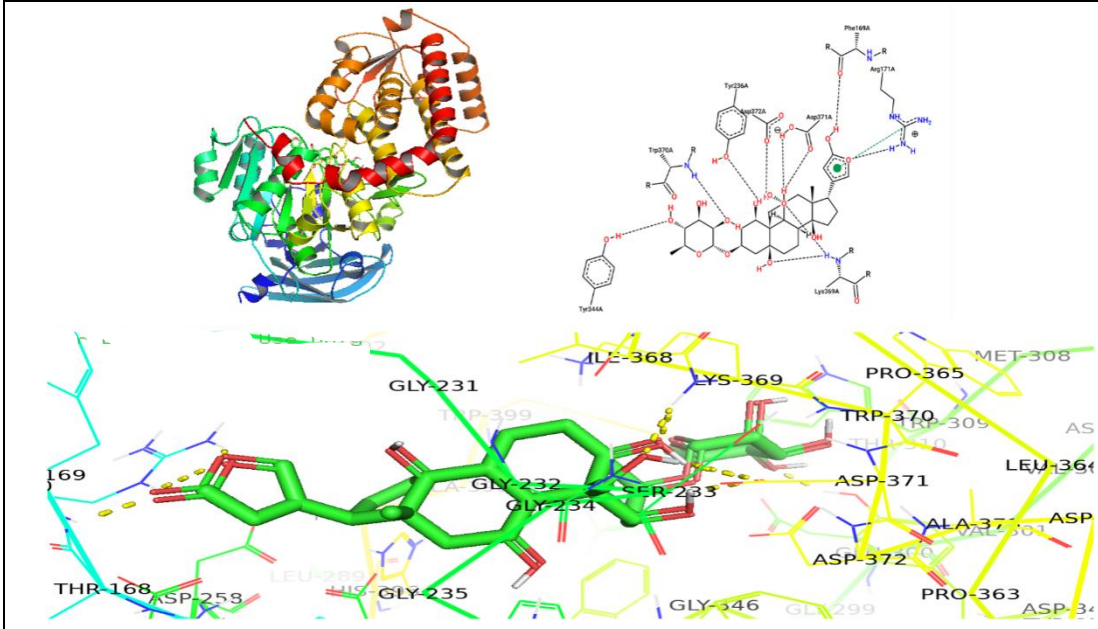

4.6.19 *GlfT2*-DB01092

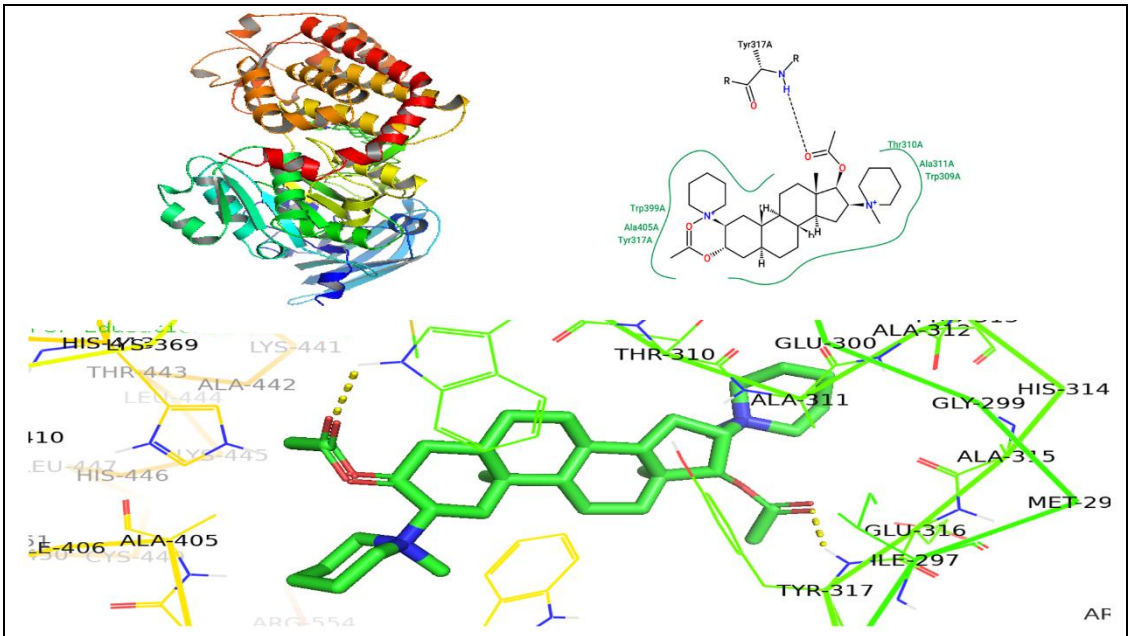

4.6.20 *GlfT2*-DB01337

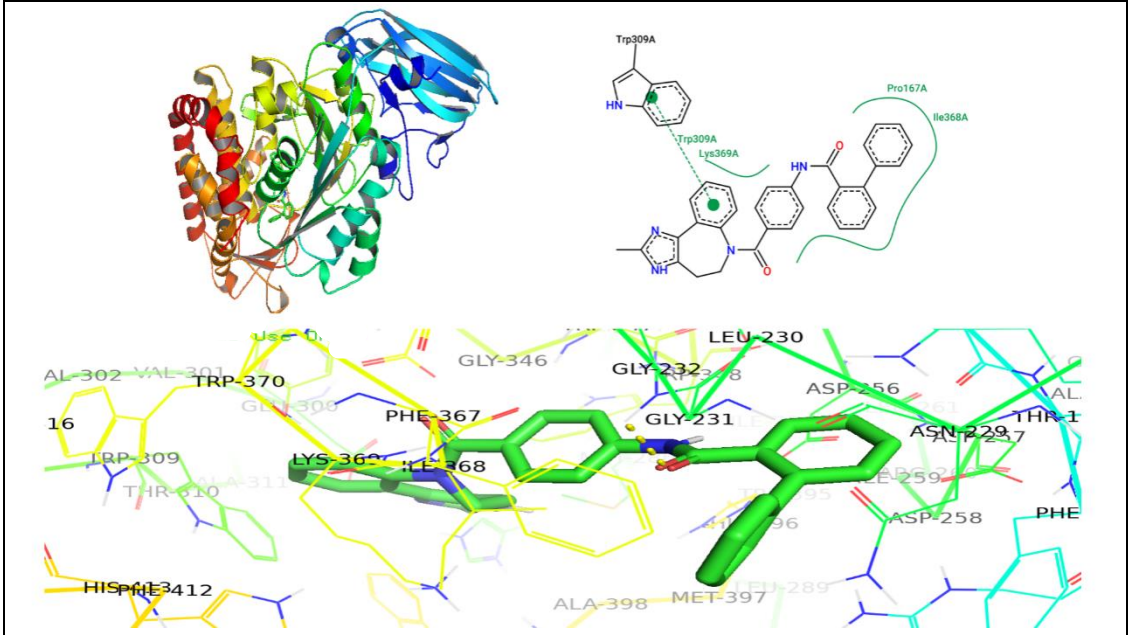

4.6.21 *GlfT2*-DB00872

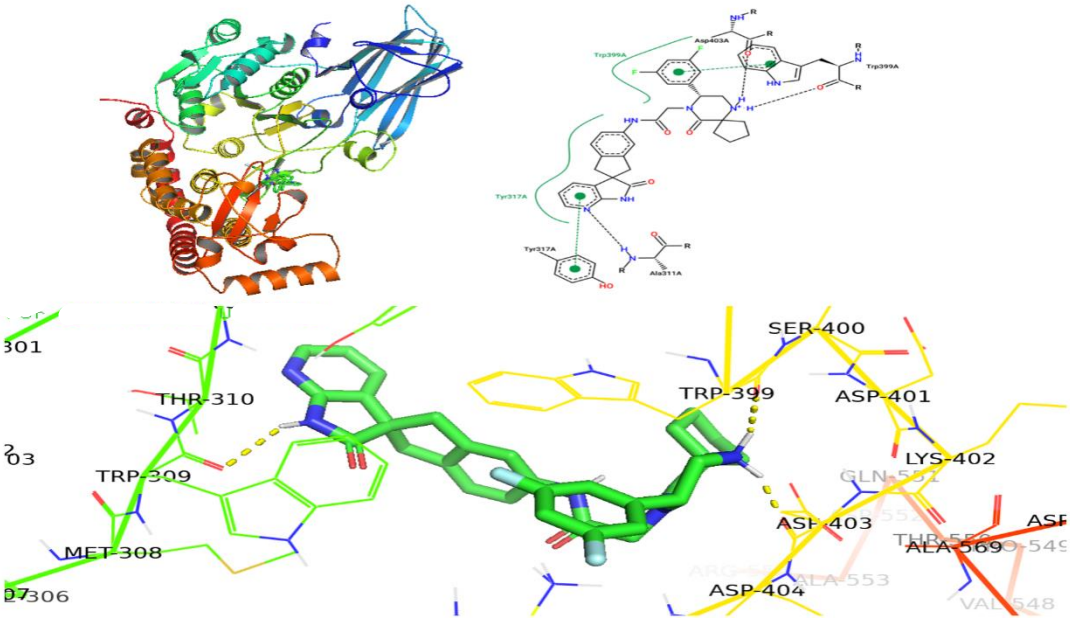

4.6.22 *GlfT2*-ZINC000043203371

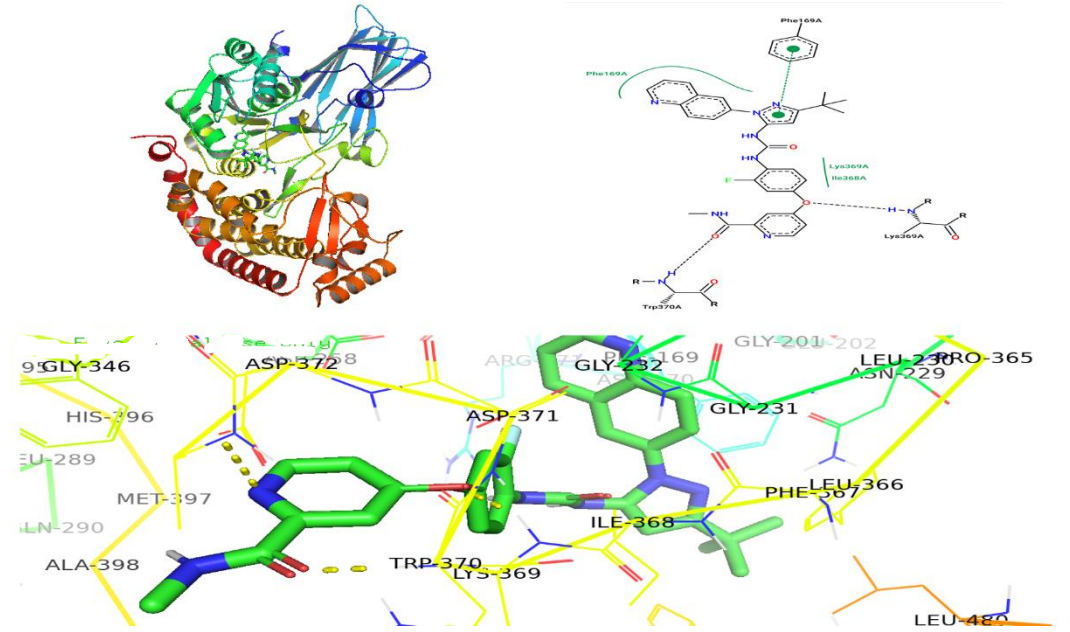

4.6.23 *GlfT2*-ZINC000063933734

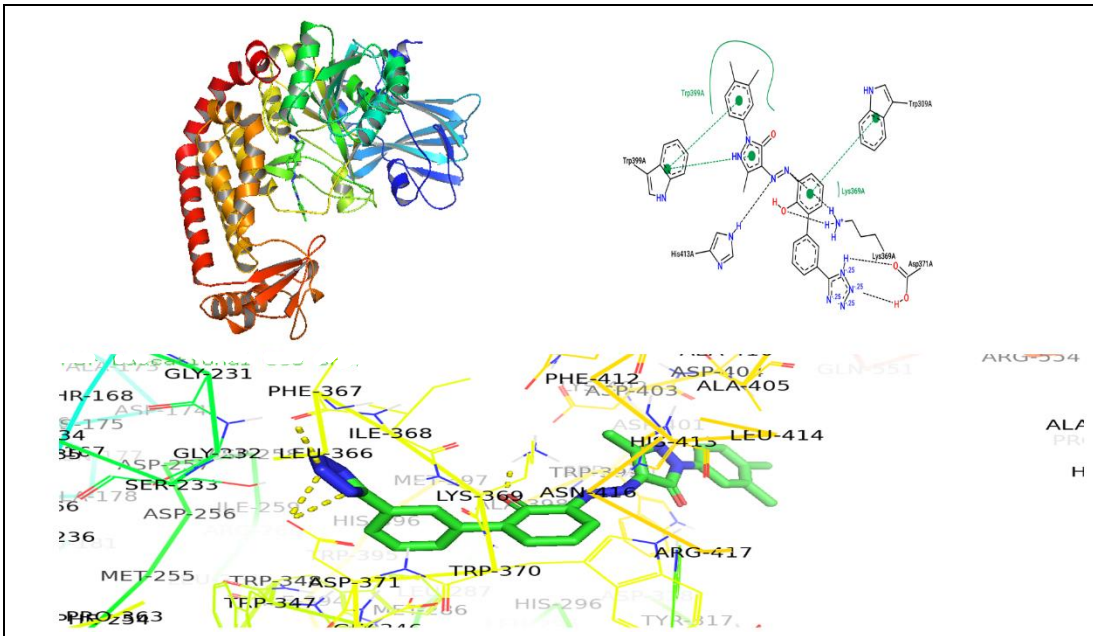

4.6.24 *GlfT2*-ZINC000095092808

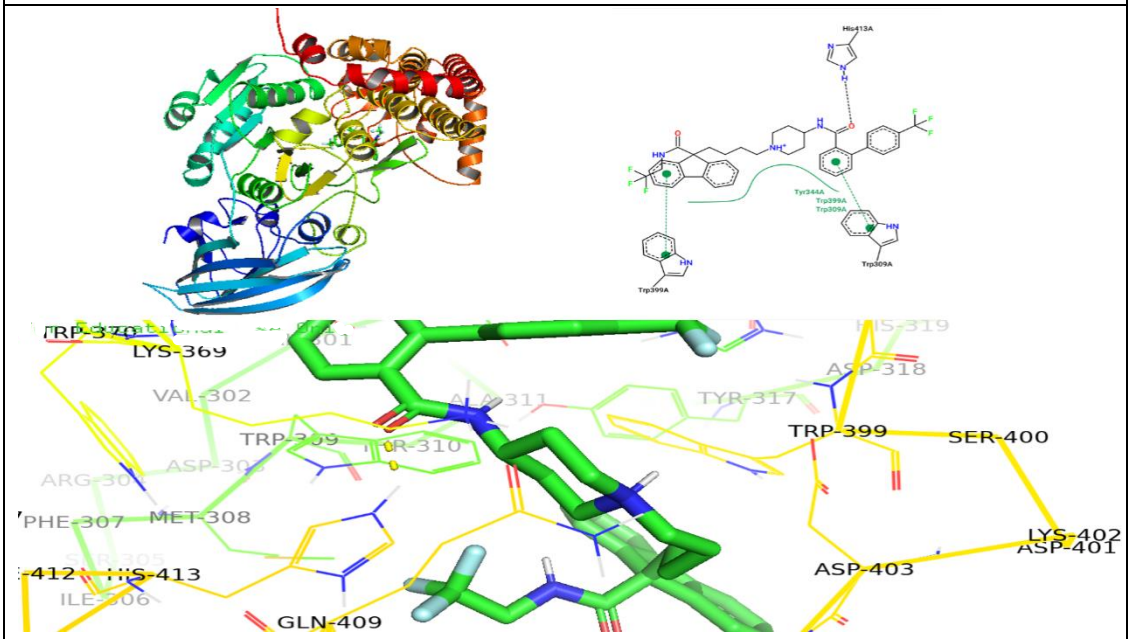

4.6.25 *GlfT2*-ZINC000027990463

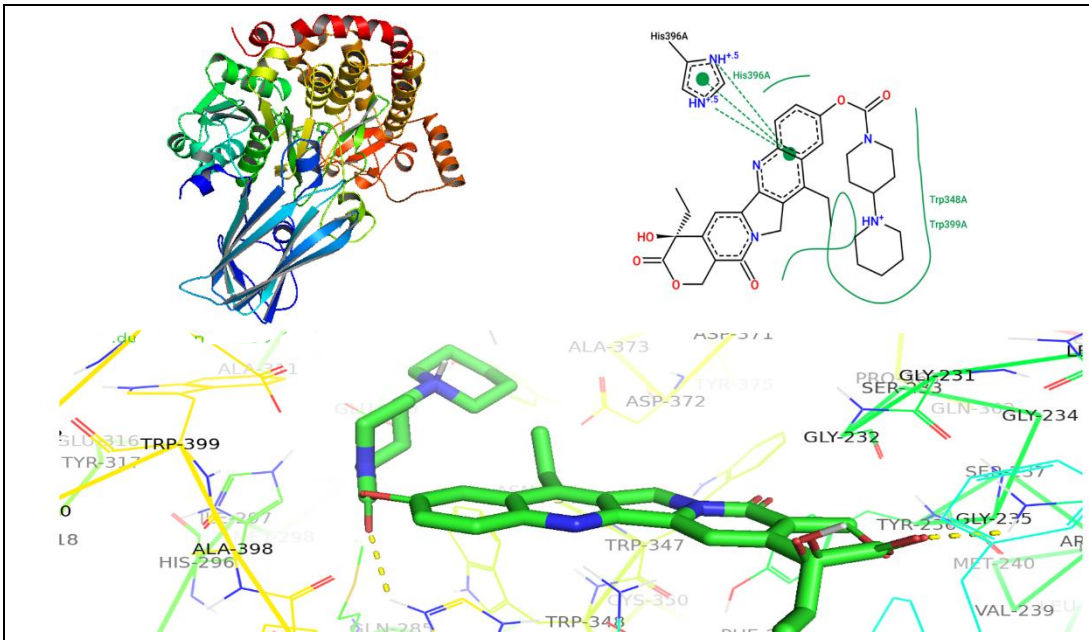

4.6.26 *GlfT2*-ZINC000001612996

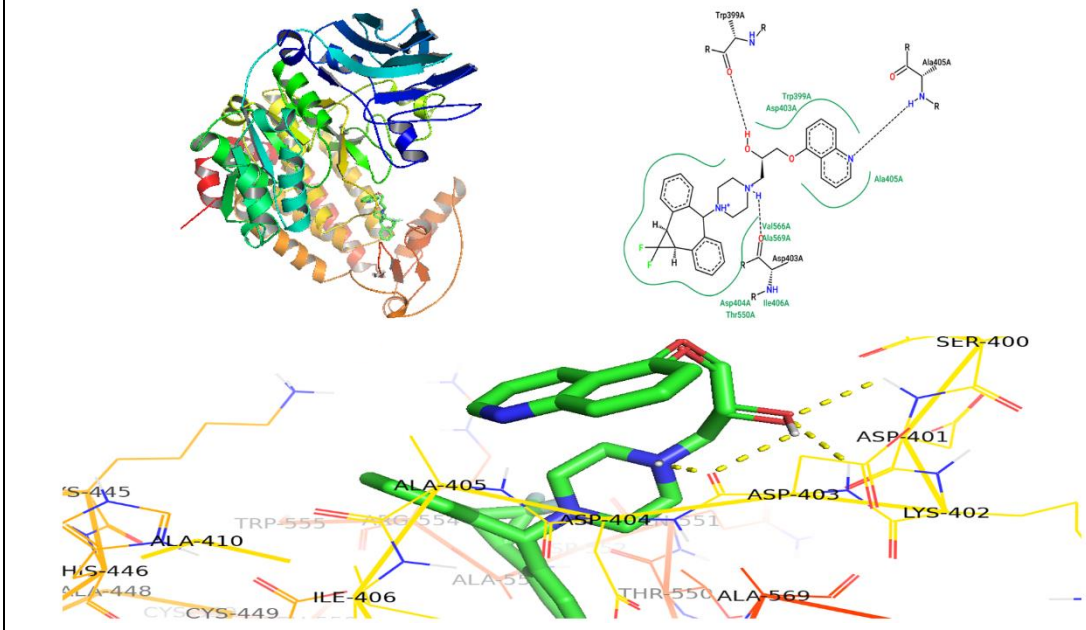

4.6.27 *GlfT2*-ZINC000253633622

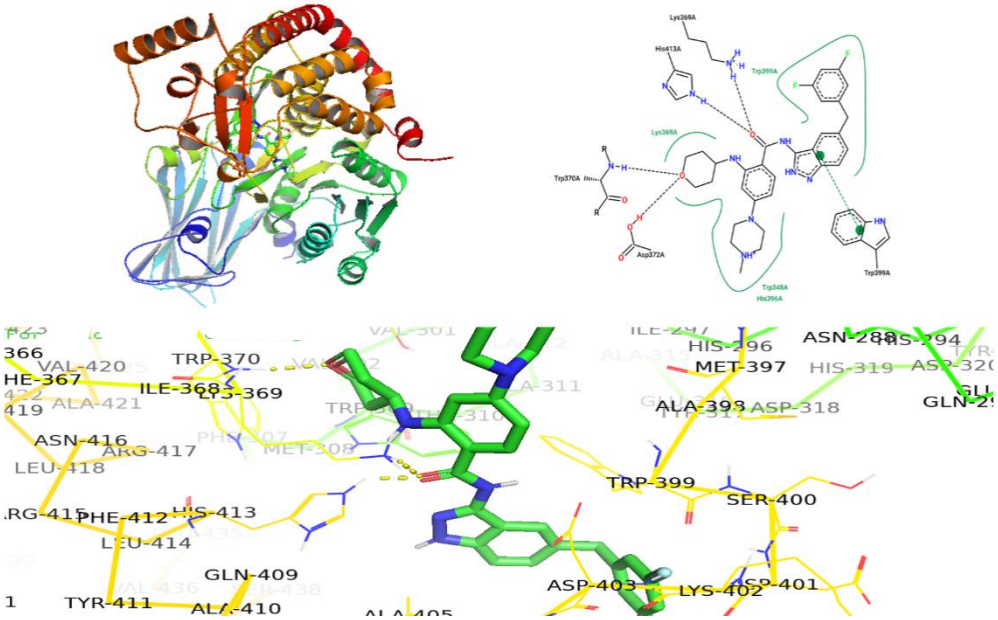

4.6.28 *GlfT2*-ZINC000043204146

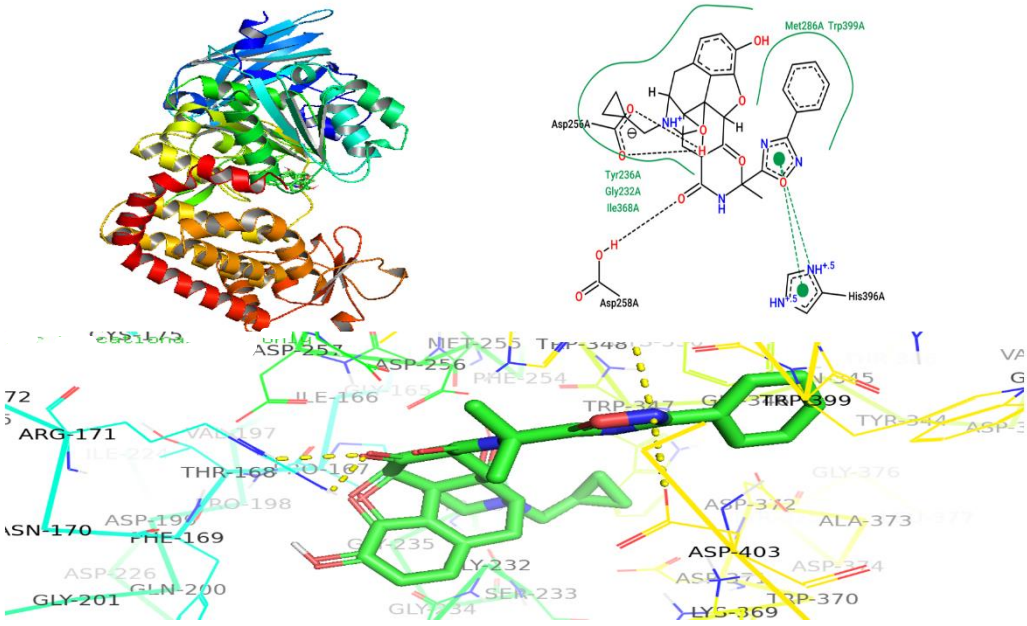

4.6.29 *GlfT2*-ZINC000100378061

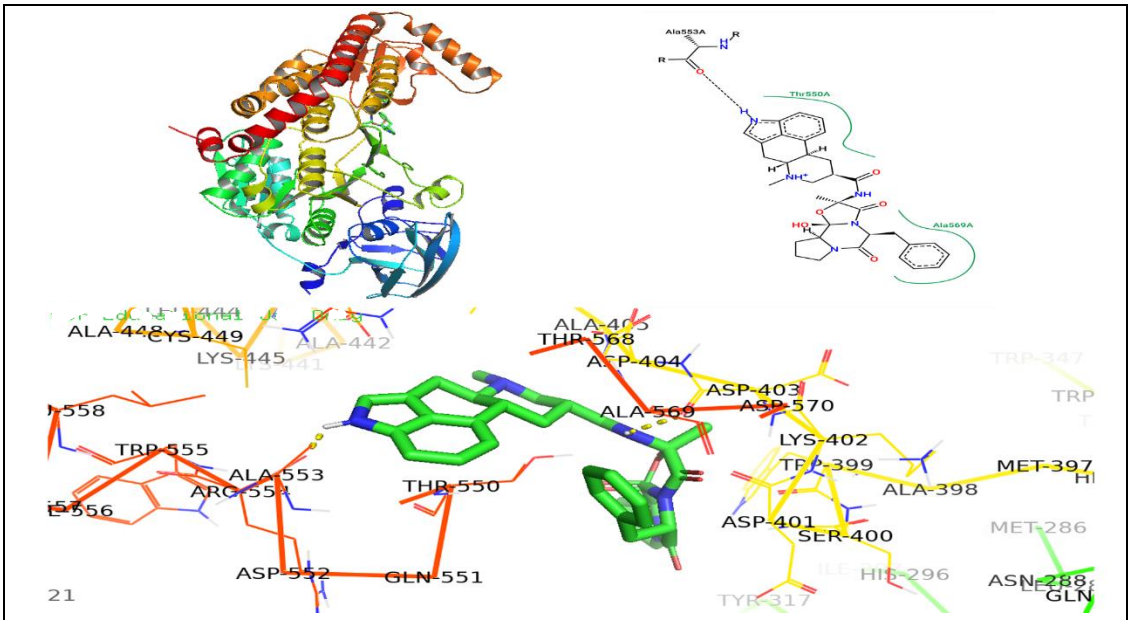

4.6.30 *GlfT2*-ZINC000003978005

Figure 4.6. Top thirty hits identified against the cell wall of MTB's *GlfT2*. Molecules containing *GlfT2* are docked and in contact with antagonistic residues (left screen). Docked molecules are displayed next to interacting receptor residues in 3D poses. Yellow dotted lines show hydrogen bond interactions.

4.1.6. *Mycobacterial* Peptidoglycan membrane protein *MurB* (5JZX)

Three domains make up MTB *MurB*, two aids in producing a binding site for the FAD cofactor, and one aid in substrate binding. The substrate-binding domain III is one of the three domains that make *MurB* (amino acid 206-361), domain II (amino acid 91-205), and domain I, which bind FAD (amino acids (1-90 and 362-364). Eight α-helices, an 18-β strand, and many loops make up the structure of MTB *MurB*. It has a structure made up of eight α-helices, 18-β strands, and several loops. Overall, helixes encircle the strands. A loop that connects the fifth and sixth β-strands between domain I and domain II while a loop between the β-12th strand and the α-4th helix connects

domain III to domain II.[189] The FAD binding module's structural framework consists of two β-sheets, "β1-β2-β3" and "β6-β7-β12-β10-β11", as well as two α-helices, "α1 and α2", with the GXG motif spanning between "β3 and β4" strands. Two lobes make up the substrate-binding module, numbered I and II arranged on each side. Two helices α4-α5 in the numbered I lobe on the left are connected to domain II. Lobe II is positioned next to the domain I, with the "β13-α6-β14-β15" segment projected outside. MTB *MurB* is classified as a type I enzyme as it has a tyrosine loop at Tyr 210 and the "β13-α6-β14-β15" folds.[189] Several, 387 molecules were molecularly docked with the anticipated *MurB* enzyme. A total of fifty-one compounds were found using *in-silico* screening and thirty-two (Figure 4.7) of the top hits were chosen for further study.

A set of thirty-two compounds was opted, prioritizing those with a strong binding affinity as indicated by their high scores in the XP G-score (Table 4.3). The binding affinity is between -13.0 to -9.7 Kcal/mol (Figure 4.8). The top thirty-two hits identified against *MurB* from ChemSpider are CSID1438694 (-11.1 Kcal/mol) with *KI* 6.87 nM, CSID2166135 (-11.0 Kcal/mol) with *KI* 8.15 nM, CSID1655442 (-10.9 Kcal/mol) with *KI* 9.94 nM, CSID2154128 (-10.5 Kcal/mol) with *KI* 19.46 nM, CSID2165834 (-10.2 Kcal/mol) with *KI* 32.80 nM, CSID2156566 (-10.2 Kcal/mol) with *KI* 33.62 nM, CSID2140363 (-10.1 Kcal/mol) with *KI* 34.00 nM, CSID2156621 (-10.0 Kcal/mol) with *KI* 44.61, CSID3866834 (-9.9 Kcal/mol) with *KI* 54.31, CSID2158441 (-9.7 Kcal/ mol) with *KI* 68.21 nM, CSID2156999 (-9.7 Kcal/mol) with *KI* 75.09 nM. The next compounds are from Drug Bank, DB15688 (-13.0 Kcal/mol) with *KI* 55.06 pM, DB12983 (-11.8 Kcal/mol) with *KI* 172.62 pM, DB14773 (-11.5

Kcal/mol) with *KI* 909.21 pM, DB06229 (-11.4 Kcal/mol) with *KI* 182.65 pM, DB12424 (-11.2 Kcal/mol) with *KI* 153.07 pM, DB15396 (-11.1 Kcal/mol) with *KI* 591.56 pM, DB15401 (-11.1 Kcal/mol) with *KI* 5.35 nM, DB03461 (-11.0 Kcal/mol) with *KI* 49.86 nM, DB11852 (-11.0 Kcal/mol) with *KI* 440.33 pM, DB08901 (-11.0 Kcal/mol) with *KI* 19.59 pM.

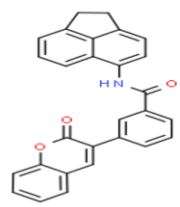

CSID1438694

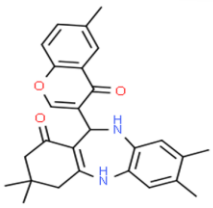

CSID2166135

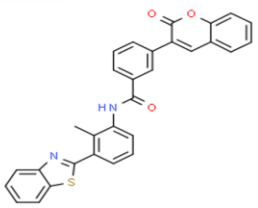

CSID1655442

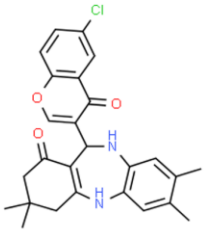

CSID2154128

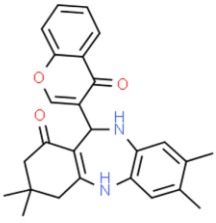

CSID2165834

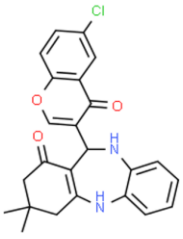

CSID2156566

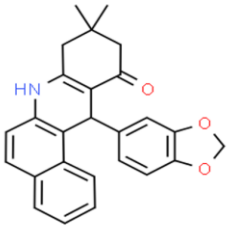

CSID2140363

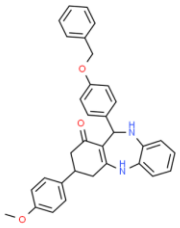

CSID2156621

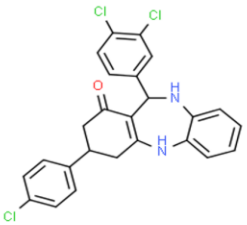

CSID38668341

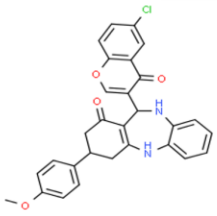

CSID2158441

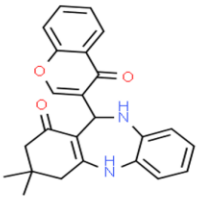

CSID2156999

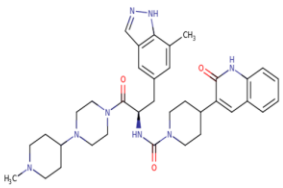

DB15688

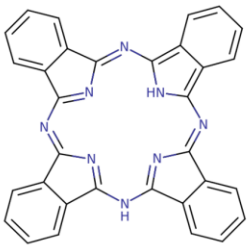

DB12983

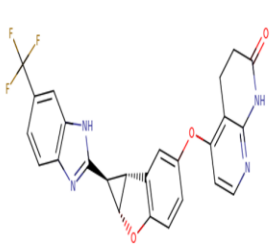

DB14773

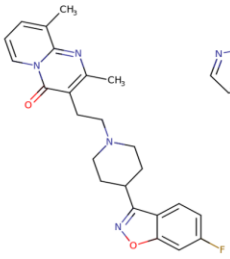

DB06229

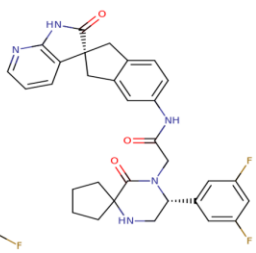

DB12424

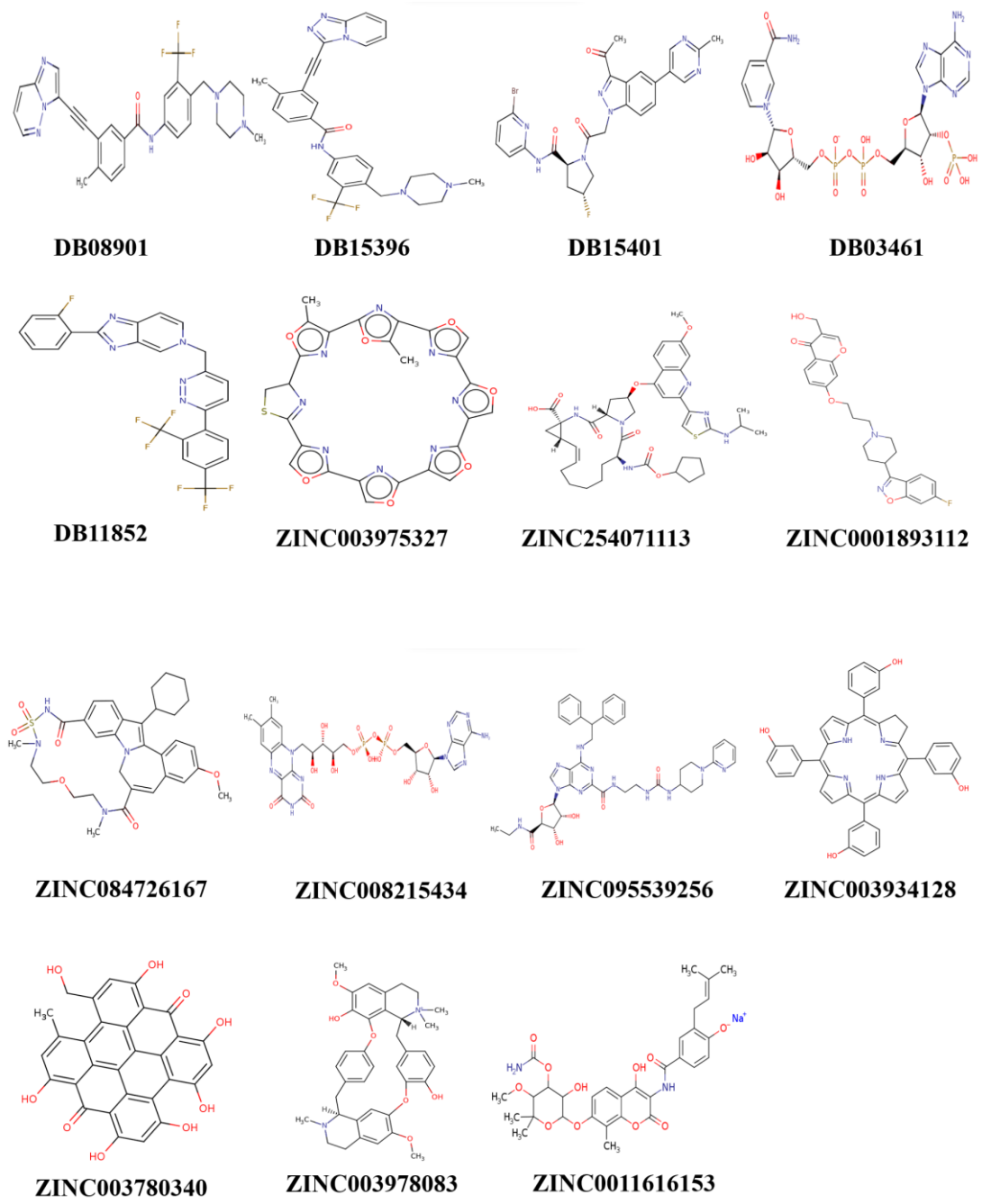

Figure 4.7. 2D Structure of top hits identified against MTB's protein *MurB.*

The last ten compounds are from the ZINC database with ID, ZINC003975327 (-11.9 Kcal/mol) with *KI* 12.34 nM, ZINC254071113 (-11.6 Kcal/mol) with *KI* 5.21 nM, ZINC084726167 (-11.5 Kcal/mol) with *KI* 557.57, ZINC008215434 (-11.3 Kcal/mol)

with *KI* 6.89 nM, ZINC09559256 (-11.1 Kcal/mol) with *KI* 4.35 nM, ZINC003934128 (-11.0 Kcal/mol) with *KI* 711.53 pM, ZINC004215770 (-11.0 Kcal/mol) with *KI* 5.93 nM, ZINC003780340 (-11.0 Kcal/mol) with *KI* 19.28 nM, ZINC0001893112 (-10.9 Kcal/mol) with *KI* 18.00 nM, ZINC003978083 (-10.9 Kcal/mol) with *KI* 56.90 nM, ZINC0011616153 (-9.5 Kcal/mol) with *KI* 159.32 nM.

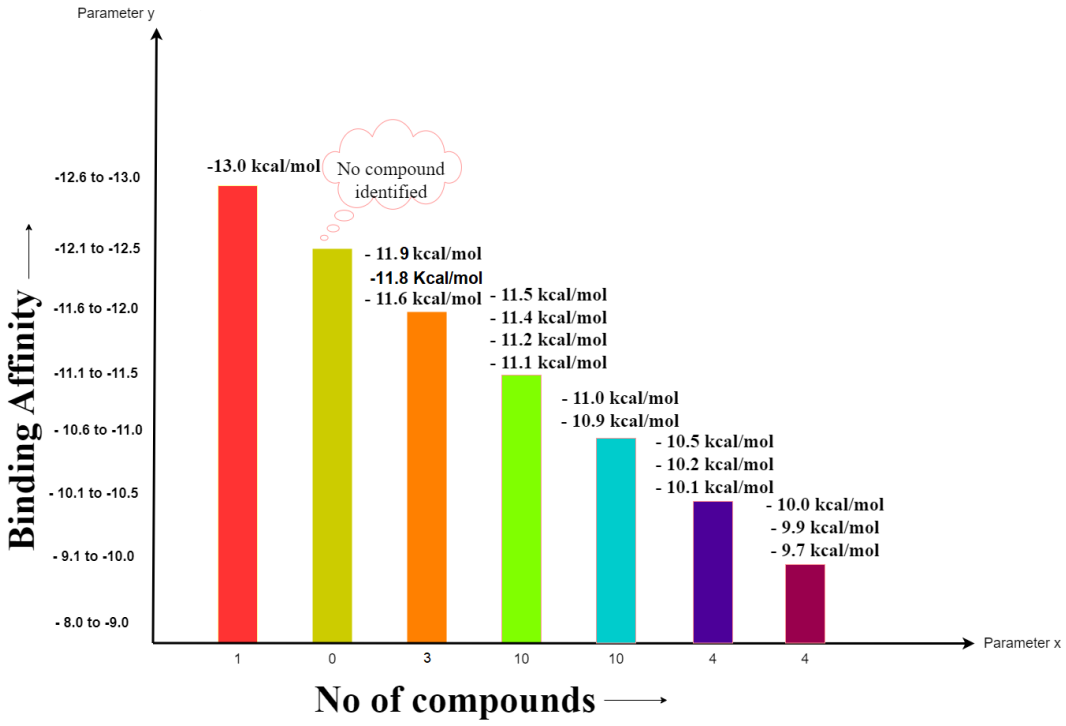

Figure 4.8. Free Binding affinity of identified compounds against *MurB.*

4.1.7. Identified compounds-*MurB* interactions

Thirty-two potential compounds targeting MTB's *MurB* protein in the peptidoglycan were identified. The first eleven compounds are from ChemSpider. The next ten compounds are from Drug Bank and the last ten compounds are from the Zinc

Database (Figure 4.9). The compounds from ChemSpider, CSID1438694 (Fig 4.9.1) show nine hydrophobic interactions which include Asn 71, Leu 72, Ile 127, Ala 133,

Table 4.3. Drug-likeness characteristic of top thirty-two hits against target *MurB.*

S.NO	Compound ID	Binding Affinity	Inhibition constant (KI)	Molecular Weight	LOGP	H-Bond Acceptors	H-Bond Donors	Drug-likeness Score
1	CSID1438694	-11.1	6.87 nM	417.14	5.96	3	1	-0.26
2	CSID2166135	-11	8.15 nM	428.52	5.94	5	2	-0.53
3	CSID1655442	-10.9	9.94 nM	488.55	7.29	5	1	-0.33
4	CSID2154128	-10.5	19.46 nM	448.95	6.28	5	2	-0.16
5	CSID2165834	-10.2	32.80 nM	414.19	4.52	3	2	-0.17
6	CSID2156566	-10.2	33.62 nM	420.88	4.14	5	2	0.1
7	CSID2140363	-10.1	34.00 nM	397.46	5.13	4	1	0
8	CSID2156621	-10	44.61 nM	502.6	5.53	5	2	0.21
9	CSID3866834	-9.9	54.31 nM	469.79	5.7	3	2	0.66
10	CSID2158441	-9.7	68.21 nM	498.95	5.58	4	2	1.25
11	CSID2156999	-9.7	75.09 nM	386.44	3.59	5	2	-0.2
12	DB15688	-13	55.06 pM	638.37	3.53	8	3	1.3
13	DB12983	-11.8	172.62 pM	514.17	7.42	6	2	-1.06
14	DB14773	-11.5	909.21 pM	478.13	4.68	5	2	0.39
15	DB06229	-11.4	182.65 pM	420.2	4.01	5	0	1.05
16	DB12424	-11.2	153.07 pM	557.22	4.27	5	3	1.11
17	DB15396	-11.1	591.56 pM	532.22	4.64	5	1	1
18	DB15401	-11.1	5.35 nM	579.1	2.13	7	1	0.73
19	DB03461	-11	49.86 nM	743.08	-5.74	20	10	0.66
20	DB11852	-11	440.33 pM	517.11	5.97	4	0	0.08
21	DB08901	-11	19.59 pM	532.22	4.66	5	1	1.06
22	ZINC003975327	-11.9	12.34 nM	582.51	5.76	16	0	-0.99
23	ZINC254071113	-11.6	5.21 nM	775.94	6.05	12	3	0.99
24	ZINC084726167	-11.5	557.57 pM	606.74	4.73	7	0	0.17
25	ZINC008215434	-11.3	6.89 nM	785.55	-2.42	23	6	0.77
26	ZINC095539256	-11.1	4.35 nM	777.88	1.91	13	7	1.29
27	ZINC003934128	-11	711.53 pM	680.76	9.86	6	6	-0.13
28	ZINC004215770	-11	5.93 nM	653.63	1.72	13	5	0.61
29	ZINC003780340	-11	19.28 nM	504.45	5.08	8	4	-1.01
30	ZINC0001893112	-10.9	18.00 nM	452.48	4.21	6	2	1.1
31	ZINC003978083	-10.9	56.90 nM	609.74	6.7	6	3	1.11
32	ZINC0011616153	-9.5	159.32 nM	612.63	3.62	11	4	1.11

Val 136 (two contacts), Val 139, Val 188 (two contacts), and two interactions via hydrogen bonding include Gly 68, Ser 130. The second compound, CSID2166135 (refer to Fig 4.9.2), exhibits five hydrophobic interactions and four hydrogen bond interactions. Specifically, it engages in hydrophobic interactions with Thr 26, Ile 127, Pro 128, Ala 141, and Leu 245, while forming hydrogen bond interactions with Ser 70, Arg 238, Ser 257, and Glu 361.

The third compound CSID1655442 (Fig 4.9.3) shows a total of seven interactions out of which four are hydrophobic and three are hydrogen bond interactions. The hydrophobic interactions are Tyr 175, Arg 176, Pro 262, and Leu 364 while hydrogen bond interactions are Thr 177, Lys 181, and Lys 359. The fourth compound CSID2154128 (Fig 4.9.4) shows a total of thirteen interactions of which six are hydrophobic while seven are hydrogen bond interactions. The hydrophobic interactions are Ala 141, Tyr 142, Glu 145, Tyr 175, Lys 241, and Ala 296 while the Gly 140, Tyr 142, Tyr 175, Arg 176, Tyr 210, Asn 261, and Lys 294 are hydrogen bond interactions. The fifth compound CSID2165834 (Fig 4.9.5) shows five hydrophobic interactions with Pro 128, Gln 137, Val 139, Ala 141, and Glu 361 and three hydrogen bond interactions with Gln 140, Arg 238 (two contacts).

The next compound CSID2156566 (Fig 4.9.6) shows four hydrophobic and hydrogen bond interactions respectively. The hydrophobic interactions include Ile 127, Pro 128, Ala 141, and Leu 245 while Ser 70, Arg 238, Ser 257, and Glu 361 are hydrogen bond interactions. The seventh compound CSID2140363 (Fig 4.9.7) shows a total of fourteen interactions out of which eleven are hydrophobic while three are hydrogen bond interactions. The hydrophobic interactions are Ala 67, Asn 71, Leu 72, Ala 133,

Val 136 (two contacts), Gln 137, His 182, Val 188 (two contacts), and Val 363 while Ala 67, Asn 71, and Val 192 are hydrogen bond interactions. The eighth compound CSID2156621 (Fig 4.9.8) shows nine hydrophobic interactions with Tyr 175 (two contacts), Arg 176, Thr 260, Val 263 (two contacts), Ile 256, Lys 359, and Pro 360 while the hydrogen bond interactions are Lys 181, Asn 261, Val 263, Thr 357, Lys 359. The ninth compound CSID3866834 (Fig 4.9.9) shows seven interactions, three are hydrophobic while four are hydrogen bond interactions. The hydrophobic interactions are Ala 141, Ala 296, and Leu 326 while Tyr 142, Tyr 210, and Ser 257 (two contacts) are hydrogen bond interactions. The tenth compound, CSID2158441 (Fig 4.9.10) shows four hydrophobic interactions with Glu 145, Tyr 175, Tyr 210, and Tyr 287 while three hydrogen bond interactions with Tyr 142, Gly 143, and Lys 294. The last compound from ChemSpider CSID2156999 (Fig 4.9.11) shows a total of six interactions with three each included in hydrophobic and hydrogen bonding. The hydrophobic interactions are Pro 360, Val 363, and Leu 364 while hydrogen bond interactions are Ala 183, Gly 366, and Cys 367.

The following compounds are sourced from the Drug Bank repository. DB15688 (refer to Fig 4.9.12) exhibits five hydrophobic interactions involving Ile 127 (two contacts), Val 139, Ala 141, and Tyr 175. Additionally, it forms seven hydrogen bond interactions with Arg 176, Tyr 210, Ser 257, Asn 261, Glu 302, Ala 325, and Glu 361. The thirteenth compound, DB12983 (refer to Fig 4.9.13), displays five hydrophobic interactions and three hydrogen bond interactions. The hydrophobic interaction is Glu 145, Asn 261, Tyr 287, Pro 288, and Ala 296 while the hydrogen bond interactions are Tyr 210, Asn 261, and Lys 294. The fourteenth compound DB14773 (Fig 4.9.14)

shows a total of ten interactions of which five are hydrophobic and five are hydrogen bond interactions. The hydrophobic interactions are Tyr 175, Val 263, Lys 359, Pro 360, and Leu 364 while hydrogen bond interactions include Lys 181, Gly 185, Thr 260, Leu 364, and Leu 354. The fifteenth compound DB06229 (Fig 4.9.15) shows a total of ten interactions. The seven are hydrophobic interactions with Ala 67, Asn 71, Leu 72, Ile 127, Pro 128, Ala 133, and Met 243 while three are hydrogen bond interactions with Gly 68, Ser 130, and Arg 238. The next compound DB12424 (Fig 4.9.16) shows hydrophobic interactions with Ala 183, Asp 184, and Val 363 while Leu 364 and Gly 366 interact with a hydrogen bond.

The seventeenth compound DB15396 (Fig 4.9.17) shows three hydrophobic interactions with Ala 141, Glu 145, and Tyr 175, and four hydrogen bond interactions with Gly 143, Arg 238 (two contacts), and Glu 361. The next compound DB15401 (Fig 4.9.18) shows a total of ten interactions of which three are hydrophobic interactions with Ile 127, Tyr 175, and Tyr 210, and eight are showing hydrogen bond interactions with Gly 143, Arg 176 (two contacts), Arg 238 (two contacts), Ser 257 (three contacts). The nineteenth compound DB03461 (Fig 4.9.19) shows only one hydrophobic interaction with Val 263 and nine hydrogen bond interactions which include Tyr 175, Thr 260, Val 263, Asp 291 (two contacts), Thr 357 (two contacts), Lys 359, and Pro 360. The twentieth compound is DB11852 (Fig 4.9.20) which shows five hydrophobic interactions with Asp 184, Leu 186, Lys 359, Pro 360, and Leu 364 while two hydrogen bond interactions including Lys 181 and Gly 185. The twenty-one compound is DB08901 (Fig 4.9.21) shows six hydrophobic interactions with Val

136, Lys 181, Val 188, Pro 360, and Val 363 (two contacts) while three hydrogen bond interactions which include Lys 181, His 182, and Val 263.

The next and twenty-second compound are from the ZINC database ZINC003975327 (Fig 4.9.22) which shows a total of five interactions. The first three are hydrophobic interactions with Tyr 175 (two contacts) and Val 263 while two are hydrogen bond interactions with Tyr 175 and Thr 177. The next compound ZINC25407113 (Fig 4.9.23) shows three hydrophobic interactions with Tyr 210, Pro 283, and Tyr 287 while four hydrogen bond interactions with Asn 261, Val 284, His 286, and Gly 298. The next compound ZINC084726167 (Fig 4.9.24) shows a total of nine interactions of which three are hydrophobic while six are hydrogen bond interactions. The hydrophobic interactions include Tyr 210, Tyr 287, and Ala 296 while Tyr 174, Arg 176 (two contacts), Ser 257, Asn 261, and His 325 interact via hydrogen bonds. The twenty-fifth compound ZINC008215434 (Fig 4.9.25) shows a total of eleven interactions with two hydrophobic and nine hydrogen bond interactions. The hydrophobic interactions include Tyr 210, and Glu 212 while Gly 143, Ala 144 (two contacts), Arg 176 (two contacts), Tyr 210, Ser 257, Asn 261, and Lys 294 show hydrogen bond interactions.

The next compound ZINC095539256 (Fig 4.9.26) shows hydrophobic interactions with Tyr 175, Arg 176, Tyr 210, Thr 260, and Pro 290 while hydrogen bond interactions are Gly 143, Ala 144 (two contacts), Arg 176 (two contacts), and Tyr 210. Ser 257, Asn 261, Lys 294. The twenty-seventh compound ZINC003934128 (Fig 4.9.27) shows four hydrophobic interactions with Arg 172, Phe 173 (two contacts), and Pro 290 while seven hydrogen bond interactions are Glu 145, Ser 147, Asp 170,

Arg 172, Phe 173 (two contacts), and Asp 291. The twenty-eight compound ZINC0004215770 (Fig 4.9.28) shows a total of eight interactions. The hydrophobic interactions include Tyr 210, Tyr 287, and Pro 288 while hydrogen bond interactions are Gly 143, Arg 176 (two contacts), Tyr 210, and Asn 261. The next and twenty-nine compound ZINC003780340 (Fig 4.9.29) shows hydrophobic interactions with three residues including Tyr 210, Tyr 287, and Ala 296 while four hydrogen bond interactions with Gly 140, Arg 176 (two contacts), Asn 261, and His 286. The thirty compound ZINC0001893112 (Fig 4.9.30) shows six hydrophobic interactions with Ala 67, Asn 71, Leu 72, Ile 127, Ala 133, and Ala 141 while seven hydrogen bond interactions with Gly 69, Ser 70, Asn 71, Arg 176, Arg 238 (two contacts), and Ser 257. The thirty-first compound ZINC003978083 (Fig 4.9.31) shows hydrophobic interactions with Glu 145, Tyr 175, Tyr 210 (two contacts), Tyr 287, and Ala 296 while four hydrogen bond interactions with Gly 143, Tyr 175, Gly 211, and Asn 261. The last and thirty-second compound ZINC0011616153 (Fig 4.9.32) shows a total of seven interactions of which two are hydrophobic with Pro 360 and Ile 365 while five are hydrogen bond interactions with Lys 181, Leu 186, Leu 364 (two contacts), and Gly 366.

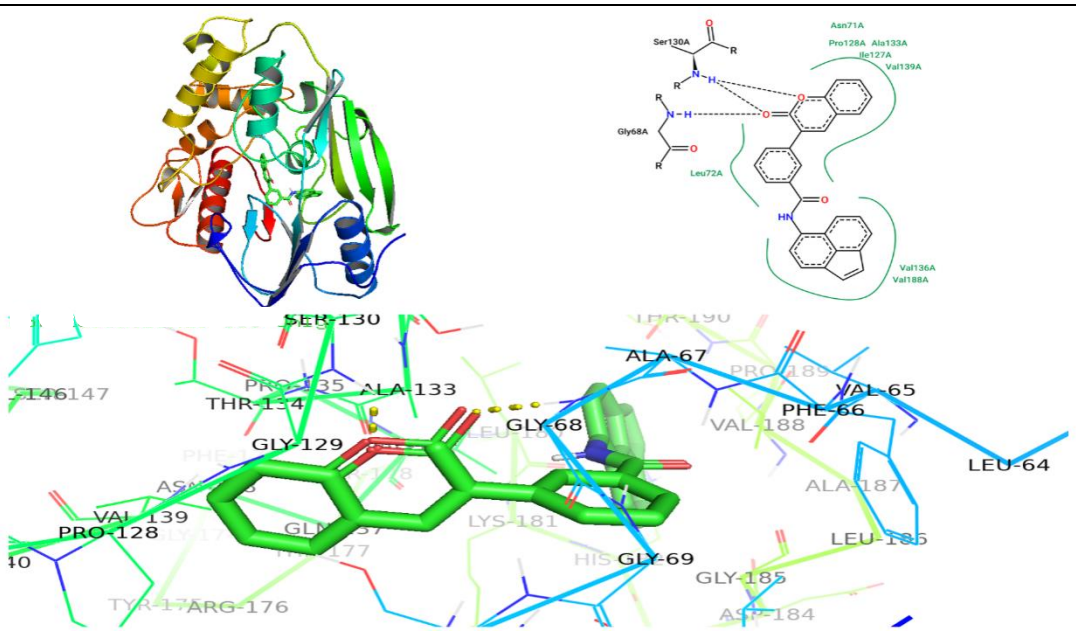

4.9.1 *MurB*-CSID1438694

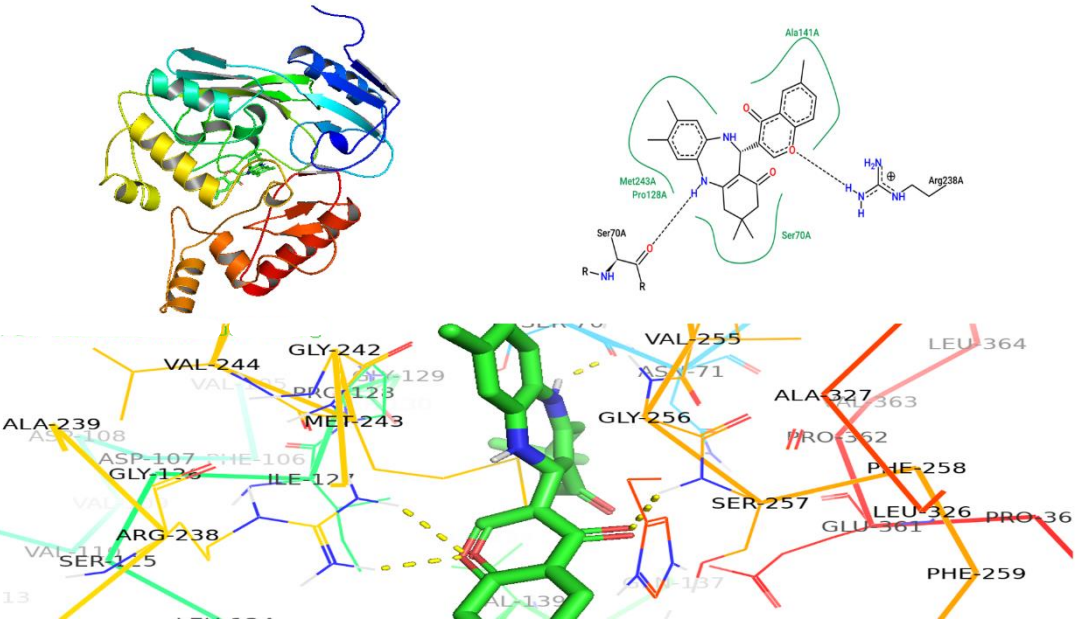

4.9.2 *MurB*- CSID2166135

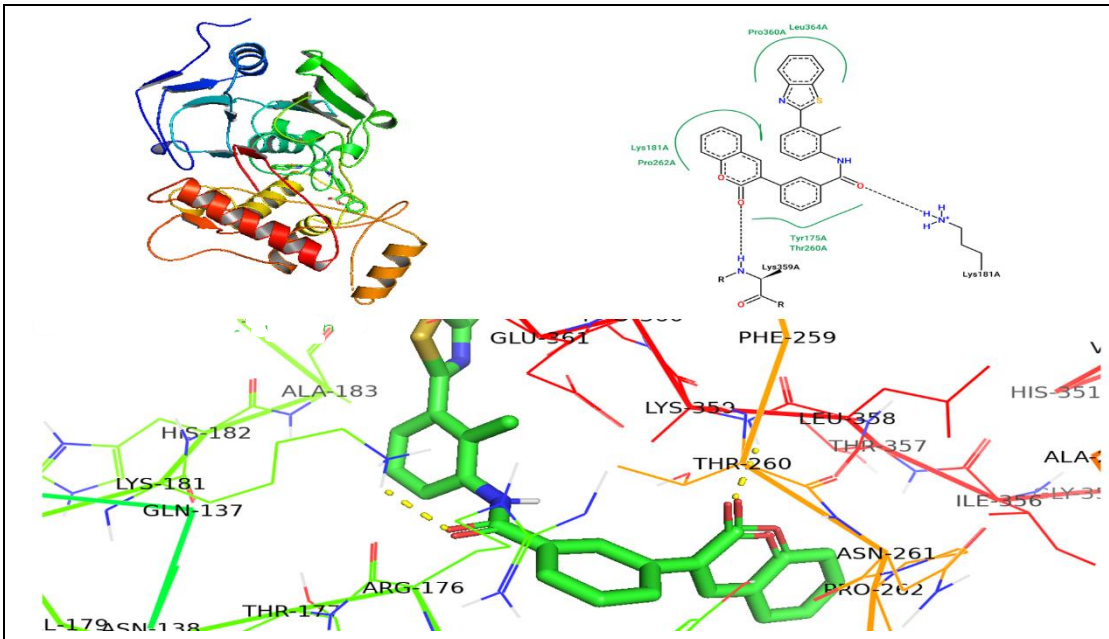

4.9.3 *MurB*- CSID1655442

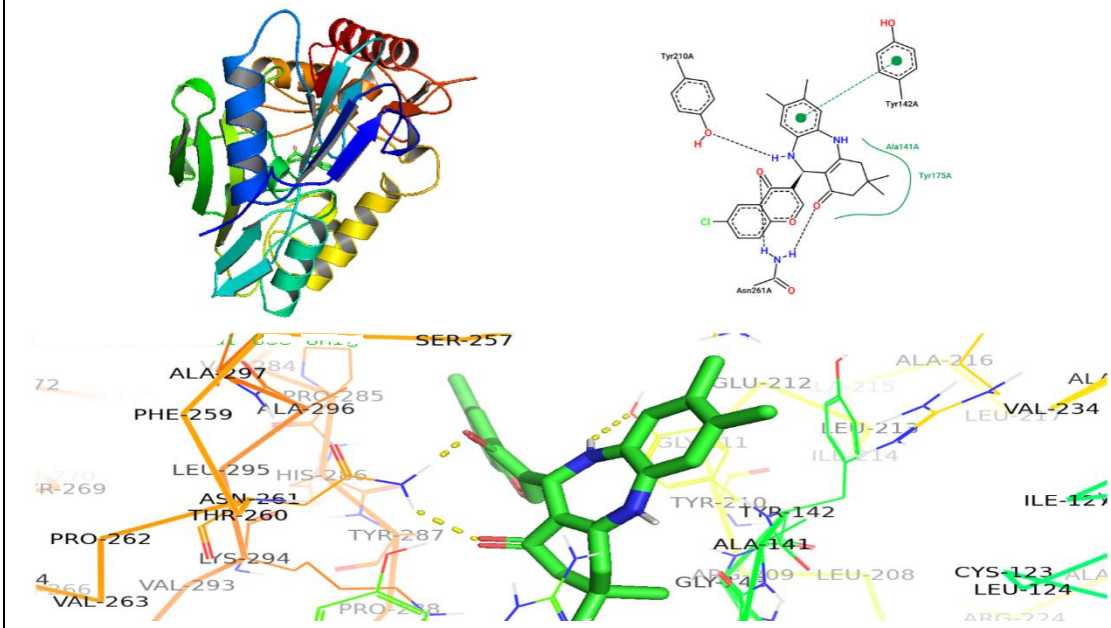

4.9.4 *MurB*- CSID2154128

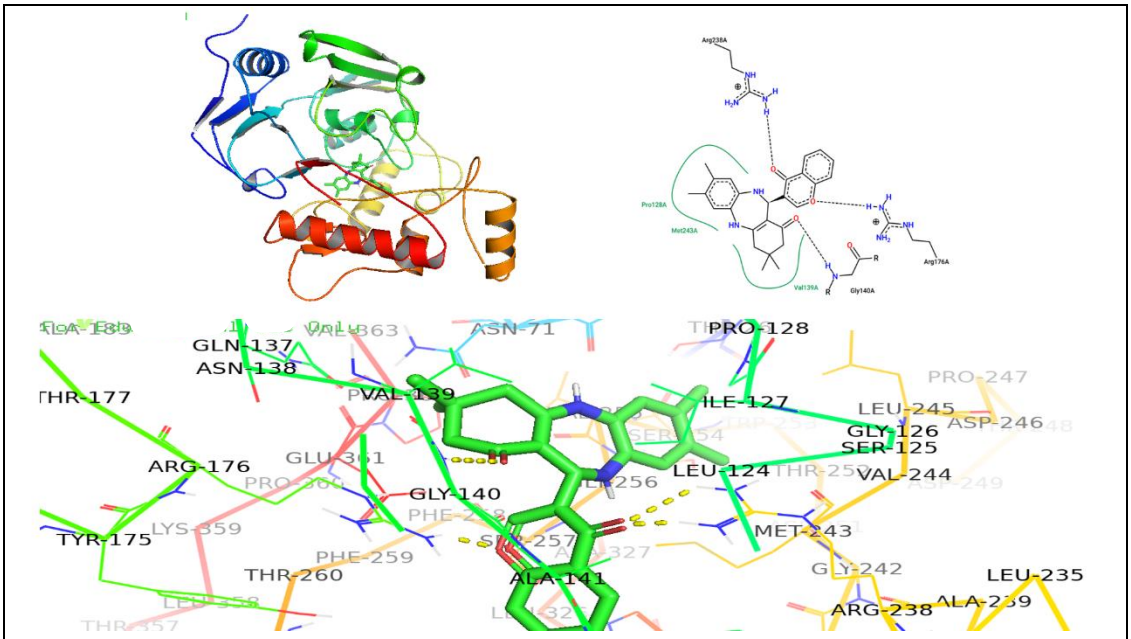

4.9.5 *MurB*- CSID2165834

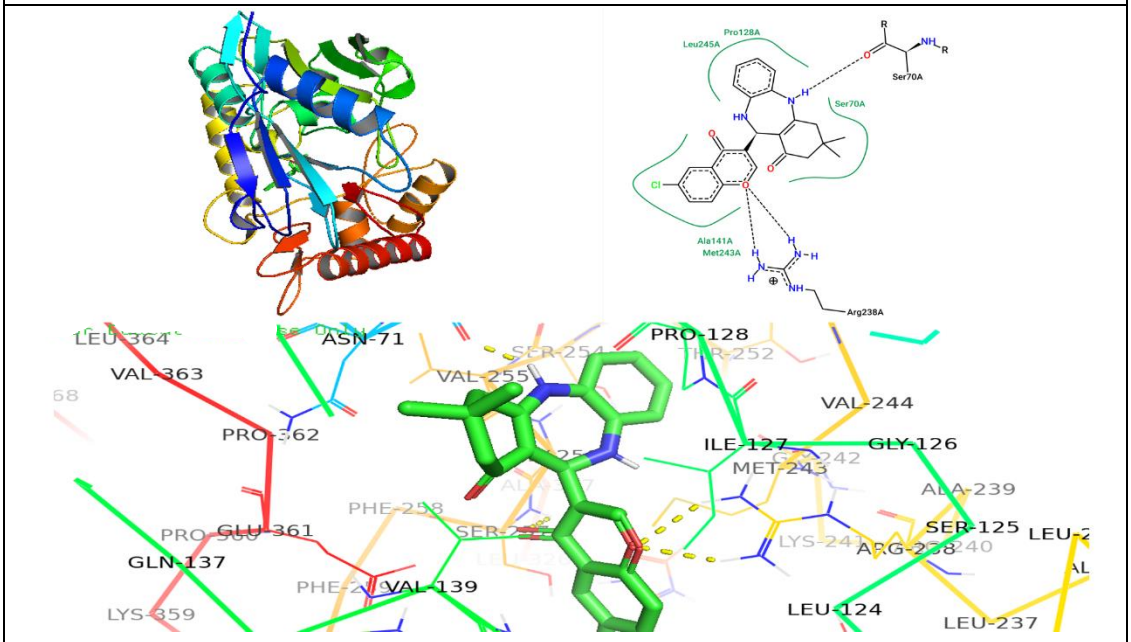

4.9.6 *MurB*- CSID2156566

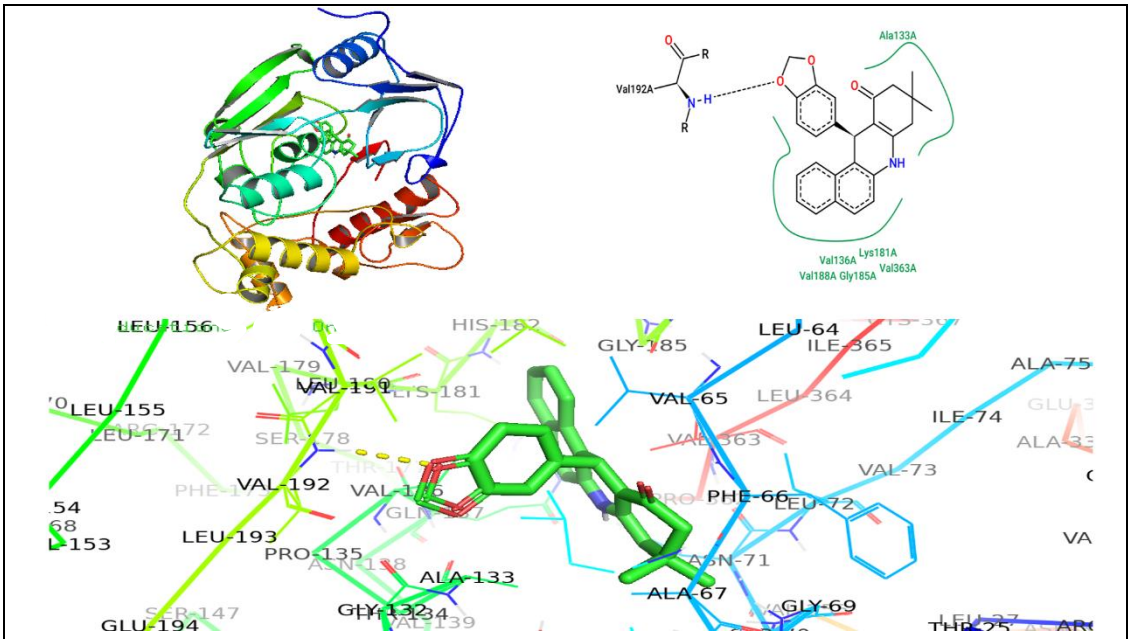

4.9.7 *MurB*- CSID2140363

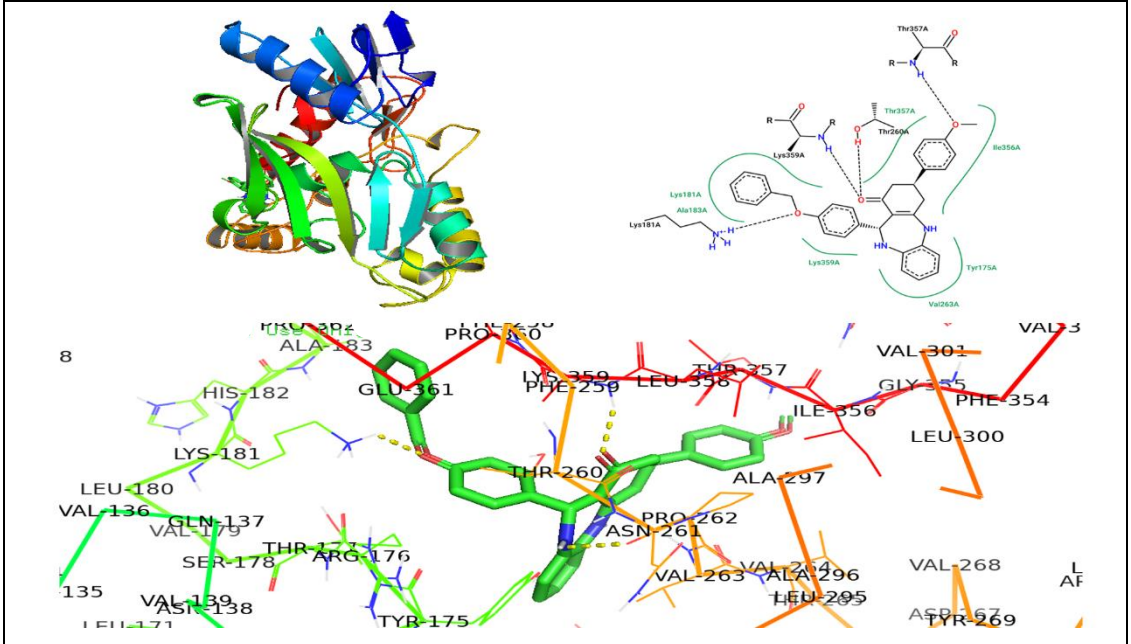

4.9.8 *MurB*- CSID2156621

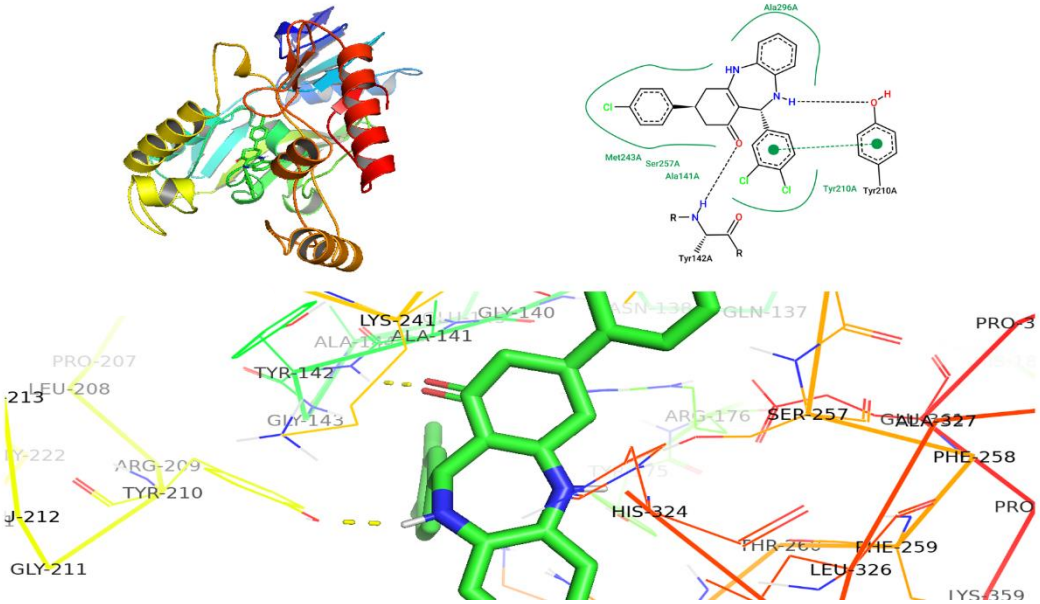

4.9.9 *MurB*- CSID3866834

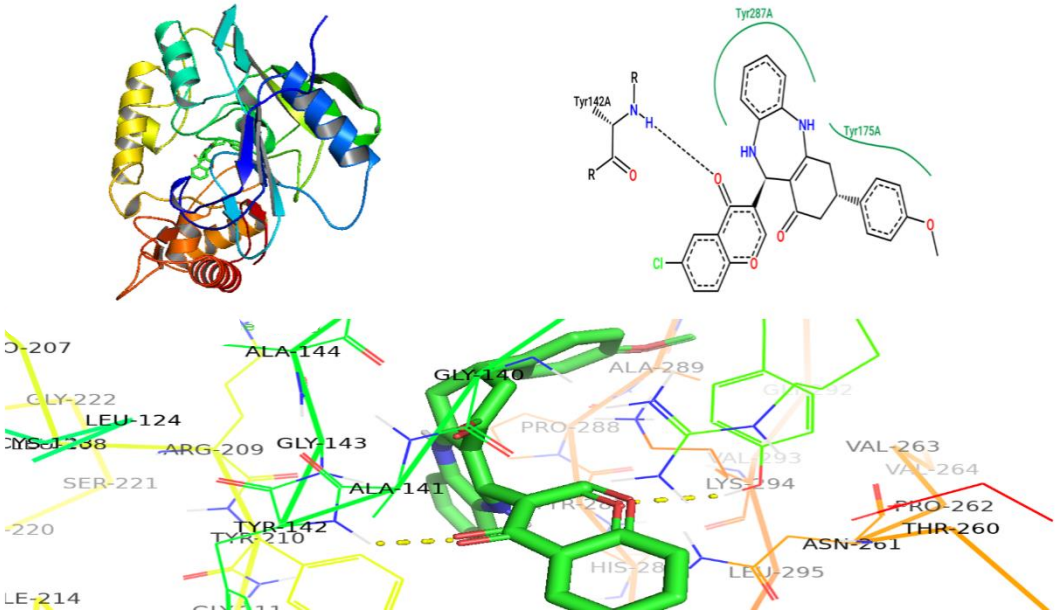

4.9.10 *MurB*- CSID2158441

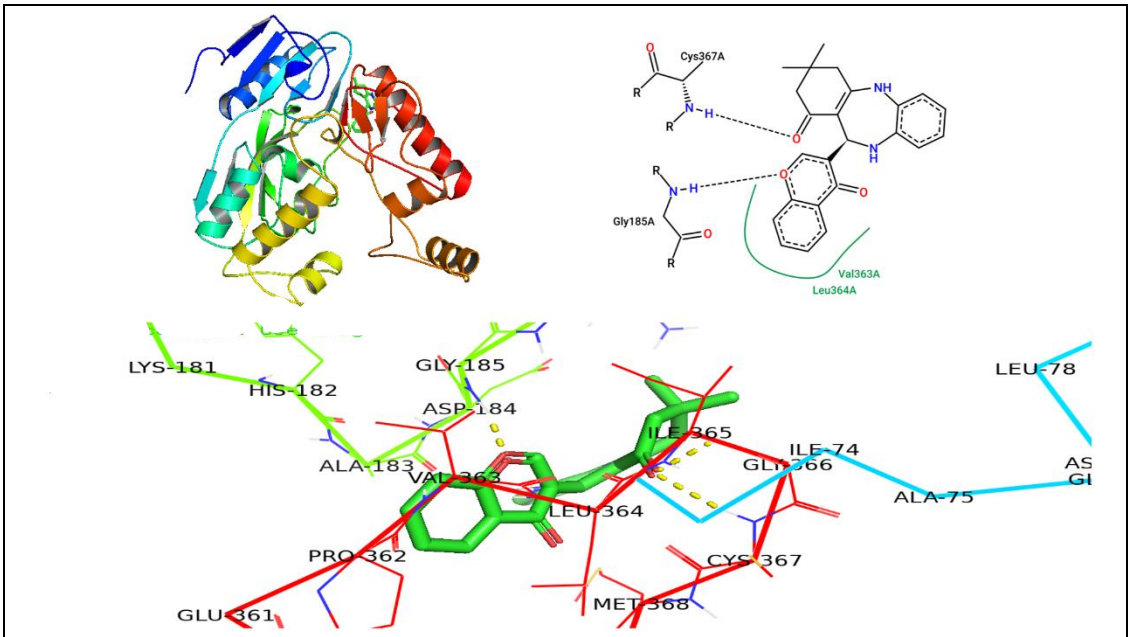

4.9.11 *MurB*-CSID2156999

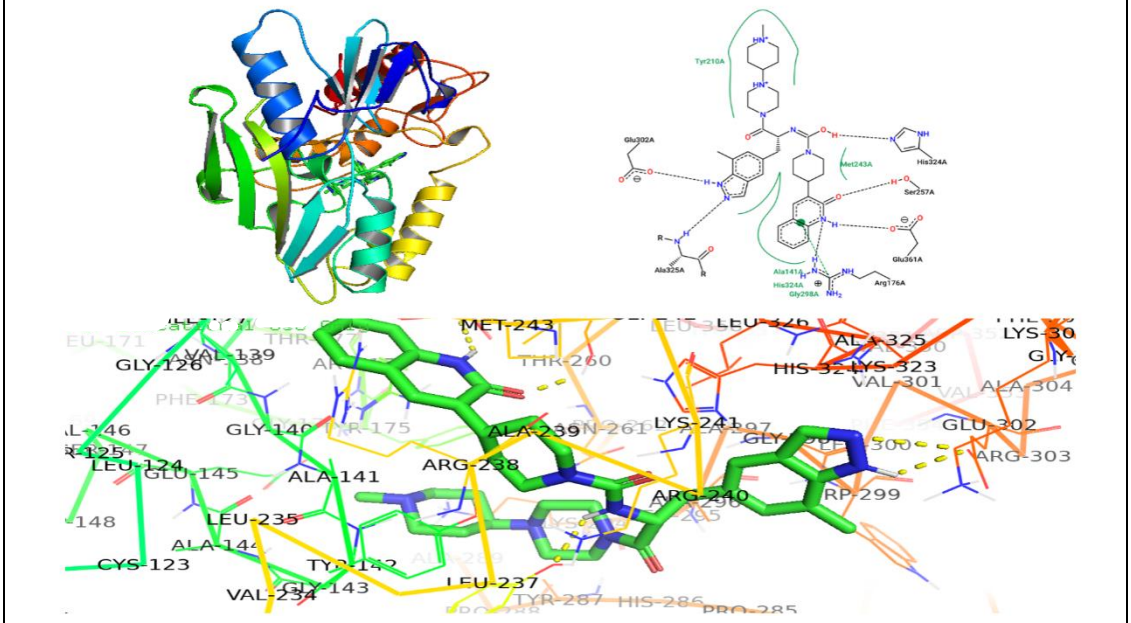

4.9.12 *MurB*- DB15688

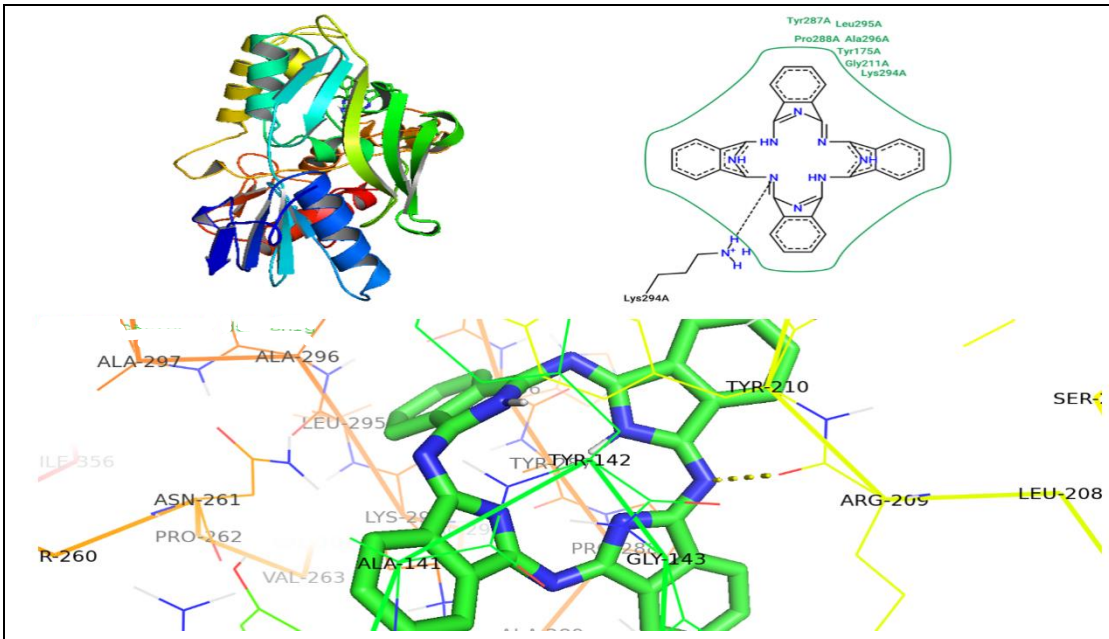

4.9.13 *MurB*- DB12983

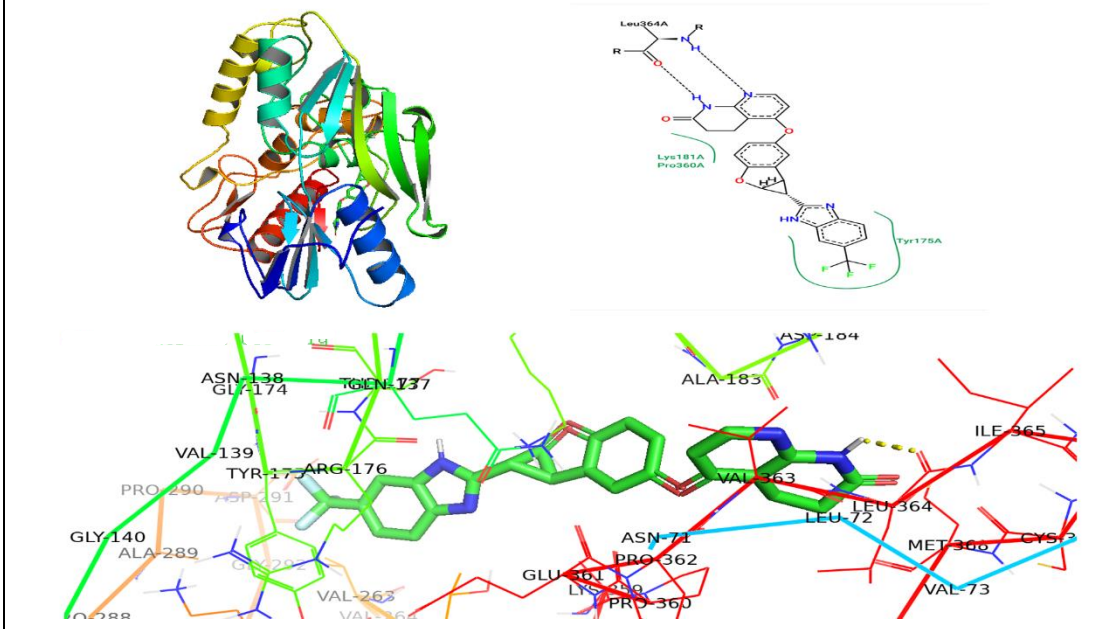

4.49.14 *MurB*- DB14773

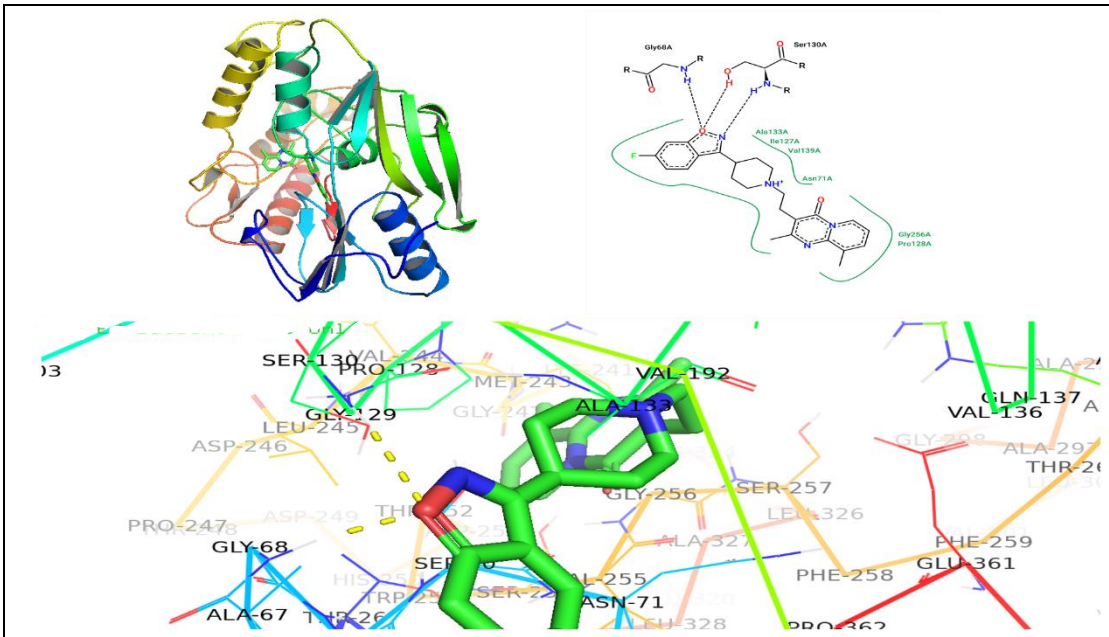

4.9.15 *MurB*- DB06229

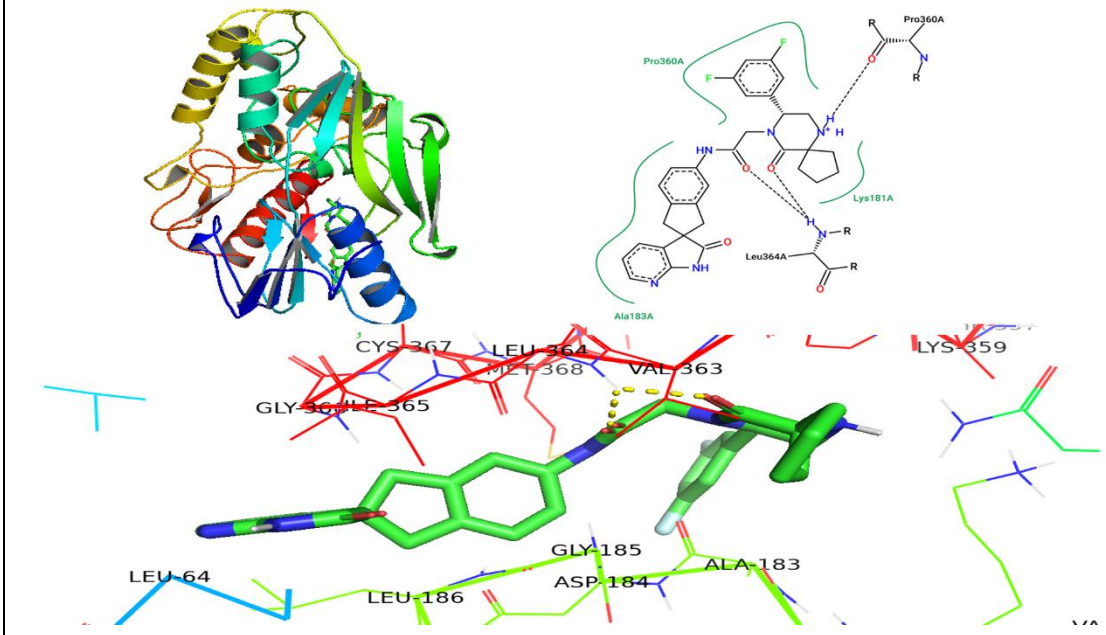

4.9.16 *MurB*- DB12424

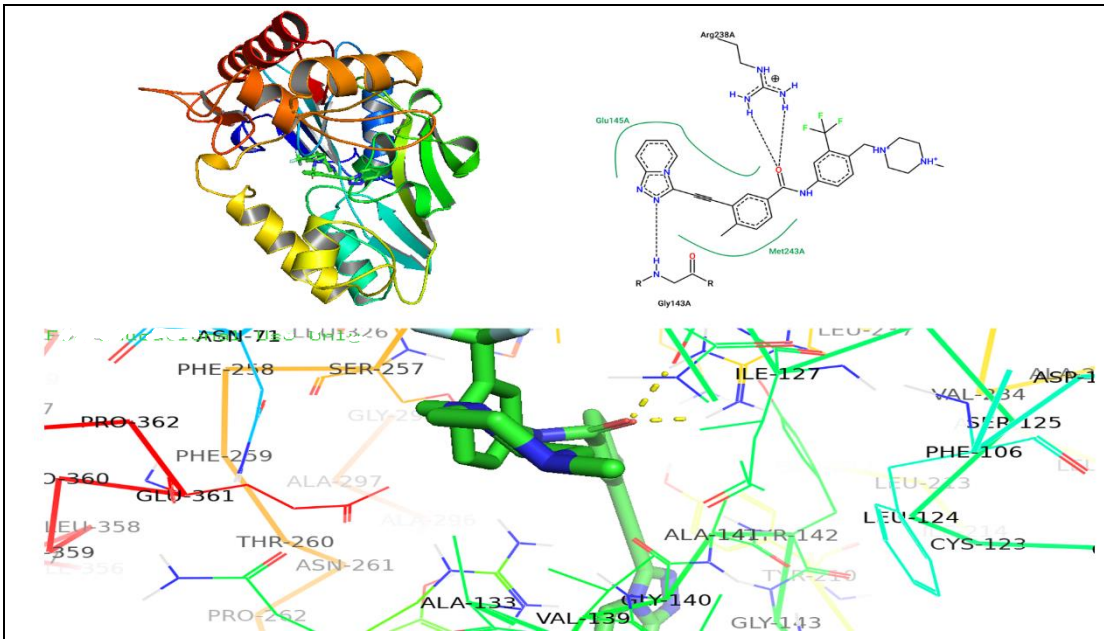

4.9.17 *MurB*- DB15396

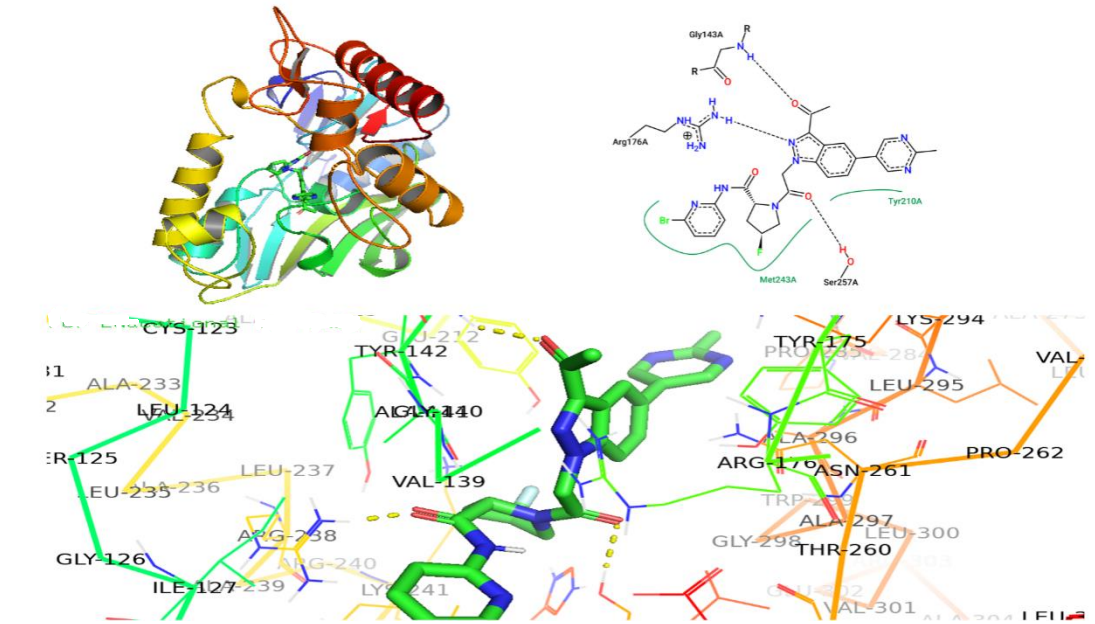

4.9.18 *MurB*- DB15401

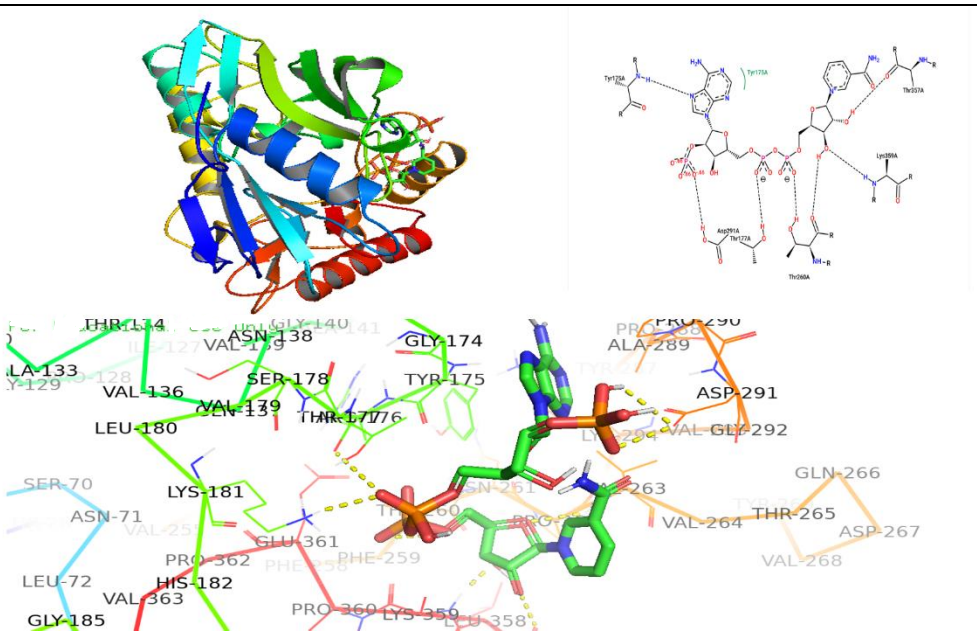

4.9.19 *MurB*- DB03461

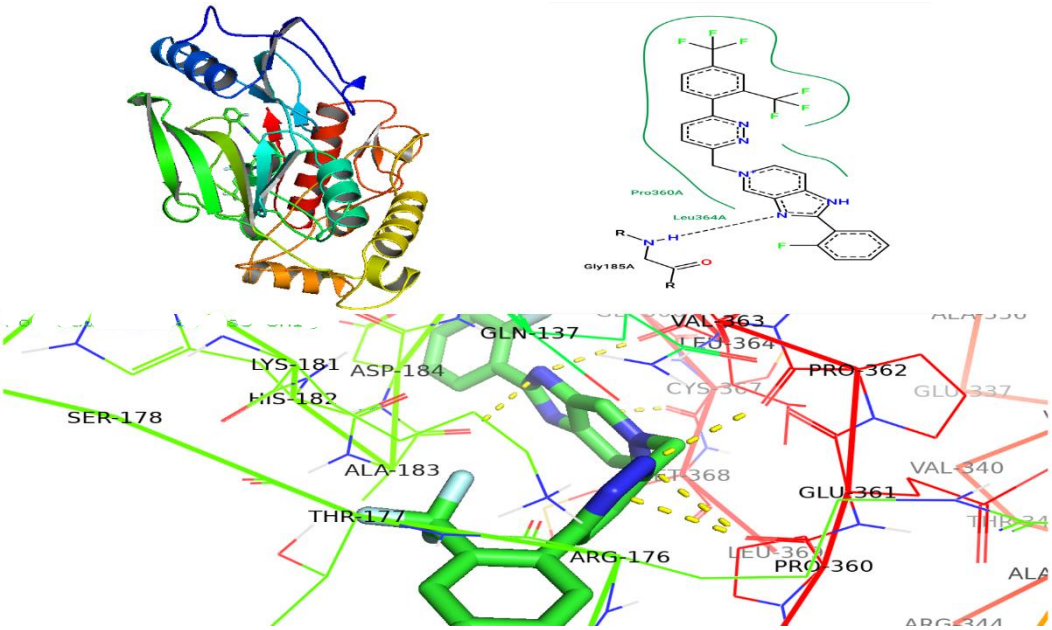

4.9.20 *MurB*- DB11852

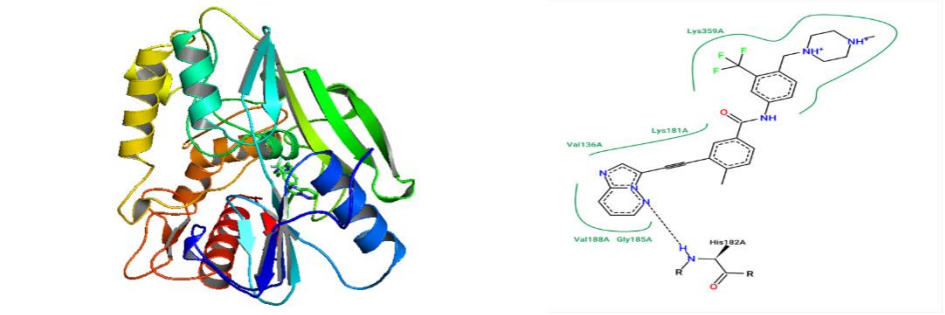

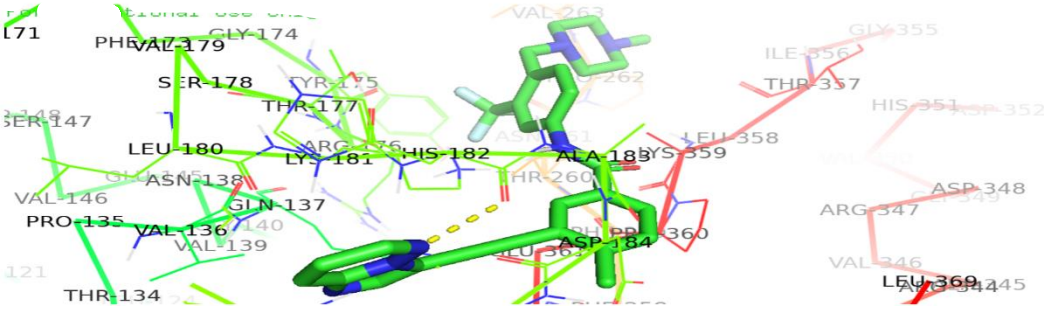

4.9.21 *MurB*- DB08901

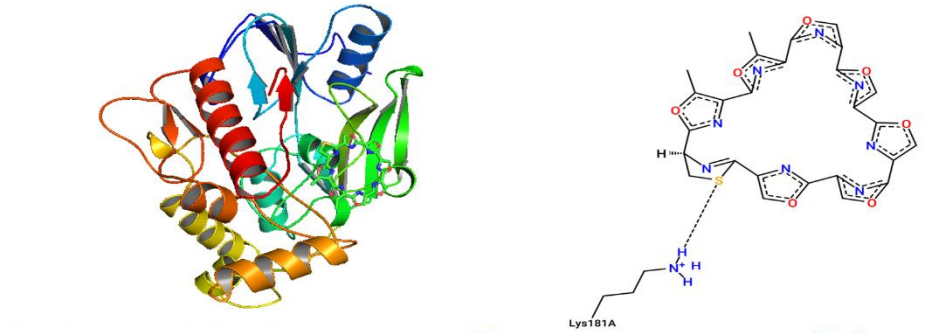

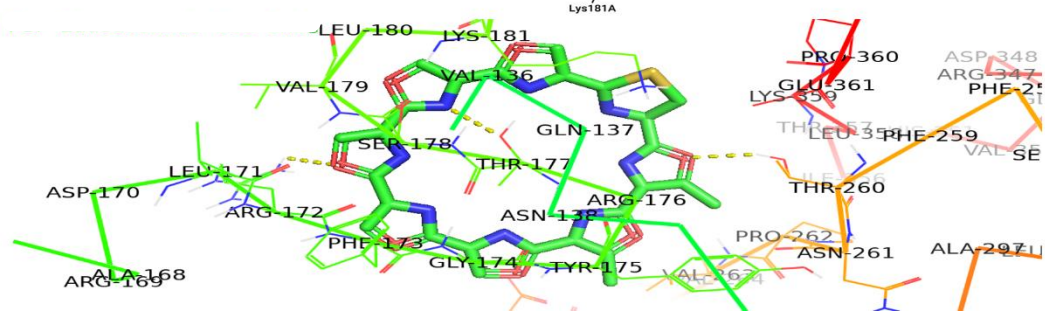

4.9.22 *MurB*- ZINC003975327

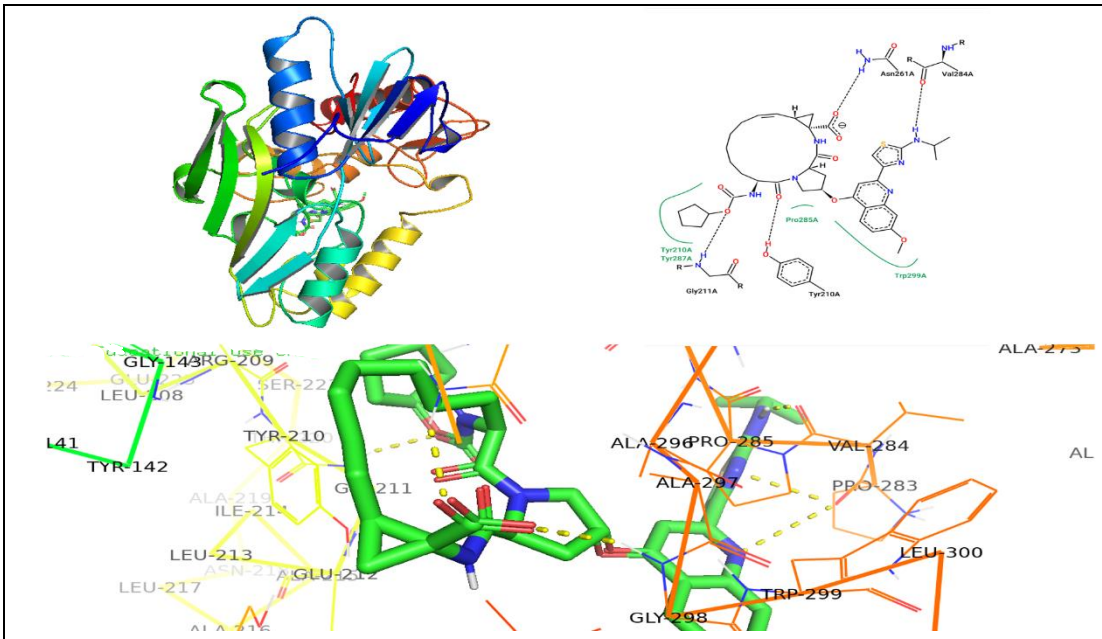

4.9.23 *MurB*- ZINC254071113

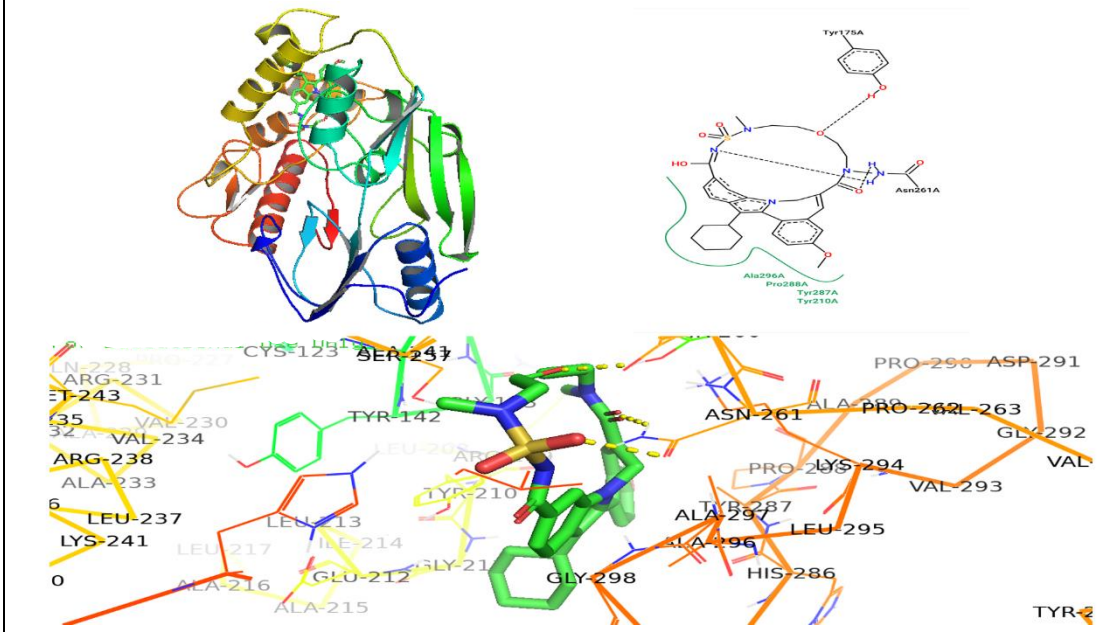

4.9.24 *MurB*- ZINC084726167

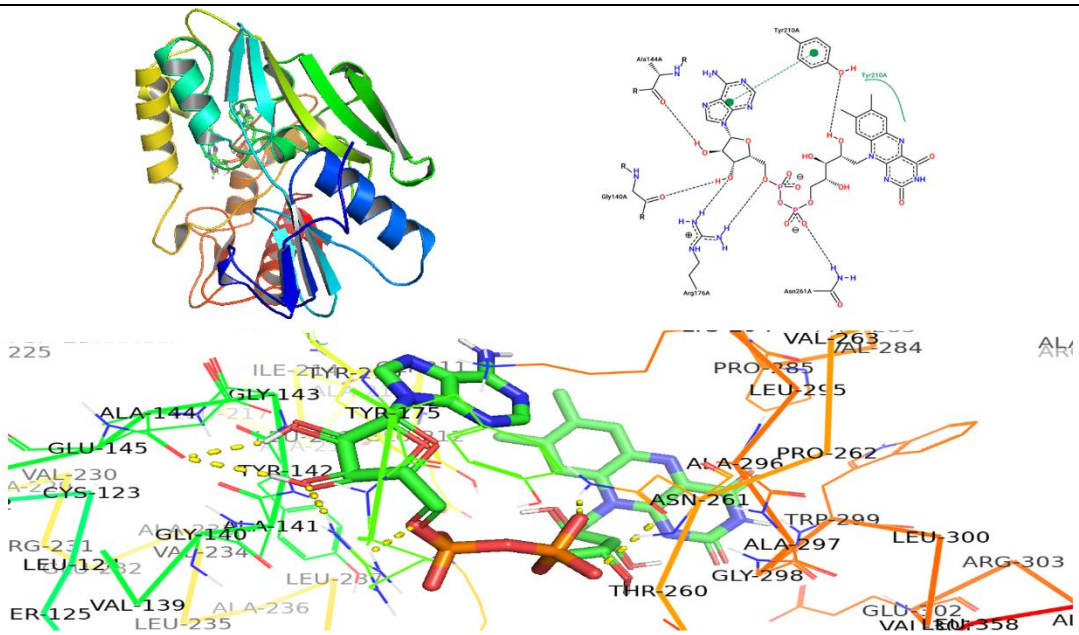

4.9.25 *MurB*- ZINC008215434

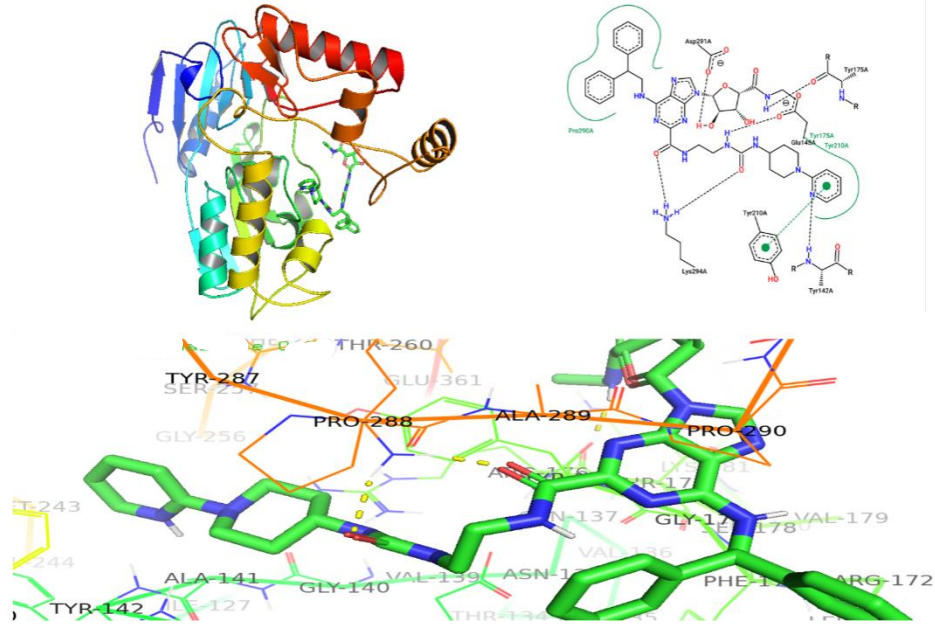

4.9.26 *MurB*- ZINC095539256

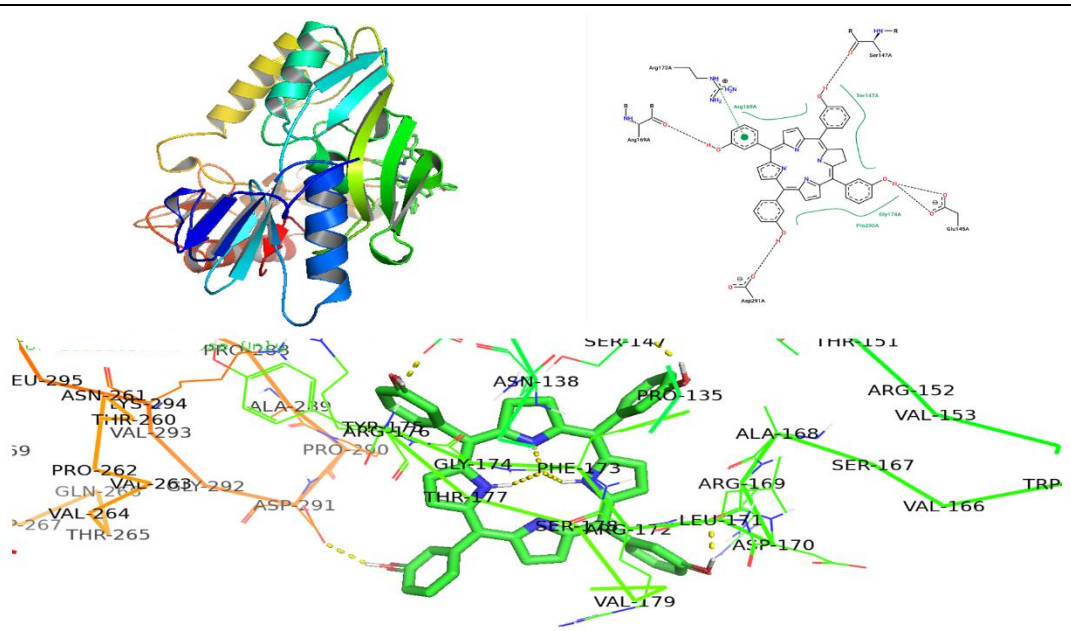

4.9.27 *MurB*- ZINC003934128

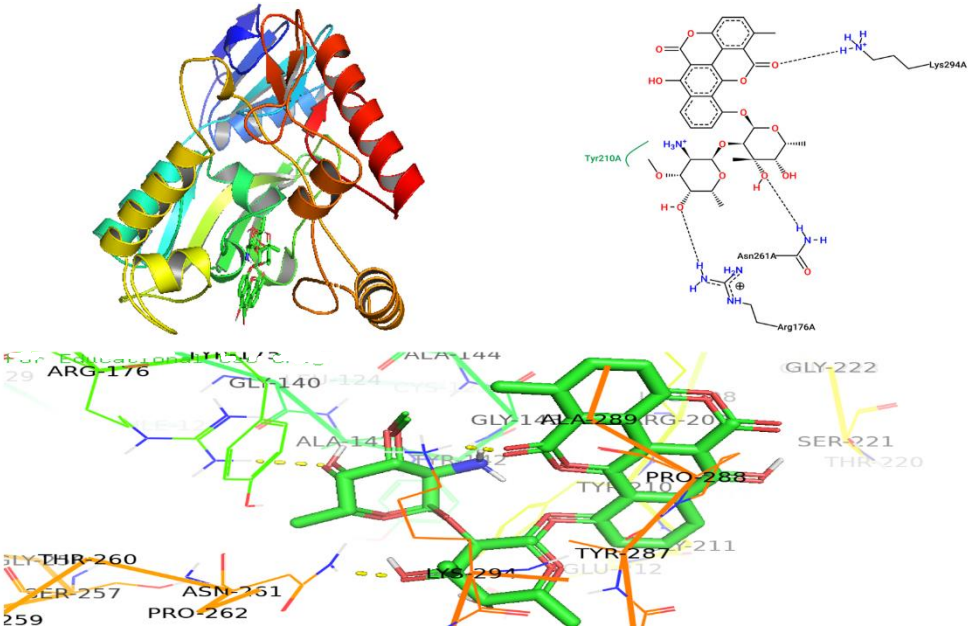

4.9.28 *MurB*- ZINC004215770

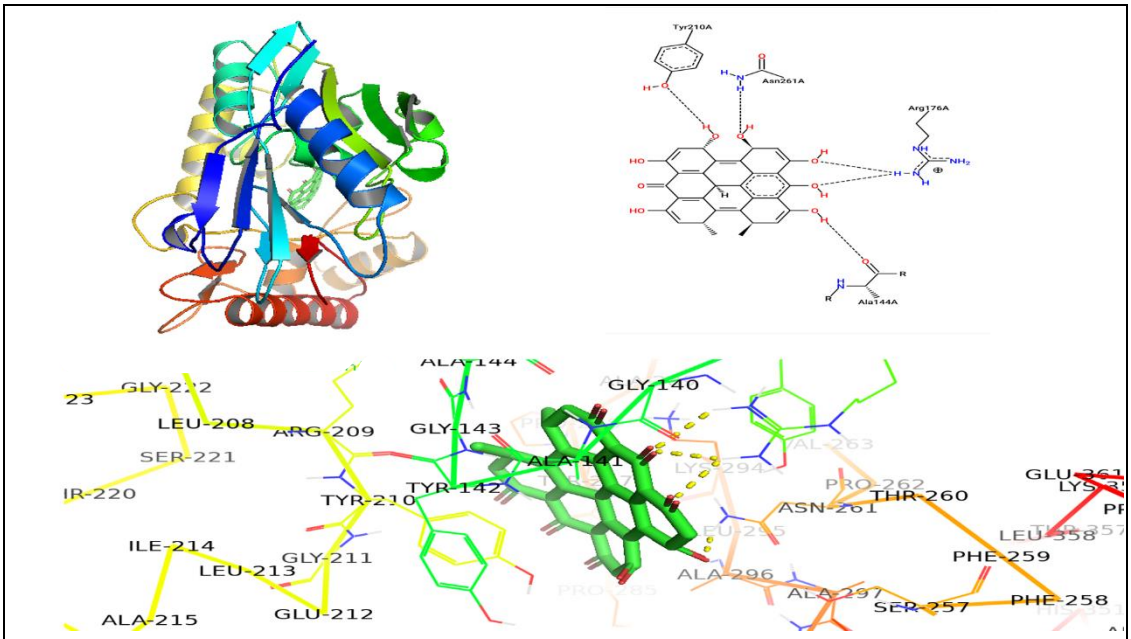

4.9.29 *MurB*- ZINC003780340

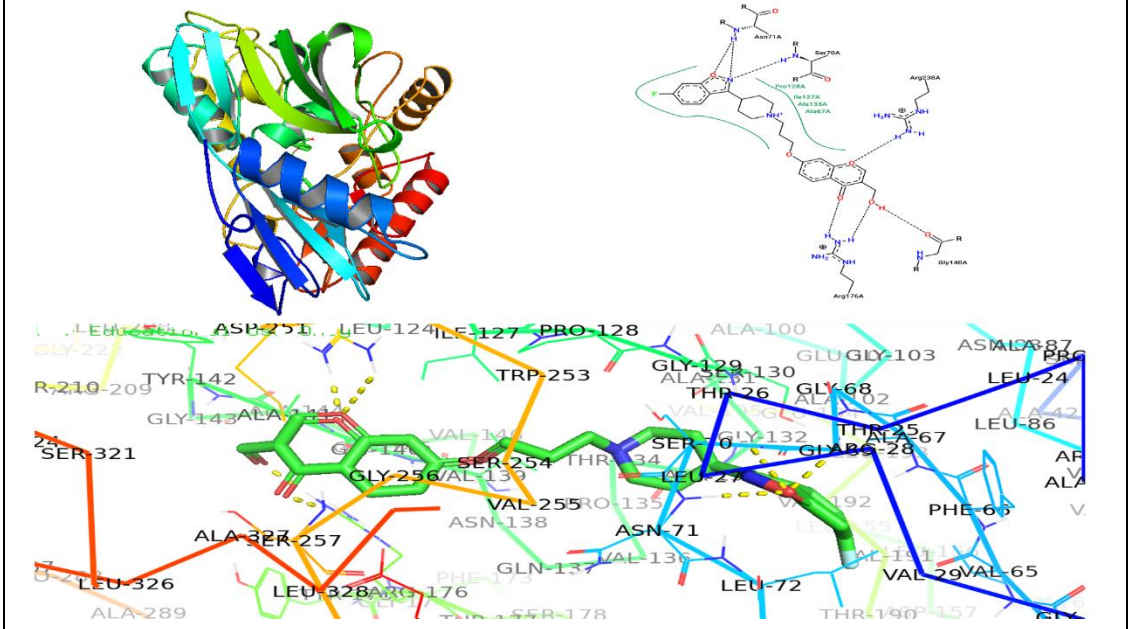

4.9.30 *MurB*- ZINC0001893112

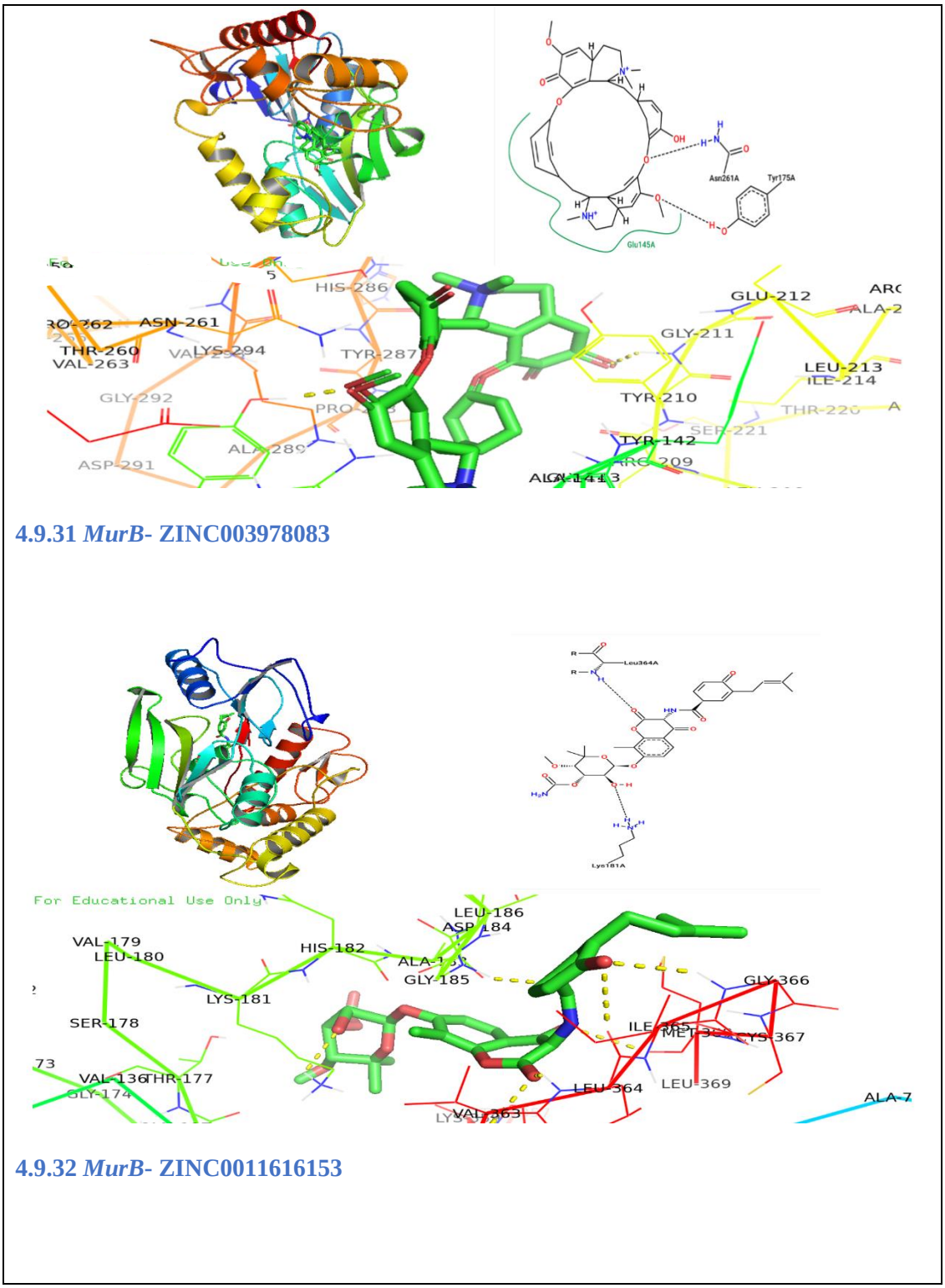

4.9.31 *MurB*- ZINC003978083

4.9.32 *MurB*- ZINC0011616153

Figure 4.9. Top thirty-two hits against the cell wall of MTB's *MurB*. Molecules containing *MurB* are docked and in contact with antagonistic residues. Docked compounds are displayed next to interacting receptor residue in 3D poses. Yellow dotted lines show hydrogen bond interactions.

4.1.8. ADMET and Pharmacophore Characteristics

As the pharmacokinetic and pharmacodynamic characteristics of these compounds are unknown, computations were performed using various online modules. It has also been demonstrated experimentally that the ADMET: Absorption, Distribution, Metabolism, Excretion, and Toxicity prediction is reliable. Moreover, the selected compounds underwent an assessment for drug-likeness and potential ADME properties. The webservers pkCSM,[182] Molsoft L.L.C (https://molsoft.com/mprop/), and ADMET lab 2.0[183] were used to assess the compounds' varied physiochemical characteristics and drug-likeness. The web server received the SMILES of these molecules as input, and it calculated several attributes including lipophilicity, physiochemical properties, drug-likeness, and medicinal chemistry analysis. The key findings and results are summarized in Table 4.4, Table 4.5, and Table 4.6. A crucial stage in pharmacokinetics for estimating drug-likeness is quality assessment. Some of the factors including lipophilicity (Log*P*), inhibitory constant (*KI*), etc. are employed in identification to assess the compound's quality.[190] These values were calculated using the binding energy that was discovered from the molecular docking investigations. Equation (1) establishes that the inhibitory constant (*KI*) can be computed based on the binding energy ΔG. In this equation, T represents the absolute temperature of the protein-ligand complex, which is 298.15 K, and R denotes the gas constant with a value of 1.987 x 10^{-3} Kcal/K-mol.

$$Ki = e\ \Delta G/RT \qquad (1)$$

The partition coefficient is used to determine a compound's lipophilicity (Log*P*). A crucial metric is known as LELP, which stands for ligand efficiency-dependent

lipophilicity. The LELP metric, developed by Keseru and Makara in 2009, amalgamates the notions of size and lipophilicity into a unified efficiency index. To compute, LELP, the Log*P* values (a measure of lipophilicity) are divided by LE (ligand efficiency), resulting in a quantitative assessment of the compound's efficiency in terms of both size and lipophilicity.[191]

$$LELP = logP/LE \quad (2)$$

The results demonstrated the compounds' strong potential to resemble inhibitors and their capacity to be tested against targets *in vitro*.

Table 4.4. ADMET analysis of top thirteen hits identified against *MmpL 11D2*.

S.No	Compound ID	PPB (%)	BBB	HIA	Aqueous Solubility (moles/L)	Ames Toxicity	Hepato-Toxicity	Max. Tolerated dose
1	CSID1653545	102.56	0.128	78.39	-2.89	YES	NO	0.438
2	CSID1655442	102.31	-0.062	95.99	-4.14	NO	YES	0.465
3	CSID1438694	100.62	-0.047	95.18	-5.55	YES	YES	0.56
4	CSID2153432	98.58	-0.083	91.48	-5.41	YES	YES	0.461
5	CSID0930923	96.61	-0.438	94.91	-3.47	YES	YES	0.221
6	DB12983	95.91	-0.877	78.53	-2.89	YES	NO	0.438
7	DB15039	97.55	-0.068	87.45	-2.89	YES	NO	0.438
8	DB14785	78.45	0.143	86.71	-2.89	YES	NO	0.438
9	DB15688	81.32	-0.724	87.05	-2.89	YES	NO	0.438
10	ZINC000051951669	80.95	-1.031	100	-3.47	YES	NO	0.571
11	ZINC000001612996	76	-1.05	86.66	-3.76	NO	YES	-0.039
12	ZINC000003780340	77.53	-1.69	100	-2.89	NO	NO	0.438
13	ZINC000028827350	84.83	-2.07	77.33	-2.82	NO	YES	0.562

Table 4.5. ADMET analysis of top thirty hits identified against *GlfT2*.

S.No	Compound ID	PPB (%)	BBB	HIA	Aqueous Solubility (moles/L)	Ames Toxicity	Hepato-Toxicity	Max. Tolerated dose
1	CSID541554	73.38	-0.05	95.13	-5.612	NO	NO	0.749
2	CSID67239	102.7	0.015	100	-2.892	YES	NO	0.438
3	DB12983	95.91	-0.877	78.53	-2.892	YES	NO	0.438
4	DB12424	93.08	0.322	80.94	-2.892	YES	NO	0.438
5	DB04016	98.57	-1.11	69.56	-2.892	YES	NO	0.438
6	DB08827	97.76	0.214	78.13	-2.892	YES	NO	0.438
7	DB12154	74	-0.326	91.73	-2.892	YES	NO	0.438
8	DB15637	95.85	-0.259	83.23	-2.892	YES	NO	0.438
9	DB03044	97.69	-0.238	81.76	-2.892	YES	NO	0.438
10	DB06589	94.34	-0.524	86.06	-2.892	YES	NO	0.438
11	DB12228	84.83	-0.582	89.31	-2.892	YES	NO	0.438
12	DB11691	96.33	-0.691	80.07	-2.892	YES	NO	0.438
13	DB13676	92.34	0.135	100	-2.892	YES	NO	0.438
14	DB01988	95.05	0.412	84.17	-2.892	YES	NO	0.438
15	DB08815	98.41	0.362	82.06	-2.892	YES	NO	0.434
16	DB14773	99.15	-0.236	83.69	-2.892	YES	NO	0.438
17	DB14703	85.86	0.111	16.02	-2.892	YES	NO	0.448
18	DB04868	98.03	-0.156	89.09	-2.892	YES	NO	0.438
19	DB01092	65.58	-0.034	72.85	-2.858	YES	NO	0.639
20	DB01337	69.84	0.348	86.71	-3.919	YES	NO	1.371
21	DB00872	99.99	-0.112	82.46	-2.892	YES	NO	0.438
22	ZINC000043203371	93.08	-0.79	94.67	-4.008	YES	NO	-0.083
23	ZINC000063933734	97.52	-1.929	92.78	-3.362	NO	YES	0.736
24	ZINC000095092808	100.8	-1.609	87.41	-2.955	NO	YES	0.665
25	ZINC000027990463	97.76	-0.339	88.44	-3.472	NO	YES	0.488
26	ZINC000001612996	76	-1.053	88.66	-3.763	NO	YES	-0.039
27	ZINC000253633622	97.46	-0.143	92.07	-4.48	YES	YES	0.294
28	ZINC000043204146	96.4	-1.399	92.15	-3.268	NO	YES	0.556
29	ZINC000100378061	96.33	-1.091	80.93	-3.346	NO	YES	0.122
30	ZINC000003978005	91.04	0.589	69.37	-3.311	NO	YES	-0.327

Table 4.6. ADMET analysis of top thirty-two hits identified against *MurB.*

S.No	Compound ID	PPB (%)	BBB	HIA	Aqueous Solubility (moles/L)	Ames Toxicity	Hepato-Toxicity	Max. Tolerated dose
1	CSID1438694	100.62	-0.04	95.18	-5.55	Yes	Yes	0.56
2	CSID2166135	97.47	0.14	92.73	-4.79	Yes	Yes	0.654
3	CSID 1655442	97.36	-0.56	89.63	-4.66	Yes	Yes	0.465
4	CSID2154128	93.78	0.1	93.16	-5	No	Yes	-0.551
5	CSID2165834	93.7	-0.08	87.68	-2.89	Yes	No	0.438
6	CSID2156566	94.15	3.99	90.89	-4.7	No	Yes	-0.152
7	CSID2140363	97.05	0	96.81	-6.03	Yes	Yes	0.003
8	CSID2156621	96.56	-0.27	81.73	-2.89	Yes	No	0.438
9	CSID3866834	99.7	4.37	87.12	-5.22	No	Yes	-0.032
10	CSID2158441	95.75	0.101	89.66	-5.46	No	No	0.181
11	CSID2156999	90.29	3.95	92.55	-4.58	No	Yes	-0.169
12	DB15688	81.32	-0.72	87.05	-4	Yes	No	0.438
13	DB12983	95.91	-0.87	78.53	-6.67	Yes	No	0.438
14	DB14773	99.15	-0.23	83.69	-4.81	Yes	No	0.438
15	DB06229	95.56	-0.13	88.71	-4.02	Yes	No	0.438
16	DB12424	93.08	-0.32	80.94	-4.31	Yes	No	0.438
17	DB15396	93.51	0.295	87.5	-4.13	Yes	No	0.438
18	DB15401	95.37	0.62	86.37	-2.7	Yes	No	0.438
19	DB03461	11.77	-5.17	0	-1.15	No	No	0.438
20	DB11852	97.51	0.24	83.96	-6.16	Yes	No	0.438
21	DB08901	93.43	0.39	87.5	-4.22	Yes	No	0.438
22	ZINC003975327	84.03	-2.7	100	-2.89	No	Yes	0.436
23	ZINC254071113	96.9	-2.15	61.57	-3.4	No	Yes	0.52
24	ZINC084726167	83.57	-1.2	92.64	-4.57	No	Yes	-0.214
25	ZINC008215434	67.03	-3.28	22.49	-2.89	No	No	0.274
26	ZINC095539256	89.47	-1.85	50.32	-2.9	No	No	0.335
27	ZINC003934128	98.93	-1.44	100	-2.89	No	No	0.434
28	ZINC004215770	73.46	-1.75	67.67	-3.14	Yes	No	0.176
29	ZINC003780340	77.53	-0.39	100	-2.89	No	No	0.438
30	ZINC003978083	51.37	-2.89	91.33	2.9	Yes	Yes	0.142
31	ZINC011616153	85.38	-2.058	61.41	-3.46	No	Yes	0.957
32	ZINC001893112	96.67	3.37	92.69	-4.28	No	Yes	0.346

4.1.9. Molecular Dynamics (MD) Simulations of Receptor-Ligand Complexes

No compounds have been identified for our initial target *MmpL* 11D2, as none have demonstrated a binding affinity of -10.5 Kcal/mol or greater. Seven compounds namely, CSID541554, CSID67239, DB12983, DB12424, ZINC000043203371, ZINC000063933734, and ZINC000095092808 against target *GlfT2* (Figure 4.10) were found to have good binding affinities through molecular docking analysis. Similarly, another seven compounds namely, CSID1438694, CSID2166135, DB15688, DB12983, ZINC003975327, ZINC084726167, and ZINC254071113 against target *MurB* (Figure 4.11) were found with binding energies lower than that of FAD cofactor (reported). These fourteen compounds were selected for further analysis based on their best binding energies and their ability to interact with the residues in the substrate binding site. The compounds underwent MD simulation analysis to investigate their dynamic behavior and interactions within the system.

Most highly rated docked complexes underwent 100 ns MDS at 300 K and 1.0 bar using Schrodinger-Maestro V 10.4's[184] Desmond 4.4 module to evaluate the stability of the compound following molecular docking and ADMET analysis.[183] The root mean square deviation (RMSD) was computed as a measure to assess the stability of the complex. Indeed, the RMSD serves as a metric for quantifying the disparity between two sets of atomic coordinates, like those of the protein-ligand complex and the native protein structure. By contrasting the RMSD values of the protein-ligand complex with those of the native protein, valuable information regarding the complex's stability can be gleaned. This analysis can help determine whether the ligand maintains its binding within the active site or undergoes movement throughout the simulation.

Variations in RMSD can signify conformational alterations or fluctuations in the ligand's binding within the active site, shedding light on the dynamic behavior of the complex.

By examining the RMSD values, one can assess the stability of the protein-ligand complex and the dynamics of the protein during the simulation. The MD simulations found that the characteristics and energy of docked complexes were stable and equilibrated. Throughout the simulation, the stabilization of the protein-ligand complex is depicted through the RMSD values and visualized in the accompanying figures.

The simulation studies conducted on fourteen compounds against *Mycobacterium tuberculosis* (MTB), seven compounds each against *GlfT2* and *MurB* have provided substantial evidence to support their suitability as inhibitors.

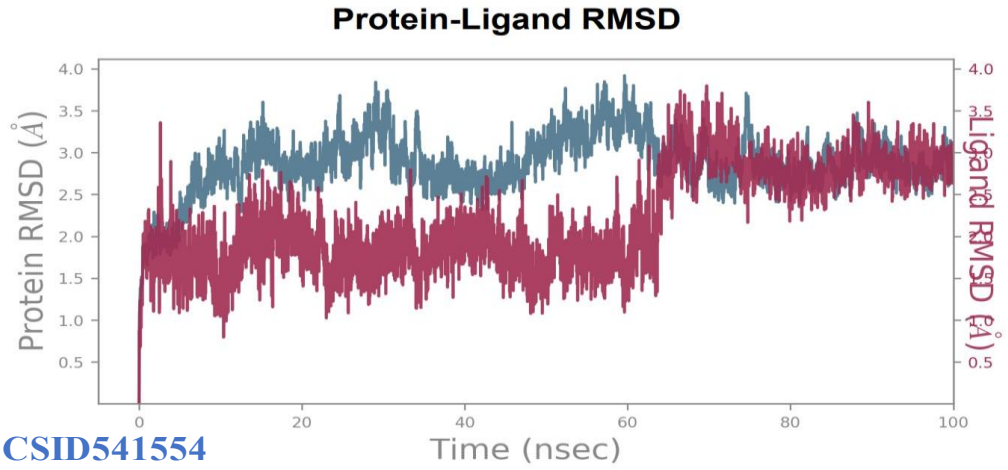

A. CSID541554

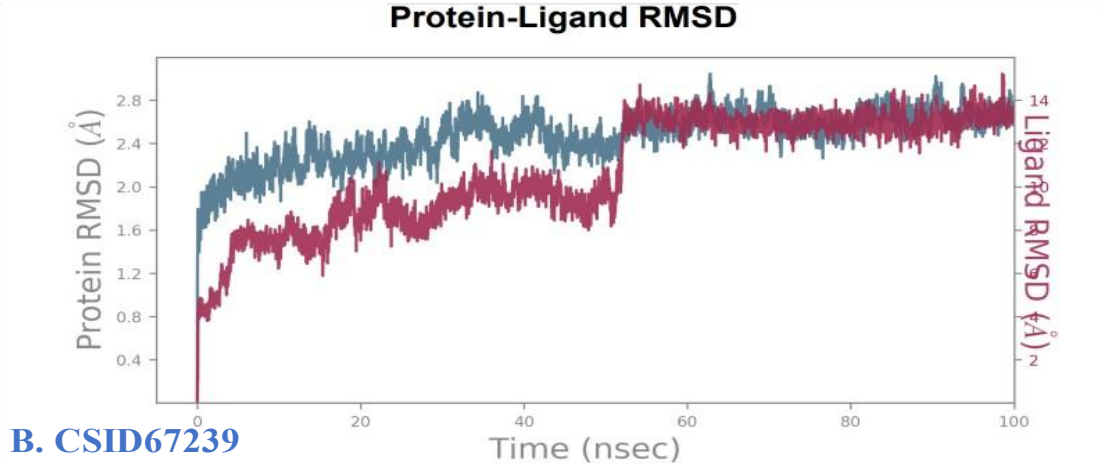

B. CSID67239

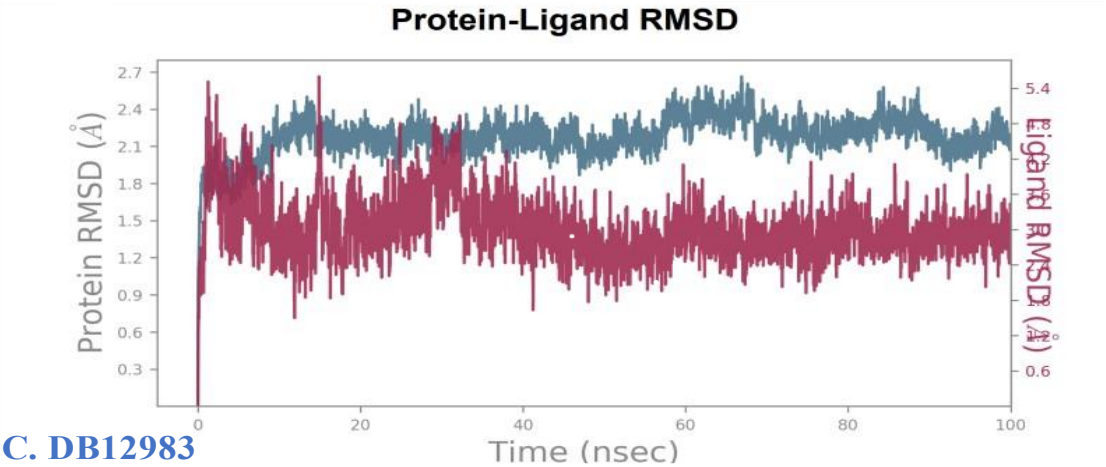

C. DB12983

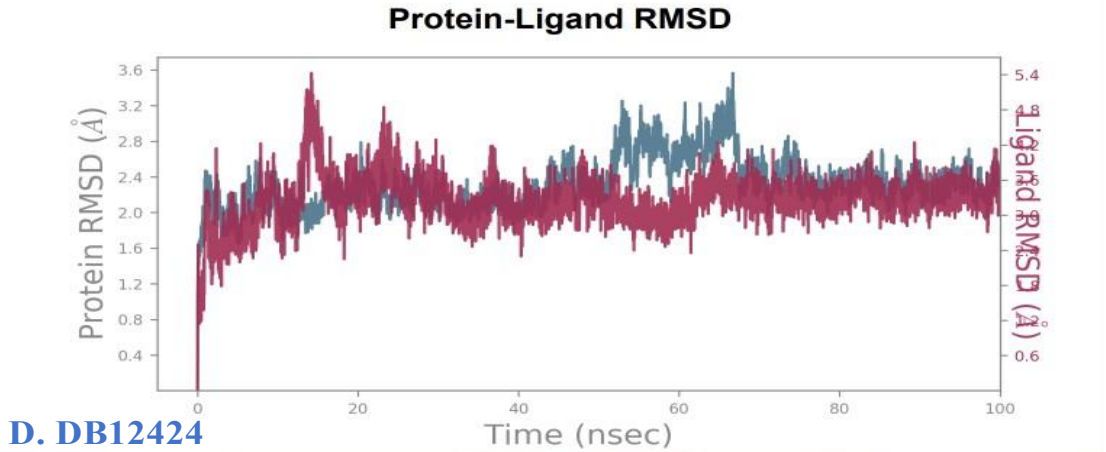

D. DB12424

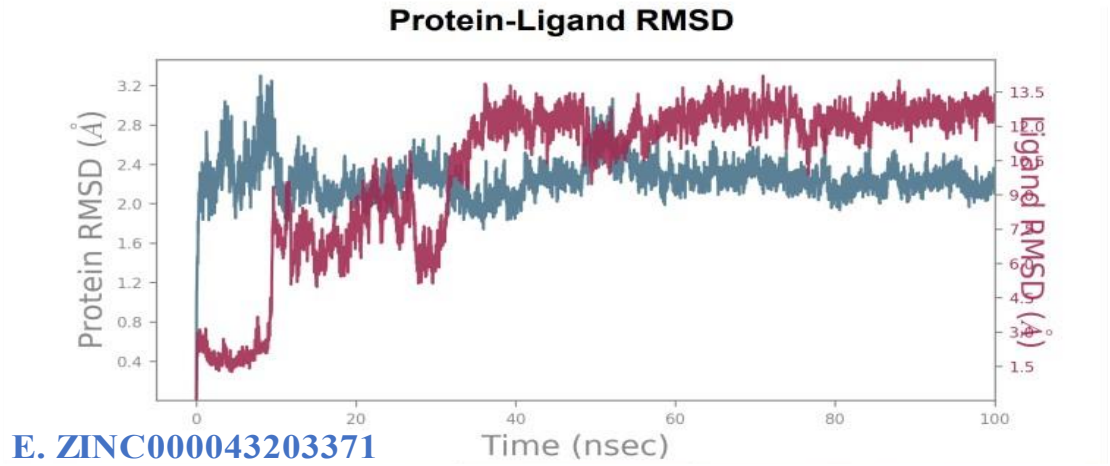

E. ZINC000043203371

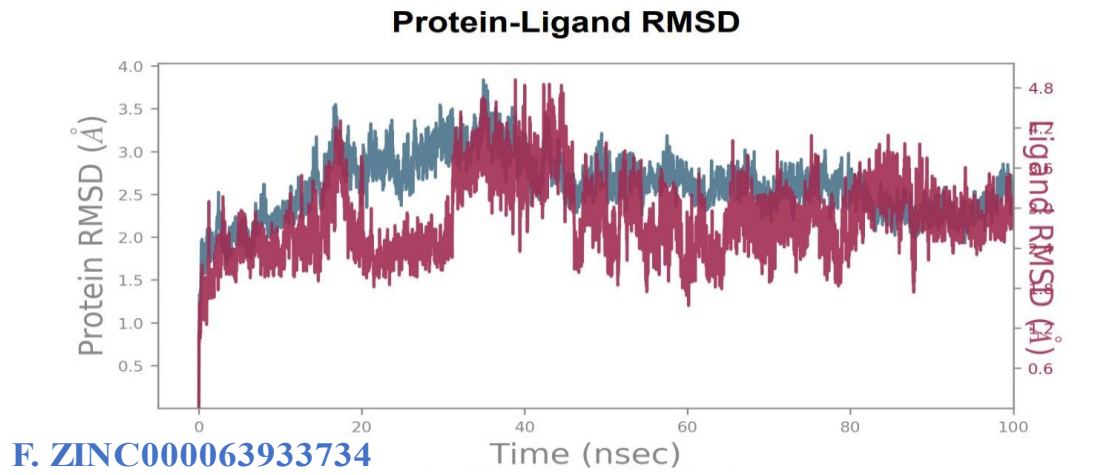

F. ZINC000063933734

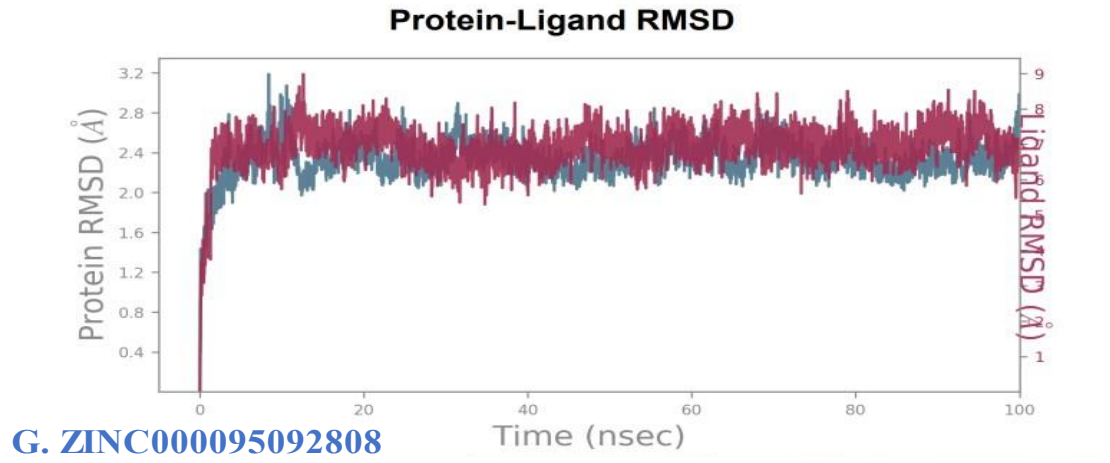

G. ZINC000095092808

Figure 4.10. Root Mean Square Deviation (RMSD) evaluation of complexes with target *GlfT2* (cyan) and ligand (red) is shown in Fig (A-G) respectively.

In the context of the *GlfT2*-ligand complexes studies, Fig 4.10A shows that the protein and ligand CSID541554 exhibit diffusion in the initial phase of 0-70 ns, but a stable and strong binding interaction is observed after 70 ns with a maximum deviation of 3.8Å. Similarly, Fig 4.10B indicates that ligand CSID67239 exhibits synchronous fluctuations in the first half-time frame of 0-50 ns, but a stable and consistent binding is observed in the second half of 50-100 ns, with an RMSD of the protein at 2.9Å. However, the ligand DB12983 (Fig 4.10C) displays weak, transient interactions with the *GlfT2* protein around 5 ns, indicating that it is not strongly binding to the protein. In contrast, ligand DB12424 (Fig 4.10D) demonstrates good stability and binding throughout most of the simulation, with slight diffusion of the ligand observed in the timeframe of 50-70 ns. However, in the timeframe of 70-100 ns, a strong binding affinity is observed, with an RMSD of the protein at 2.7Å, suggesting that it consistently and stably interacts with *GlfT2*.

On the other hand, Fig 4.10E shows that ligand ZINC000043203371 is not demonstrating stable interactions with the target protein *GlfT2*, with an RMSD ranging from 0.7-13.5Å for the ligand and maximum fluctuations observed in the complex. In Fig 4.10F, the RMSD of the *GlfT2*-ZINC000063933734 complex equilibrates at 0-15 ns and 35-45 ns but fluctuates between 20-30 ns. After that, a weak to moderate binding is observed during the 45-100 ns timeframe. Finally, ligand ZINC000095092808 (Fig 4.10G) exhibits a strong, consistent, and stable binding throughout the 100 ns simulation. Based on the RMSD values, and the steadiness of the protein-ligand interactions witnessed, it appears that the most stable and best interactions are exhibited by the ligands DB12424 (Fig 4.10D), ZINC000063933734

(Fig 4.10F), and ZINC000095092808 (Fig 4.10G), which demonstrate a good binding affinity towards the *GlfT2* protein. In summary, these results indicate that these ligands show promise as potential candidates for further refinement and advancement in their role as inhibitors of *GlfT2*.

For the complexes of *MurB*, it has been observed that the ligand CSID1438694 (Fig 4.11A) shows good binding with the *MurB* protein, except for a slight diffusion in the timeframe of 15-20 ns and between 60-80 ns. This observation implies that the interaction between the ligand and the protein is not consistently stable throughout the simulation, with some periods of fluctuation and diffusion of the ligand away from the protein. However, in the last time frame of 80-100 ns, the ligand shows strong binding affinity and fluctuates sharply, indicating that the protein-ligand complex has stabilized once again. The RMSD value of the protein at 3.2Å and the ligand at 3.6Å suggest that the overall structure of the complex remains relatively stable during this time frame. Ligand CSID2166135 (Fig 4.11B) did not show good binding and a complete diffusion was observed during a 0-100 ns time frame and did not bind well to its intended target and quickly diffused away during the experiment, which could be problematic for its probable use as a drug candidate. In the case of ligand, DB15688 (Fig 4.11C) initially shows diffusion between 0-30 ns but a good, stable, and consistent binding is observed between 30-100 ns time frame.

Ligand DB12983 (Fig 4.11D) shows strong and consistent binding with the protein from 10-60 ns but diffuses away after that, with some aberrant fluctuations. During the first 50 nanoseconds of the simulation, the ligand strongly and consistently binds to the protein. This is a positive sign as strong binding is often desirable for a ligand

intended for use as an inhibitor. Ligand ZINC003975327 (Fig 4.11E) does not show steady collaboration with the target protein and has a fluctuating RMSD. This suggests that the ligand did not form an even complex or bond with the respective target protein, indicating that it may not be an effective inhibitor. Further experiments or simulations may be necessary to determine whether this ligand has the potential to be an effective inhibitor. The ligand, ZINC084726167 (Fig 4.11F) exhibits diffusion during the 0-20 ns timeframe, however, a strong binding interaction was observed between 20-80 ns. Subsequently, the ligand molecules display erratic fluctuations.

The ligand, ZINC254071113 (Fig 4.11G) exhibits a stable and consistent binding behavior throughout the time frame of 0-80 ns. Yet, afterward 80 ns, the ligand demonstrates a tendency to diffuse, indicating weaker interaction with the receptor. This diffusion behavior can potentially impact the stability of the ligand-receptor complex and may compromise the overall efficacy as an inhibitor. Among the ligands studied against *MurB*, DB15688 (Fig 4.11C), DB12983 (Fig 4.11D), ZINC084726167 (Fig 4.11F), and ZINC254071113 (Fig 4.11G) exhibit the most stable RMSD values within the range of 2.1Å-3.6Å and demonstrate a good binding affinity with the *MurB* protein. However, it is noteworthy that the ligand ZINC254071113 (Fig 4.11G) shows a diffusion behavior away from the target after the time step of 80 ns. Although this ligand demonstrates favorable binding characteristics, its diffusion behavior could potentially compromise the stability of the complex, which may affect its overall efficacy. Further investigation into the underlying factors contributing to the diffusion behavior of this ligand may be necessary to optimize its binding interaction with the *MurB* protein. In summary, the molecular dynamics (MD) simulation analysis offers

valuable insights into the stability and binding interactions of these ligands with the *MurB* protein.

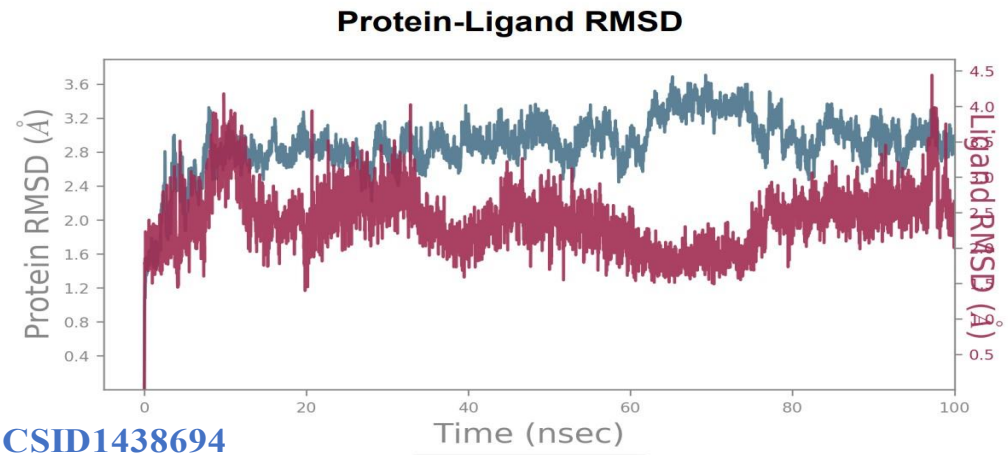

A. CSID1438694

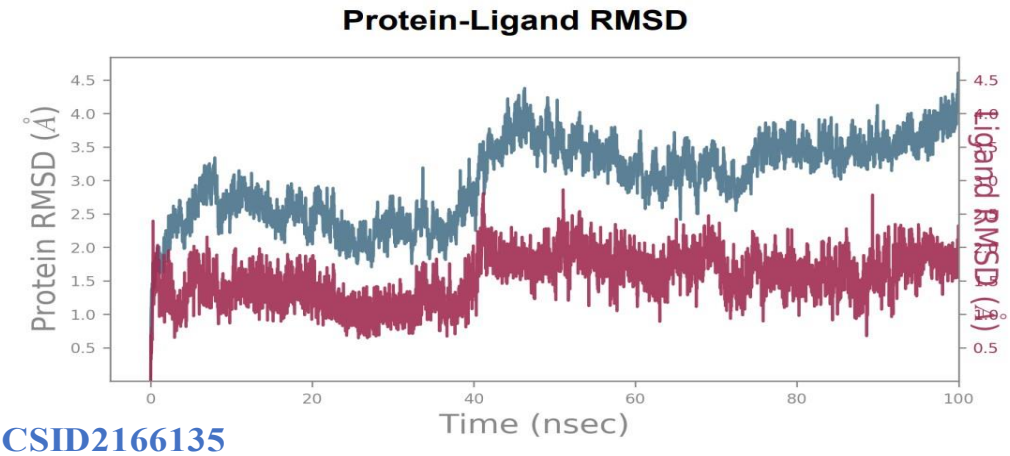

B. CSID2166135

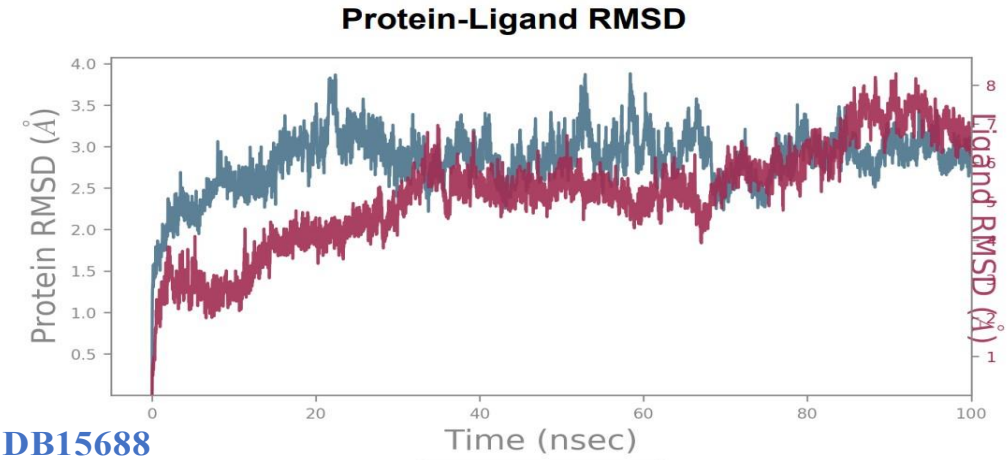

C. DB15688

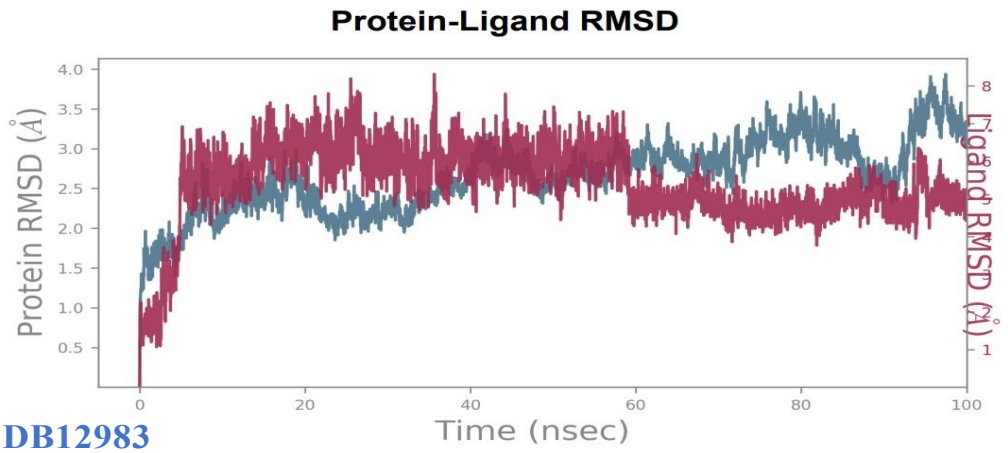

D. DB12983

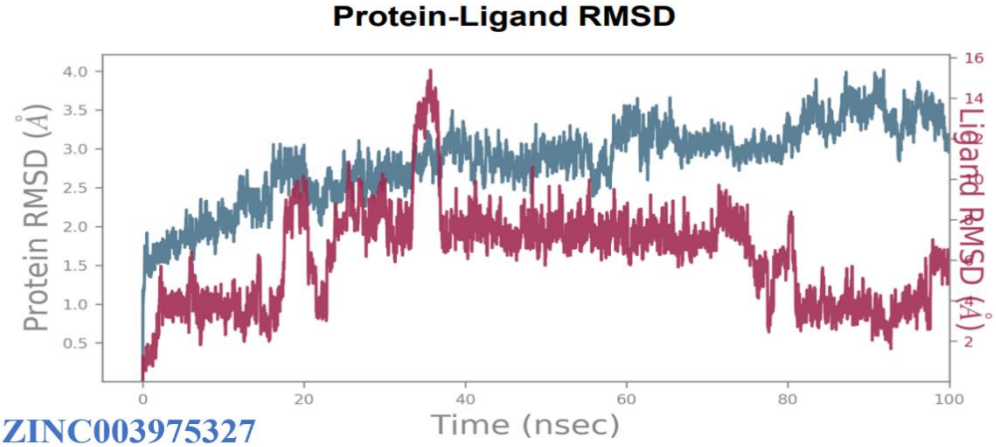

E. ZINC003975327

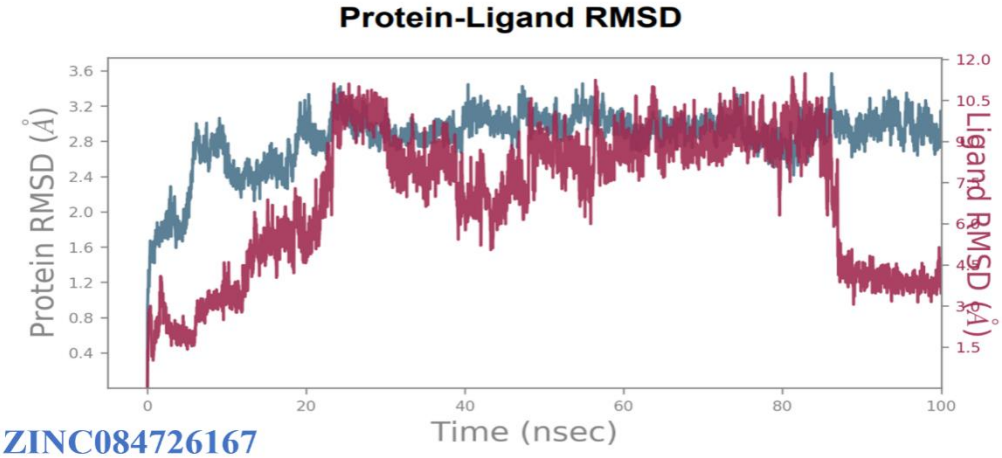

F. ZINC084726167

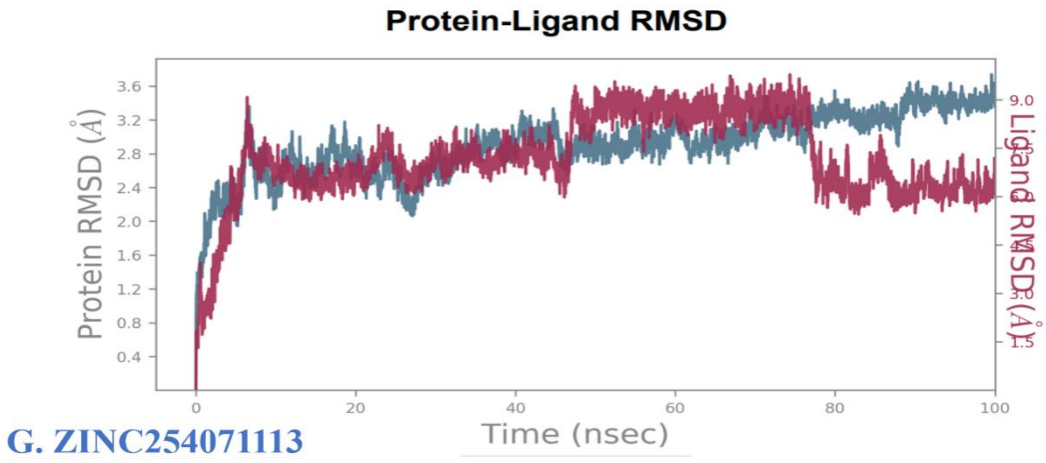

Figure 4.11. Illustrates the simulation analysis of *MurB* using the most highly ranked compounds obtained from ChemSpider CSID1438694 (A), CSID2166135 (B); from Drug Bank DB15688 (C), DB16292 (D); from ZINC database ZINC003975327 (E), ZINC084726167 (F), ZINC254071113 (G).

4.2. *In-vitro* Validation

In the process of identifying potential inhibitors, *in-silico* screening is a widely employed method to identify promising compounds that exhibit potential therapeutic properties. However, it is crucial to validate the predicted results with *in-vitro* experiments to confirm the efficacy of the selected compounds.

Subsequently, *in-vitro* experiments were performed to test the activity of the identified compounds against the target enzymes. After conducting meticulous analysis, the four chemical compounds are designated as A, B, C, and D and were chosen based on their *in-silico* screening outcomes and accessibility for further investigation. These compounds were found effective against *M. smegmatis*, and *M. phlei* in disc diffusion test (Fig 4.12). The inhibition zone diameter (IZD) of compounds A, B, C, and D against *M. phlei* was 20.00±1.33, 22.21±0.92, 28.33±0.44, 10.00±0.00 mm respectively while IZD of A against *M. smegmatis* was 28.12±1.44 and B, C, and D

have equal values of 18.00±0.00 mm. Among these compounds, two ZINC000095092808 (A) and DB12424 (B) were found to be effective against *GlfT2*, while the other two, ZINC254071113 (C) and DB15688 (D) showed promising inhibitory activity against *MurB.*

The selection of these compounds was made by employing a combination of computational and experimental approaches, and their availability was also taken into consideration to ensure that they can be readily obtained for experimental studies. These findings provide valuable insight into the potential use of these compounds as novel inhibitors that can target key enzymes involved in bacterial cell wall biosynthesis.

The MIC value was determined against *Mycobacterium phlei* MTCC 1724, *M. smegmatis* MTCC 6, *M. tuberculosis* H_{37}Rv ATCC 27294, *M. tuberculosis* H_{37}Ra ATCC 25177 and *M. tuberculosis* SRHU-1. The control antibiotics tested included rifampicin and moxifloxacin. The findings indicated that two compounds, namely ZINC000095092808 (referred to as compound A) and ZINC254071113 (referred to as compound C), exhibited promising antituberculosis effects against the tested strains.

The MIC values of compounds A and C ranged from 0.25 to 0.5 µg/mL. On the other hand, compounds B and D also displayed activity but were less as compared to A, C, rifamycin, and moxifloxacin. The MIC values of B and D ranged from 2 to 8 and 2 to 6 µg/mL respectively. Notably, ZINC000095092808 (Compound A) demonstrated significant potency against *Mycobacterium phlei* MTCC 1724, *M. smegmatis* MTCC

6, *M. tuberculosis* H_{37}Rv ATCC 27294, *M. tuberculosis* H_{37}Ra ATCC 25177, and *M. tuberculosis* SRHU-1 with MIC values ranging from 0.25 to 0.5 µg/mL (Table 4.7). Similarly, compound C showed MIC values ranging from 0.25 to 0.5. Overall, these results suggest that ZINC000095092808 (compound A) and ZINC254071113 (compound C) may be effective antimicrobial agents as compared to rifampicin and moxifloxacin against the bacterial strains tested (Table 4.7).

Further investigation is essential to explore the potential clinical applications of these compounds. Understanding their safety and effectiveness in living organisms is paramount. This necessitates comprehensive research efforts and studies. Only through rigorous exploration can the full potential of these compounds be unlocked in the field of medicine. Therefore, a commitment to ongoing research is crucial.

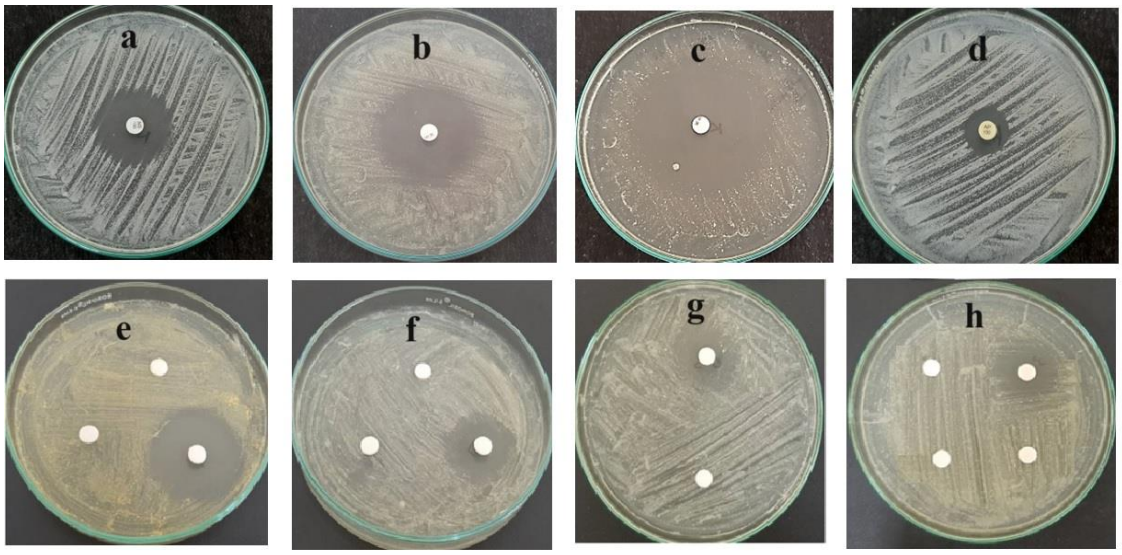

Figure 4.12. Evaluation of Antimicrobial Activity: a-d *M. phlei* and e-h: *M. smegmatis*; The disc showing inhibition zones are: a and e- ZINC000095092808; b and f-DB12424; c and g-ZINC254071113; d and h-DB15688; the disc without inhibition zone diameter is control (methanol) in which the compound was dissolved.

Table 4.7. MIC value of different compounds against pathogenic and non-pathogenic strains of *Mycobacterium* species.

Targets	**Compounds**	***Mycobacterium* species**				
		M.Phlei MTCC 1724*	*M. Smegmatis* MTCC6*	MTB (H_{37} Rv) ATCC 27294**	MTB (H_{37} Ra) ATCC25177**	Clinical Isolate SRHU-1
GlfT2	Compound A (µg/mL)	0.25	0.25	0.25	0.5	0.5
	Compound B (µg/mL)	8	4	4	2	2
MurB	Compound C (µg/mL)	0.25	0.25	0.5	0.5	0.5
	Compound D (µg/ml)	2	2	3	2	6
Control	Rifampicin (µg/mL)	0.25	0.25	0.25	0.5	1.0
	Moxifloxacin (µg/mL)	0.06	0.06	0.06	0.06	0.25

*MIC value determined by broth dilution method; ** MIC by Radiometric BACTEC assay

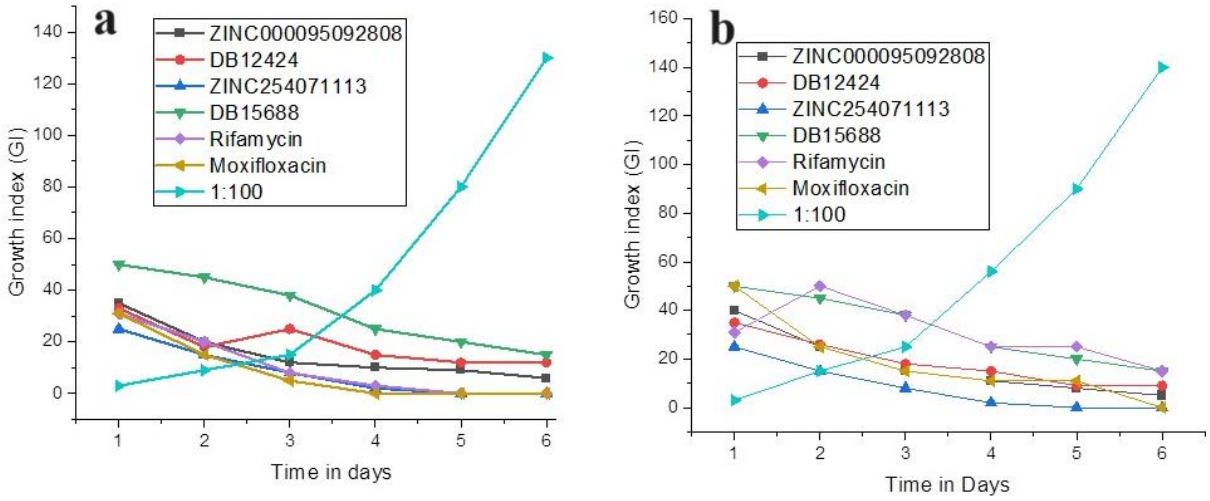

Figure 4.13. Graph illustrating the inhibition of Growth Index (GI) values of *M. tuberculosis* H_{37}Rv strain (a) and clinical isolate *M. tuberculosis* SRHU-1 (b) over a period of days in the presence of identified compounds and control.

The results showed that ZINC000095092808 (compound A) and ZINC254071113 (compound C) exhibited potent anti-tuberculosis activity against both *M. tuberculosis* H_{37}Rv and clinical isolate *M. tuberculosis* SRHU-1 with a decrease in the value of GI indicating a substantial reduction in bacterial growth. The compound DB12424 (compound B) and DB15688 (compound D) also exhibited reasonable activity against both strains (Fig 4.13 a and b). The results are comparable with compounds A, C, rifamycin, and moxifloxacin.

Overall, these findings suggest that ZINC000095092808 (compound A) and ZINC254071113 (compound C) has strong potential as a lead compound for the development of new anti-tuberculosis inhibitor while DB12424 (compound B) and DB15688 (compound D) may have the potential for combination therapy. Our findings reveal that these compounds exhibited comparable effects on the growth index. Further investigations are desirable to determine these compounds' mode of action and potential toxicity.